NOSC

NOSC TR 634

Technical Report 634

HIGH-PRESSURE VIEWPORTS FOR INFRARED SYSTEMS

Phase 2 – Chalcogenide Glass

JD Stachiw
SL Bertic

28 January 1982

Final Report for Period October 1980—September 1981

Prepared for
Naval Material Command
Director of Navy Laboratories

Approved for public release; distribution unlimited

NAVAL OCEAN SYSTEMS CENTER
SAN DIEGO, CALIFORNIA 92152

NAVAL OCEAN SYSTEMS CENTER, SAN DIEGO, CA 92152

AN ACTIVITY OF THE NAVAL MATERIAL COMMAND

SL GUILLE, CAPT, USN
Commander

HL BLOOD
Technical Director

ADMINISTRATIVE INFORMATION

Work was performed under direction of the Naval Material Command, Director of Navy Laboratories, as part of NOSC IR/IED Technical Project F61512, by members of the Ocean Technology Department. This report covers work from October 1980 to September 1981 and was approved for publication 28 January 1982.

The chalcogenide glass, composition AMTIR-1, was supplied for this study by Amorphous Materials, Inc, of Garland, Texas, while the process for applying AMTIR-1 coating to germanium test specimens and windows was developed by Optic Electronic Corp, of Dallas, Texas. Technical advice by AR Hilton, of Amorphous Materials, Inc, and WC Herrmann Jr, of Optic Electronic Corp, was crucial for the successful completion of this study. The interest and administrative support by JA Morreal, Dark Eyes Program Manager, NOSC Code 713, made feasible the application of chalcogenide glass coatings to germanium hyperhemispherical windows for the Dark Eyes thermal imager system.

Released by
JD Stachiw, Staff Scientist,
Materials

Under authority of
IP Lemaire, Head
Ocean Technology Department

METRIC EQUIVALENTS

To convert from	to	Multiply by
mils	μm	25.4
inches (in)	mm	25.4
feet, ft/s	m, m/s	$\sim 3.05 \times 10^{-1}$
angstroms (Å)	nm	10^{-1}
degrees (°) of arc	rad	$\sim 1.75 \times 10^{-2}$
minutes of arc	rad	$\sim 2.91 \times 10^{-4}$
pounds (lb)	kg	$\sim 4.54 \times 10^{-1}$
pounds of force per square inch (psi)	Pa	$\sim 6.89 \times 10^{3}$
temperature, °F	temperature, °C	5/9 after subtracting 32
cal (thermochemical)/cm · s · °C	W/m·K	4.184×10^{2}
cal (thermochemical)/g·°C	J/kg·K	4.184×10^{3}
W/inch^2	W/m^2	$\sim 1.55 \times 10^{3}$

UNCLASSIFIED

SECURITY CLASSIFICATION OF THIS PAGE *(When Data Entered)*

REPORT DOCUMENTATION PAGE

READ INSTRUCTIONS BEFORE COMPLETING FORM

1. REPORT NUMBER: NOSC Technical Report 634 (TR 634)	2. GOVT ACCESSION NO.: AD-A119495
3. RECIPIENT'S CATALOG NUMBER:	
4. TITLE *(and Subtitle)*: HIGH-PRESSURE VIEWPORTS FOR INFRARED SYSTEMS Phase 2 - Chalcogenide glass	5. TYPE OF REPORT & PERIOD COVERED: Final October 1980 – September 1981
	6. PERFORMING ORG. REPORT NUMBER:
7. AUTHOR(s): JD Stachiw SL Bertic	8. CONTRACT OR GRANT NUMBER(s):
9. PERFORMING ORGANIZATION NAME AND ADDRESS: Naval Ocean Systems Center San Diego CA 92152	10. PROGRAM ELEMENT, PROJECT, TASK AREA & WORK UNIT NUMBERS: NOSC IR/IED Technical Project F61512
11. CONTROLLING OFFICE NAME AND ADDRESS: Naval Material Command Director of Navy Laboratories Washington DC 20360	12. REPORT DATE: 28 January 1982 13. NUMBER OF PAGES: 122
14. MONITORING AGENCY NAME & ADDRESS *(if different from Controlling Office)*:	15. SECURITY CLASS. *(of this report)*: Unclassified 15a. DECLASSIFICATION/DOWNGRADING SCHEDULE:

16. DISTRIBUTION STATEMENT *(of this Report)*

Approved for public release; distribution unlimited

17. DISTRIBUTION STATEMENT *(of the abstract entered in Block 20, if different from Report)*

18. SUPPLEMENTARY NOTES

19. KEY WORDS *(Continue on reverse side if necessary and identify by block number)*

High-pressure viewports	Thermal imagers
Marine environment	Chalcogenide glass
Infrared systems	Laser windows
Viewports	

20. ABSTRACT *(Continue on reverse side if necessary and identify by block number)*

An experimental study established the effectiveness of chalcogenide glass composition AMTIR-1 ($Ge_{33}As_{12}Se_{55}$) as structural material and/or coating material for windows in IR systems operating in a marine environment. Test results show that the optical and structural properties of the material are not degraded by continuous or intermittent submersion in seawater. A tremendous potential reduction in expenditures would result from its application wherever feasible.

DD FORM 1 JAN 73 1473 EDITION OF 1 NOV 65 IS OBSOLETE

S/N 0102-LF-014-6601

UNCLASSIFIED

SECURITY CLASSIFICATION OF THIS PAGE *(When Data Entered)*

OBJECTIVE

For the infrared imaging and/or tracking systems of undersea vehicles, develop a pressure-resistant window construction that "sees" infrared energy during surface operations and that protects their electro-optical receivers from seawater incursion while submerged. Select (1) a material that is transparent to IR energy, resistant to seawater corrosion, and structurally feasible, (2) a window shape that is resistant to pressure, (3) a mounting that holds the window securely in place without generating stress concentrations, (4) seals that provide a leakproof joint between the mounting and the window, and (5) an optical coating that both decreases the reflection of IR energy from interior and exterior surfaces and protects the exterior surface from chemical and galvanic corrosion by seawater. Optimize the structural design of the window to equalize stress distribution and minimize stress magnitudes under the high hydrostatic pressures at maximum operational submerged depths.

RESULTS

1. Spherical sector windows of massive AMTIR-1 chalcogenide glass ($Ge_{33}As_{12}Se_{55}$) set in compliant mountings were fabricated with a thickness-to-inside-radius ratio of 0.33 and an included spherical angle of 150°. The mounting consisted of Monel K-500 seats covered with composite gaskets of neoprene-impregnated nylon cloth bonded to epoxy-impregnated Kevlar cloth. The assemblies performed satisfactorily in marine environments both above and below the surface.

2. The assembly withstood, without fracturing, 500 cyclic pressurizations in the 0–2250 psi range and short-term static pressurization up to 17 000 psi. It will withstand without failure 10 000 pressure cycles to 1000 psi hydrostatic loading.

3. Typical values for short-term uniaxial compression and flexural strengths were 21 000 and 2500 psi, respectively; for long-term uniaxial compression and flexure, 15 000 and 1500 psi, respectively. Typical strength values under short-term biaxial compression and flexure were 50 000 and 1250 psi, respectively. For a fatigue life of 10 000 cycles, the cyclic biaxial compression must be limited to 2500 psi.

4. Both massive chalcogenide glass specimens and germanium specimens coated with 0.001-inch-thick chalcogenide glass showed excellent resistance to seawater corrosion.

5. The 8–11 μm transmittance of uncoated windows fabricated from chalcogenide glass composition AMTIR-1 is in excess of 65%, while that of windows coated on both sides with an antireflective (AR) composition exceeds 90%. The 10 μm transmittance of germanium windows with and without a chalcogenide glass corrosion-resistant coating is as follows:

Bare	~45%
Wet side coated with AMTIR-1	~55%
Wet side coated with AMTIR-1; dry side coated with AR composition	~75%
Wet side coated with AMTIR-1 overlaid with AR composition; dry side coated with AR composition	~90%

6. Chalcogenide glass AMTIR-1 is ideally suited for infrared system windows in marine applications such as surface ships, buoys, offshore platforms, piers, and lighthouses, where hydrostatic and hydrodynamic pressures are low. It is less ideally suited for submarine service, since this glass has low structural strength and thus by itself is applicable only in very massive applications such as submarine periscopes.

7. One useful application of chalcogenide glass in the submarine service is as a thick ($\geqslant$0.001 inch) overlay on massive germanium windows. The germanium substratum serves as the structural window member, while the chalcogenide glass overlay acts as a corrosion barrier.

8. Regardless of whether windows are fabricated from massive AMTIR-1 glass or from germanium overlaid with a thick layer of AMTIR-1, both the dry and wetted surfaces of the windows must be coated with AR compositions to insure a transmittance of 90% in the 8–11 μm wavelength range. The AR coatings lose their optical effectiveness after about 120 days of immersion in seawater; but because both massive chalcogenide glass and chalcogenide glass overlay on massive germanium chalcogenide glass are inert, the wetted surface of coated windows remains free of pits and thus can be recoated repeatedly without extensive refinishing.

RECOMMENDATIONS

1. For windows on IR systems exposed to a marine environment, consider the use of chalcogenide glass as a prime construction material or as a window coating. Either application will extend the life of such windows to at least a year, in contrast to the current 6-month maximum life of standard AR-coated germanium windows.

2. Because of the tremendous potential reduction in expenditures that would result from these applications, use chalcogenide glass wherever feasible.

CONTENTS

INTRODUCTION . . . page 5

- Atmospheric transmission . . . 6
- Thermal imagers . . . 7
- Thermal imagers in marine environment . . . 12

MATERIALS CONSIDERATIONS FOR IR WINDOWS . . . 13

- Selection criteria . . . 13
- Alkali halides . . . 17
- Crystalline semiconductors . . . 17
- Fine-grain polycrystalline materials . . . 18
- Melt-formed glass . . . 19
- Germanium . . . 20
- Alternate window materials . . . 22

CHALCOGENIDE GLASSES AS IR OPTICAL MATERIALS . . . 22

- Early studies . . . 22
- Characteristics . . . 25
- NOSC investigation . . . 28

CHALCOGENIDE GLASS FABRICATION PROCESSES . . . 28

- Primary material . . . 29
- Coating for germanium . . . 33

PREPARATION OF TEST SPECIMENS . . . 34

- Compression cylinders . . . 34
- Flexure bars . . . 36
- Flexure disks . . . 36
- Spherical sectors . . . 36
- Bearing gaskets . . . 47
- Chalcogenide-glass-coated elements . . . 50

TEST SETUP . . . 54

- Instrumentation . . . 54
- Test fixtures for structural strength tests . . . 54
- Test fixtures for corrosion-resistance tests . . . 66

TEST PROCEDURES . . . 77

- Short-term uniaxial compression . . . 77
- Short-term uniaxial flexure . . . 77
- Long-term uniaxial flexure . . . 77
- Short-term biaxial flexure . . . 77
- Short-term biaxial compression . . . 77
- Cyclic biaxial compression . . . 77
- Dynamic impulse . . . 78
- Corrosion . . . 78

TEST RESULTS – MASSIVE CHALCOGENIDE GLASS SPECIMENS . . . 78

Short-term uniaxial compressive strength . . . 78
Short-term uniaxial flexural strength . . . 78
Long-term uniaxial flexural strength . . . 82
Short-term biaxial flexural strength . . . 84
Short-term biaxial compressive strength . . . 84
Cyclic biaxial compressive strength . . . 84
Dynamic impulse resistance . . . 95
Corrosion resistance . . . 95

TEST RESULTS – CORROSION RESISTANCE OF CHALCOGENIDE-GLASS-COATED SPECIMENS . . . 97

3-inch diameter disk . . . 97
8-inch diameter disk . . . 98
10-inch diameter hyperhemisphere . . . 106

DISCUSSION OF PHYSICAL PROPERTIES . . . 106

Massive chalcogenide glass . . . 106
Chalcogenide glass coatings . . . 108

CONCLUSIONS . . . 109

RECOMMENDATIONS . . . 109

REFERENCES . . . 110

APPENDIX A: DESIGN CONSIDERATIONS . . . 113

APPENDIX B: FUTURE DEVELOPMENTS . . . 118

INTRODUCTION

The sense of vision has served humankind well in the exploration of land and sea. Electro-optical systems operating in the 0.3–0.8 μm range of wavelengths have augmented the sense of vision by allowing humans to view objects at illumination levels below the threshold of unaided vision. Such electro-optical systems also extend human senses to locations that are either inaccessible (eg, surface of remote planet), hazardous (eg, high radiation level); or too small for human occupancy (eg, interior of drone aircraft). Still, electro-optical systems are limited by some of the same environmental parameters that limit unaided human vision. Thus in total darkness, haze, or fog, both human vision and electro-optical systems operating in the visual spectrum of light are hindered.

Furthermore, even with sufficient illumination present under atmospheric conditions that allow good visibility, information provided to a viewer is limited. Human ability to discern differences in reflectivity of surfaces (ie, colors and/or shades of gray) and to differentiate between observed objects and background depends primarily on intensity of illumination and difference in reflectivity of objects and background. Unless objects are well illuminated and the reflectivity of their surfaces differs sufficiently from the background, they will probably blend with the background and escape detection.

There exist, however, approaches for detection and classification of objects at a distance that do not rely on reflection and reflectivity differences of surfaces in the visual spectrum. Ranging and detection techniques that use high-frequency radio waves (radar) and high-frequency sound waves (sonar) rely on the reflection and reflectivity differences of surfaces to radio or sound waves. These approaches are both active, since the objects to be "viewed" must be "illuminated" by either radio or sound waves of appropriate frequency. There is an approach, however, that does not require illumination for detection and classification of objects, since it processes and converts into visual images only those signals emitted by the objects. This approach relies on thermal self-emission and emissivity differences of objects to produce thermal images in the viewing system.

A thermal imaging system relies for its operation on thermal energy patterns generated by all objects whose temperature is above absolute zero. The differences in radiated thermal energy are defined for thermal imaging work in terms of effective scene temperatures rather than in radiometric terms. Effective temperatures represent the sum of contributions made by scene temperature, reflectivity, and emissivity. Thus the effective temperature at a point can be conceived as that temperature of a blackbody radiator which would produce the measured irradiance at that point. Similarly, the irradiance measure through an attenuating atmosphere can be conceived as having been produced by an apparent temperature which is less than the effective temperature of a point on the object.

The differences in effective temperatures of a thermal scene correspond in large degree to the reflectivity differences in a visual scene and thus allow the transfer of visual concepts to thermally imaged scenes. A mechanical scanning device that converts thermal radiation to visible radiation in real time for presentation on a television screen is termed forward-looking infrared (FLIR) (ref 1). This paper focuses primarily on design considerations and materials for FLIRs operating in a marine environment.

1. Naval Air Development Center Report of Action Group JAG-1, State of the Art of Airborne Forward Looking Infrared (FLIR) Technology, vol 1, edited by PM Moser, August 1976.

ATMOSPHERIC TRANSMISSION

The major applications of FLIRs to date have been in the military arena, where they have been used for target acquisition, fire control, surveillance, intelligence gathering, and navigation (ref 1). As the cost of FLIRs decreases because of mass production for the military, they will become attractive for nonmilitary uses as well. Typical nonmilitary applications include thermal pollution surveys, forest fire detection and fighting, preventive maintenance, inspection of machinery, crime prevention, aircraft navigation, aircraft landing aids, and air-sea rescue. The reason for the popularity of thermal imaging systems over passive electro-optic imaging devices operating in the visible light spectrum lies in the ability of the thermal imagers to provide superior images over a wider range of atmospheric and illumination conditions. Thus, while image intensifiers and low-light television systems require some illumination and good atmospheric visibility, thermal imagers perform equally well during day and night even under marginal atmospheric visibility conditions (eg, haze and light fog).

There are two processes that affect the passage of thermal radiation through the terrestrial atmosphere: (1) absorption and (2) scattering by gas molecules, molecular clusters, rain, snow, and suspensions such as smoke, fog, haze, and smog (ref 2, 3). The most significant absorbers are water (2.7, 3.2, and 6.3 μm in wavelength), carbon dioxide (2.7, 4.3, and 15 μm), ozone (4.8, 9.6, and 14.2 μm), nitrous oxide (4.7 and 7.8 μm), and methane (3.2 and 7.8 μm). The water and carbon dioxide absorption bands in effect limit the thermal radiation through terrestrial atmosphere to two windows in the 2–20 μm spectral range: the 3.5–5 and 8–14 μm wavelength bands (fig 1).

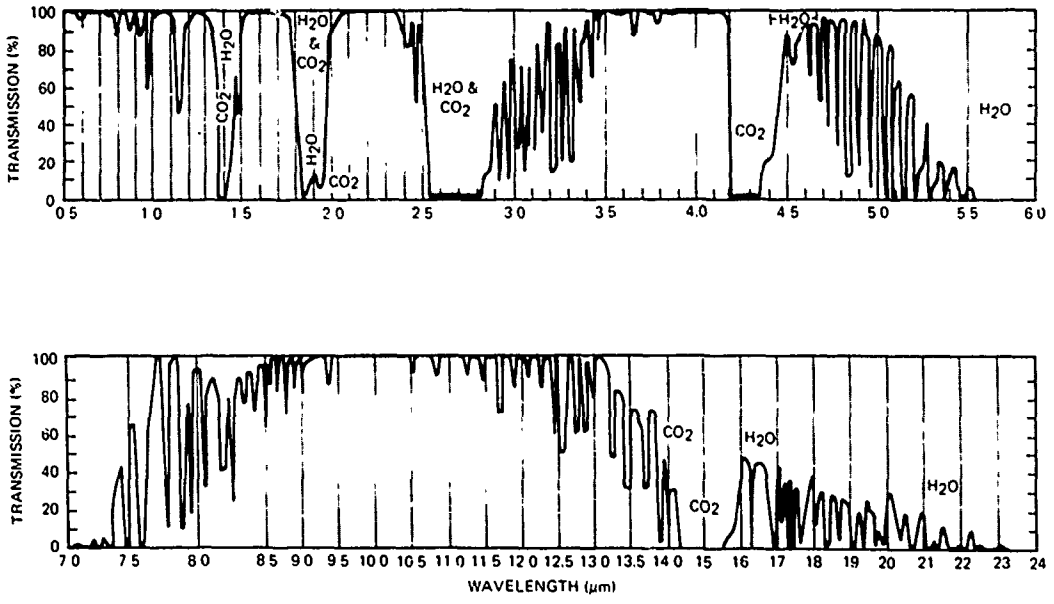

Figure 1. Atmospheric transmission of 1000-foot horizontal air path at sea level; 5.7 mm precipitable water, 79°F.

2. Lloyd, JM, Thermal Imaging System, Plenum Press, New York, London, 1975.
3. The Infrared Handbook, edited by WL Wolfe and GJ Zissis, Infrared Information and Analysis Center, Environmental Research Institute of Michigan, Ann Arbor MI, 1979.

There are several reasons why the 8–14 μm wavelength window in atmospheric transmission is preferred by FLIR designers over the lower wavelength window. Haze attenuates 8–14 μm energy less, the ratio of thermal sensitivity of a system to transmission is higher, and the peaks of radiant energy emitted by objects at ambient terrestrial temperature are centered in this band (fig 2).

THERMAL IMAGERS

Thermal imagers can be divided into many classes on the basis of the types of detectors, scene dissection procedures, scanning mechanisms, and processing of preamplified detector signals for video presentation. To date, two successful approaches have been developed for converting incoming infrared signals to visual images in thermal imaging systems (ref 3). The approach yielding the better performance relies on a mechanically scanning discrete photon detector in a technique analogous to television systems (fig 3), while the approach yielding visual images of lesser quality relies upon an electrically scanned pyroelectric vidicon (fig 4).

There is a basic distinction between scene dissection procedures, based on whether the scene is dissected serially or in parallel (fig 5). As figure 5b shows, parallel scene dissection has an array of discrete detectors oriented perpendicularly to the primary scan axis. The resulting electrical signals from each detector are individually amplified, processed, and displayed on a CRT screen simultaneously or in parallel. Serial scene dissection, on the other hand (fig 5a), has an array of detectors oriented in parallel to the primary scan axis. The array serially scans each point of the thermal image. The resulting electrical signals from each detector are, as a rule, delayed and summed by an electrical integrating delay line.

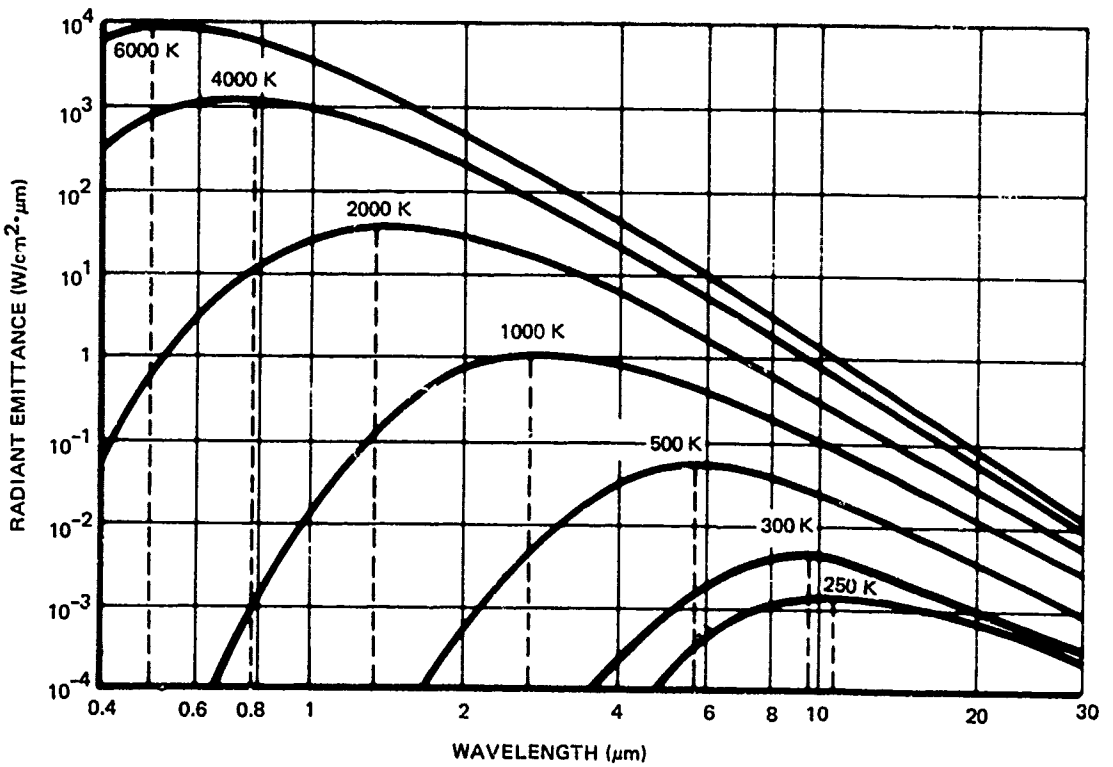

Figure 2. Blackbody spectral emittance at various temperatures.

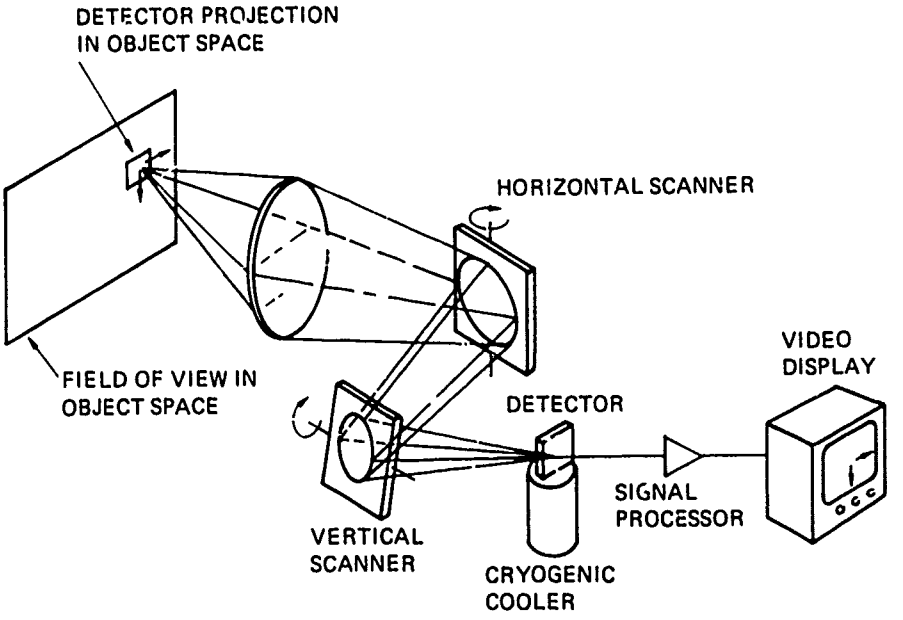

Figure 3. Basic components of a thermal imager using a single cryogenically cooled photon detector and a dual-axis mechanical scanner.

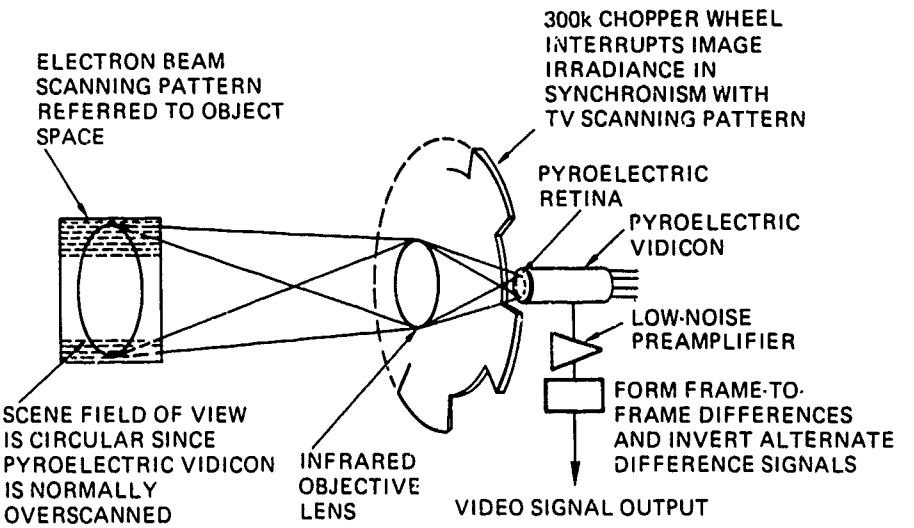

Figure 4. Basic components of a thermal imager using an electrically scanned, mechanically chopped, pyroelectric vidicon.

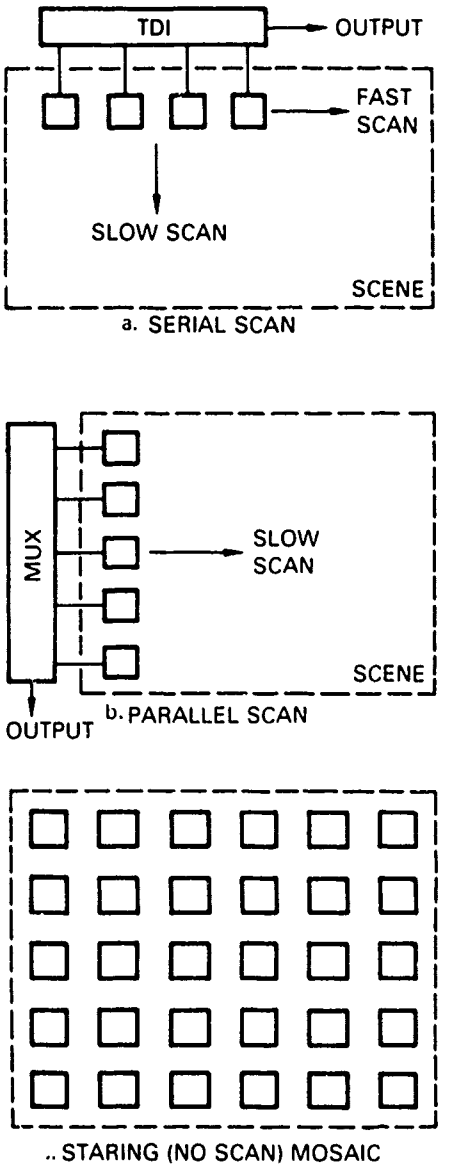

Figure 5. Techniques for dissecting the scene with arrays of discrete detectors.

Although each dissection procedure has advantages and disadvantages, serial scan is considered to be superior to parallel scan in that nonuniformities of individual detectors are eliminated by the integrating delay line, which superimposes the outputs of all detectors. Thus serial scan dissection simulates a single scanning detector. Its disadvantage is that it requires rather complex optics. The major advantage of parallel scanning is that the optics are much less complex, since in its sensor the detector and the display are scanning the same mirror. The major disadvantage of parallel scanning lies in the possibility of variations in the individually processed signals from the detectors.

The mechanical scanning mechanisms for FLIRs vary from one design to another, depending on the scene dissection procedure used, type of application, cost ceiling, space limitations, etc. The most common ones use an oscillating plane mirror, a rotating polygonal mirror, a rotating reflective carousel, a rotating refractive prism, revolving lenses, a rotating V-mirror, or other means. To scan the whole scene and generate a picture of TV quality on the picture tube, these mechanical components must rotate or oscillate at high speeds. One obvious technique for elimination of these costly and complex mechanical scanning mechanisms would be to place in the focal plane a mosaic array of detectors covering the whole field of view (fig 5c). The signals from all detectors would be individually amplified and displayed on the picture tube. This approach, in principle, promises to eliminate complex mechanisms and, as a result, to lower the cost, reduce mechanical failures, and increase optical performance. To date it has failed to achieve these objectives. Future advances in detector technology may, however, drastically revise the current position of staring (nonscanned) mosaic detector arrays.

So far, the discussion concerns only FLIRs that use discrete, solid-state photon detectors operated at cryogenic temperatures. Detectors of this type have provided military FLIRs with resolution capabilities of ≤ 0.0002 radian at $\leq 0.2^{\circ}C$. Cooling to cryogenic temperature reduces thermally generated background noise to acceptable levels so that the electrical signals generated in the detectors represent a suitable signal-to-noise ratio.

Although the optical performance of the cryogenically cooled, mechanically scanned solid-state photon detectors is excellent, a strong desire exists to eliminate the costly and failure-prone cryogenic coolers and mechanical scanners in FLIRs. This is feasible with a class of detectors having electrical characteristics (eg, resistance, magnetic orientation, potential) that change only when the impinging electromagnetic radiation in the visible and infrared spectrum induces in them a temperature change. With thermistors, thermocouples, and pyroelectric detectors it is possible to detect infrared radiation without cumbersome cryogenic cooling because these devices are capable of operating at ambient room temperatures. Furthermore, they are useful under a very wide range of atmospheric conditions since they respond to both visible and IR radiation. Unfortunately, they have two very serious disadvantages: slower response time and lower sensitivity relative to the cryogenically cooled photon detectors. Only the pyroelectric detector appears to have a response time (nanoseconds) comparable to the cryogenically cooled photon detector. Because there is considerable commercial interest in pyroelectric detectors, several thermal imaging systems have been built around them that are available for commercial applications (ref 4).

4. Levitt, RS, and T Conklin, Infrared Imaging, Heating Up, Industrial Research, July 1977.

The heart of these systems is the pyroelectric vidicon tube (PEV), which has a pyroelectric crystal material as its active target element (fig 4). When the temperature of a point on the pyroelectric target is disturbed by incident thermal radiation, the permanent microscopic dipole domain undergoes spontaneous polarization, which results in the buildup of charge on the opposite surface of the target. The electric charges on the target, which represent the electrical analog of the imaged thermal scene, are read by a scanning electron beam. The current variation in the beam as it discharges the charge pattern is the desired video signal.

The resolution and sensitivity typically achievable with the state-of-the-art pyroelectric vidicon are 0.0006 radian at $\Delta T = 0.5°C$, still short of the performance level (0.0002 radian at $\Delta T = 0.2°C$) achievable by mechanically serial-scanned, cryogenically cooled photon detectors in top-of-the-line military FLIRs. It compares rather well, however, with the optical performance of commercial FLIRs that use mechanical scanning and cryogenic cooling techniques. There are strong indications that with continued development, the resolution of pyroelectric vidicons can be improved significantly.

The discussion so far has brought out two important advantages of PEV thermal imagers: absence of the requirements for cryogenic cooling of detectors and electron-beam scanning. As a result, the PEV thermal imagers are an order of magnitude less complex and therefore less expensive. But there is one serious drawback to the PEV thermal imager: the detector responds only to changes in temperature. Thus a thermally static scene does not generate an image in it. This limitation is acceptable where a PEV thermal imager is used for an intruder surveillance system, which shows only the image of the intruder on its otherwise blank screen.

For PEV thermal imager applications wherein a thermally static scene is to be observed, the required changes in detector temperature are introduced artifically, typically either by panning the camera across the viewed scene or by mechanically chopping the camera's view of the scene. Of the two approaches, chopping at about 16 Hz results in optimum image detail with a minimum of chopper-induced flicker. The use of a rotary mechanical chopper in front of the PEV window introduces some complexity to the thermal imaging system, which otherwise has no other moving mechanical components. But because the chopper is not a part of the optical train in the PEV thermal imaging system, it contributes very little to the overall cost of the system. Contrast this to the mechanically driven optical scanner in the FLIR system with cryogenically cooled photon detectors, wherein the cost of the precision-made scanner components is the major contributor to the high cost of the FLIR.

In summary, although there are many feasible approaches to the design of thermal imagers, experience has shown that only two provide cost-effective solutions to thermal imaging requirements. Where the operational requirements call for thermal imagers with real-time maximum sensitivity and resolution capability, the expensive, serially scanned, cryogenically cooled array of photon detectors provides the best visual analog of the thermal image on the television tube. Where the requirements call for real-time thermal imagers with medium sensitivity and resolution capability, on the other hand, the inexpensive, electronically scanned pyroelectric vidicons provide a satisfactory visual analog of the thermal image on the television tube at a much lower price. The user has a clear choice between expensive thermal imagers with excellent resolution and inexpensive thermal imagers with mediocre resolution. Thus by specifying only the inexpensive, low-performance PEV thermal imagers for applications where their performance is acceptable, a major user

may save enough money to acquire at least one serially scanned, cryogenically cooled, high-performance FLIR imager for applications requiring maximum optical performance.

THERMAL IMAGERS IN MARINE ENVIRONMENT

There are many potential military and civilian applications of thermal imagers in the marine environment. Typical military applications are detection and classification of surface and airborne targets from ships, submarines, and aircraft. Because their sensitivity and resolution are optimized, the detection range of thermal imagers with cryogenically cooled, serially scanned photon detectors is essentially horizon-limited. Their classification range is several miles. The detection and classification range capabilities vary with the size and thermal intensity of the target, atmospheric conditions, diameter of the entrance aperture of the objective lens, and experience of the observer.

Besides allowing an observer to detect and classify a target in total darkness and/or haze, a thermoelectric imager provides information not available with electro-optic imagers. The observer can, for example, determine from the image on the TV monitor whether a ship's power plant is cold (ie, dead), or hot (ie, operational), whether the vessel is propelled by a fossil-burning or a nuclear power plant, and whether there are any other power plants operating on deck (ie, idling engines in aircraft, deck-mounted generators, compressors, or winches). In addition, thermal imagers can be employed in fire control of conventional weapons and in guidance of smart bombs or rockets.

Civilian applications for thermal imagers are as numerous and varied as military applications. Their performance in search and rescue at sea surpasses that of radar and visual observation from low- or high-flying aircraft because the thermal emission contrast between inflatable liferafts (with their occupants) and the surrounding sea surface is significantly higher than either the visual contrast or the contrast in radar return. Thermal imagers also allow firefighters to see the source of fire through smoke; thus they can determine the location and extent of fire on ships and offshore platforms. Because today's high-resolution imagers are bulky, their current applications in firefighting are limited to aircraft and ships that serve as firefighting control centers. As the developing PEV or photon detector technology shrinks thermal imagers in size, firefighters may have available helmet-mounted thermal imagers that will be able to provide a sense of vision in smoke-filled ship compartments.

Thermal imagers are used also as detectors of potential trouble in industrial equipment. By continuously surveying equipment prone to failure aboard an offshore platform or ship, such as pumps, electric motors and generators, and hydraulic and mechanical transmissions, incipient failure can be detected and catastrophic failure avoided. With the help of thermal imagers, it is feasible to check periodically and with great accuracy the level of fluids in bare or insulated storage tanks. Thermal imagers are excellent tools for detecting leakage of thermal and chemical pollutants into the sea, since the thermal emission of warm or oil-covered water is significantly different from that of unpolluted seawater at ambient temperature.

Thermal imagers in nonindustrial applications can serve during periods of minimum visibility for perimeter surveillance, visitor identification and control, floating debris and iceberg avoidance, and navigation among anchored or permanent platforms. Because these applications are very similar to military uses, DoD technology and operational experience

in such areas are directly transferable to industry, provided they do not compromise national security in certain critical technological areas.

The application of thermal imagers in the marine environment probably will have as great an impact on at-sea operations as radar and sonar had several decades ago. It seems incredible today that in the past, ships, submarines, offshore platforms, and aircraft operated solely on the basis of unaided vision. Several decades from now, operation without the aid of thermal imagers will seem equally incredible. It is hoped that in some small measure this report will aid prospective users and designers in selecting thermal imager housing design and construction materials appropriate to the intended service in the marine environment.

MATERIALS CONSIDERATIONS FOR IR WINDOWS

SELECTION CRITERIA

Selection of window material is of primary concern to the designer of an IR imaging system for the marine environment. The selection must be based on an evaluation of optical, mechanical, and chemical characteristics. Because the imaging system is primarily an optical system, the window must satisfy optical lens criteria such as transmissivity to the proper wavelengths of IR emissions, suitable index of refraction, and stability of optical properties with variations in temperature. And from a mechanical standpoint, the window must protect the fragile and sensitive imager components from a hostile external environment. Thus it must possess acceptable mechanical strength, hardness, scratch and fracture resistance, and thermal shock resistance. Finally it must be insoluble in seawater and resistant to corrosion.

The principal selection criterion must be the ability to transmit IR radiation with a minimum of absorption. Figure 6 illustrates the transmission regions for a variety of IR window materials (ref 3). As mentioned earlier, transmission in the 8–12 μm wavelength range is the most desirable for marine applications because the peaks of ambient energy emitted by objects at ambient terrestrial temperatures are centered in this band (fig 2). Another desirable optical characteristic is a high refractive index that changes with neither temperature nor wavelength. A high refractive index is necessary to minimize lens curvature and thickness. A low thermal coefficient for refractive index prevents abberation unbalancing and changes in focal length as the temperature changes. Refractive insensitivity to wavelength (ie, dispersion approaching zero) minimizes chromatic abberation.

Several mechanical and chemical properties directly affect the optical performance of an IR window. The lower the coefficient of thermal expansion, the smaller the change in window shape and dimensions with a change in temperature, thus minimizing aberration unbalancing and changes in the focal length as well as the mechanical stresses generated in the window by differences in thermal expansion between the window and its metallic mounting. The material surface must be compatible with antireflective coatings (ie, have good adherence) so that surface reflection losses can be minimized. The window material should also have high surface hardness and scratch resistance to prevent degradation of the lens surface. Insolubility in seawater and a high resistance to corrosion are important for preventing optical and mechanical degradation in marine environments.

The structural integrity of the housing that contains the thermal imaging system depends on the structural integrity of the window. Pressure resistant windows are found in

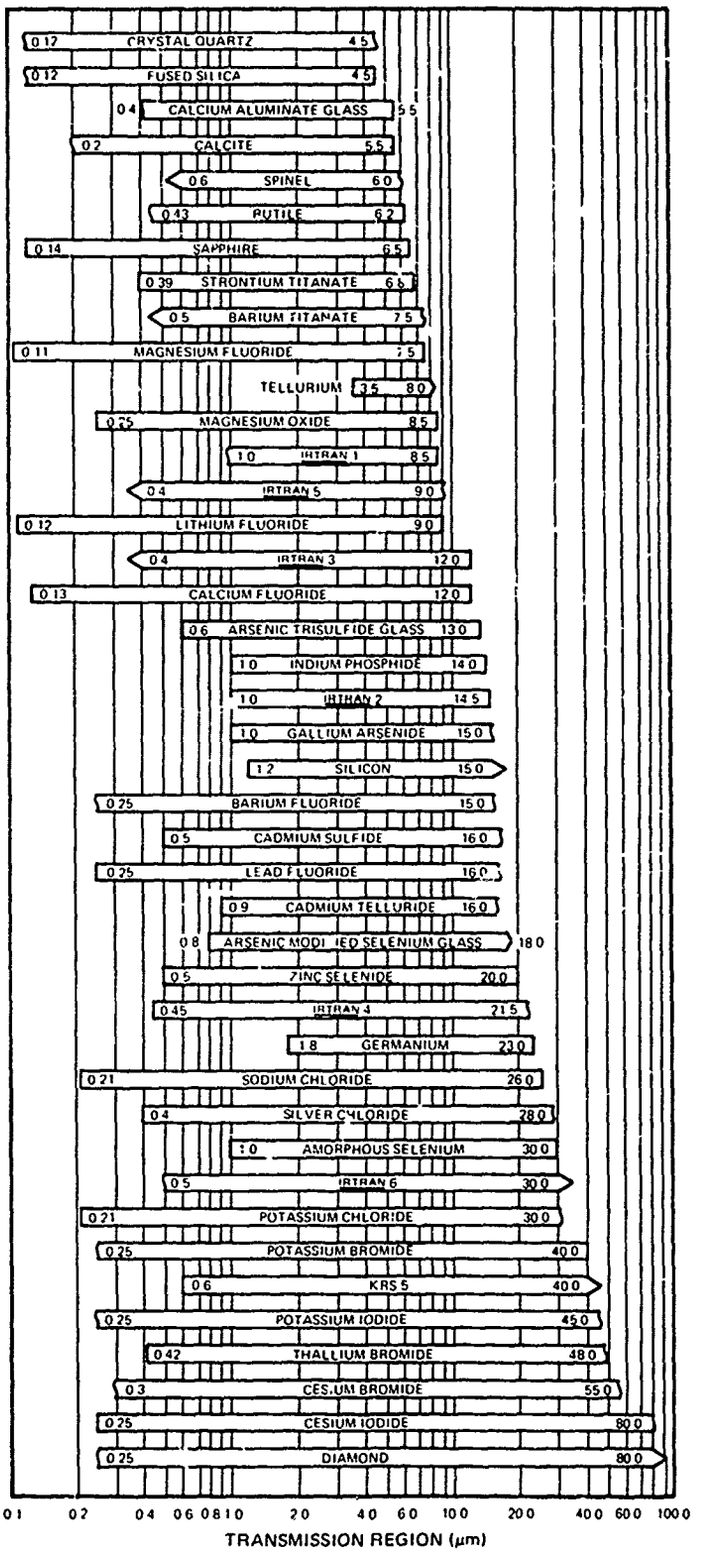

Figure 6. Transmission regions of optical materials, 2 mm thick.

six standard shapes (fig 7). All must have high mechanical strength to resist the extreme hydrostatic pressures to which they are exposed at maximum operating depths. High mechanical strength also allows them to be relatively thin and therefore more transmissive to infrared radiation. Corrosion resistance is important both in preventing optical degradation of the external surface and in maintaining the sealing of the internal components from seawater. Scratch resistance is important; most IR materials are quite brittle and notch-sensitive, and a surface scratch can reduce tensile strength by as much as 75%. Finally, the window must be capable of withstanding thermal shocks such as occur on submersion in cold seawater after prolonged exposure to elevated air temperatures, without fracturing or incipient cracking.

Although many materials meet a few of these requirements, no ideal material – ie, one that satisfies all of the criteria – has been found. The infrared optical materials may be compared in a general way by grouping them as follows:

Ionic solids – alkali halides

Crystalline semiconductors – melt formed

Crystalline semiconductors – II-VI fine grain

Amorphous solids – chalcogenide glasses

For a particular application, the suitability of a material is judged by comparing values of various pertinent physical properties among families of materials or between individual members of a group. The pertinent properties and their relation to optical applications are as follows.

Transmission range. The region in wavelength in which the bulk absorption is low enough that the desired energy is readily transmitted without appreciable loss. Broad transmission is desirable.

Refractive index at 10 μm. We desire to use the material in the 8–12 μm atmospheric window. The wavelength of 10 μm is chosen as a comparative point because it is in the middle of the band. Since the thickness and curvature of the lens are inverse functions of the refractive index, a high refractive index is desirable.

Thermal change in refractive index. All systems are subject to temperature changes. If the refractive index changes appreciably with temperature, the focal distance of the lens may vary with temperature. Therefore low values are desirable.

Upper use temperature. Generally, the upper use temperatures are adequate for most applications. However, use as a supersonic window subject to airstream heating would require that the properties exhibit little variation with temperature. High use temperatures are desirable.

Thermal expansion coefficient. This magnitude is a broad indication of the physical properties of a material. Large values indicate soft, weak, fragile solids that are subject to heat shock. Small values indicate materials that are more physically stable under heat stress.

Surface hardness. A high value is desirable from the standpoint of optical finish. Soft materials are not easily polishable.

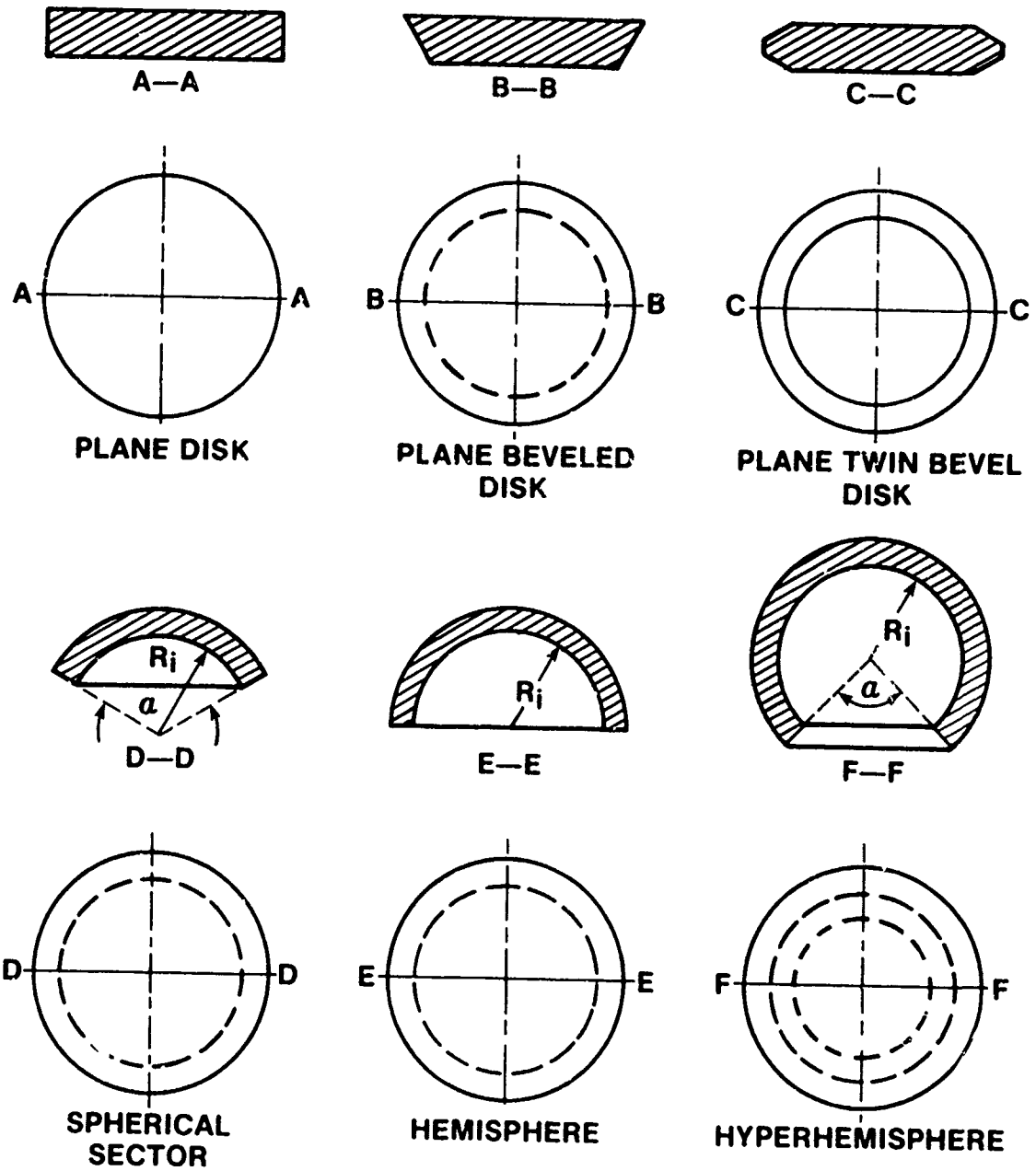

Figure 7. Standard shapes for pressure-resistant windows.

Young's modulus. An indication of the strength of the chemical bonds between the constituent elements. Large values are desirable. The true indicator of the real or practical strength of a material is its rupture modulus, a measured value that is not generally available in the published literature.

Size. Some applications require sizes that may be unattainable for a particular material.

ALKALI HALIDES

The physical properties of the alkali halides useful in the 8–12 μm range are quantified in table 1. These ionic solids show broad transmission range, low refractive indexes that do not change much with temperature, relatively high melting points, and large volume expansion coefficients. They are very soft and weak even in fine-grain structure but can be made in large sizes at relatively low cost. A pronounced disadvantage is that they all readily dissolve in water. Efforts to seal and protect their surfaces with evaporated coatings have been moderately successful. Perhaps the best source for these materials is Harshaw Chemical Company, Solon, OH.

Material	Transmission Range (μm)	Refractive Index (n) at 10 μm	Thermal Change in n	Upper Use Temp (°C)	Thermal Exp Coefficient	Surface Hardness (Knoop)	Young's Modulus (psi)	Size (inches)
NaCl	0.2-15	1.52	-25×10^{-6}/°C	800	44×10^{-6}/°C	15	6×10^{6}	24
KCl	0.4-21	1.47	-27×10^{-6}/°C	776	36×10^{-6}/°C	7	4×10^{6}	24
KBr	0.2-27	1.54	-40×10^{-6}/°C	730	43×10^{-6}/°C	6	4×10^{6}	24
CsBr	0.2-40	1.67	-79×10^{-6}/°C	636	48×10^{-6}/°C	20	2×10^{6}	8
CsI	0.2-50	1.74	-85×10^{-6}/°C	621	50×10^{-6}/°C	–	8×10^{6}	5
KI	0.3-31	1.63	-50×10^{-6}/°C	723	43×10^{-6}/°C	–	5×10^{6}	8
Summary	Broad	Low	Small	High	Large	Soft	Moderate	Large

Table 1. Alkali halides 8–12 μm applications.

CRYSTALLINE SEMICONDUCTORS

Table 2 quantifies the properties of crystalline semiconductors. The distinction refers to melt-formed materials grown either in large-grain or single-crystal form. The materials listed are silicon (used mainly for 3–5 μm applications), germanium (the most widely used 8–12 μm material), gallium arsenide, and cadmium telluride. Neither of the last two has had significant use. These materials all have broad transmission ranges and high refractive indexes. The very high thermal change in refractive indexes (especially for germanium) creates thermal defocusing problems. The low upper use temperatures for silicon and germanium are due to their low band gaps. The semiconductors are by far the hardest, strongest solids. With the exception of cadmium telluride, all are available in large pieces or plates up to 24 inches in diameter. Single-crystal sizes are much smaller and in some cases not as strong as the polycrystalline variety. The best sources of germanium in this country are Eagle-Picher (Quapah, OK) and Exotic Materials (Costa Mesa, CA).

Material	Transmission Range (μm)	Refractive Index (n) at 10 μm	Thermal Change in n	Upper Use Temp (°C)	Thermal Exp Coefficient	Surface Hardness (Knoop)	Young's Modulus (psi)	Size (inches)
Si	1.2-15	3.42	$+186 \times 10^{-6}$/°C	200	4×10^{-6}/°C	1150	19×10^{6}	12
Ge	2-23	4.00	$+427 \times 10^{-6}$/°C	100	6×10^{-6}/°C	700	15×10^{6}	24
GaAs	0.9-18	3.34	$+207 \times 10^{-6}$/°C	500	6×10^{-6}/°C	750	12×10^{6}	18
CdTe	0.9-30	2.67	$+100 \times 10^{-6}$/°C	500	6×10^{-6}/°C	45	3×10^{6}	6
Summary	Broad	High	High	Depends upon band gap	Low	High	Strong	Small for pulled single crystals

Table 2. Crystalline semiconductors.

FINE-GRAIN POLYCRYSTALLINE MATERIALS

The properties of fine-grain polycrystalline materials are quantified in table 3. Materials that have been useful in the 8-12 μm region are all II-VI compounds, ie prepared from elements of group II and group VI. Two general methods of preparation have been used. In the first, fine-grain powder of the pure material is hot pressed into disks. Such materials are named IRTRANS and are made by Eastman Kodak. The second method, developed by Raytheon, uses chemical vapor deposition (CVD) methods on inert graphite substrates. The most prominent 8-12 μm material is zinc selenide.

The table shows that these materials have moderate transmission ranges, moderate refractive indexes with small thermal changes, high upper use temperatures, and small thermal expansion coefficients. The properties of small expansion coefficient and good physical strength (due to their fine-grain structure) permit these materials to be used for high-temperature applications. Large sizes are available. But their relative softness is a problem that hampers polishing.

Material	Transmission Range (μm)	Refractive Index (n) at 10 μm	Thermal Change in n	Upper Use Temp (°C)	Thermal Exp Coefficient	Surface Hardness (Knoop)	Young's Modulus (psi)	Size (inches)
ZnSe	0.5-20	2.40	52×10^{-6}/°C	500	8.5×10^{-6}/°C	100	10×10^{6}	25
ZnSSe	0.6-15	2.38	–	500	8.3×10^{-6}/°C	190	9×10^{6}	25
ZnS	0.6-12	2.20	46×10^{-6}/°C	500	7.9×10^{-6}/°C	200	11×10^{6}	25
CdS	1.0-14	2.27	–	300	3.0×10^{-6}/°C	102	7.5×10^{6}	12
Summary	Moderate	Moderate	Small	High	Small	Soft	Moderate	Large

Table 3. Polycrystalline II-VI compounds.

MELT-FORMED GLASS

The properties of the melt-formed glasses are quantified in table 4. Only glasses that have been made in commercial quantities are listed. Glasses useful in the 8–12 μm range have broad transmission range and moderate refractive indexes with small changes in value with temperature. Upper use temperatures are low, limited by the relatively low glass transition temperatures of the materials. The glasses have large expansion coefficients and are soft and relatively weak, especially when placed in tension. (In compression they are strong.) Glasses can be cast in almost unlimited sizes and shapes, whereas crystalline materials are limited in that respect. Furthermore, glasses are much more chemically inert than crystalline materials. Previous suppliers have been Eastman Kodak and Servo Corporation, while in more recent years Texas Instruments and Amorphous Materials have become the two major sources in the US. The last two glasses listed in table 4 are the compositions produced at Texas Instruments ($Ge_{28}Sb_{12}Se_{60}$, TI 1173) and the composition produced at Amorphous Materials ($Ge_{33}As_{12}Se_{55}$, AMTIR-1). Both materials are currently specified in the packages for US Army common modules.

Material	Transmission Range (μm)	Refractive Index (n) at 10 μm	Thermal Change in n	Upper Use Temp ($^{\circ}$C)	Thermal Exp Coefficient	Surface Hardness (Knoop)	Young's Modulus (psi)	Size (inches)
As_2S_3	1.0–11	2.41	$-10 \times 10^{-6}/^{\circ}C$	210	$25 \times 10^{-6}/^{\circ}C$	109	2×10^{6}	Cast
$As_{10}Se_{90}$	1.0–19	2.48	–	70	$34 \times 10^{-6}/^{\circ}C$	–	–	Bulk
$As_{39}Se_{61}$	1.0–15	2.79	–	202	$19 \times 10^{-6}/^{\circ}C$	114	3×10^{6}	Cast
$Ge_{28}Sb_{12}Se_{60}$	1.0–14	2.62	$+90 \times 10^{-6}/^{\circ}C$	200	$15 \times 10^{-6}/^{\circ}C$	150	3×10^{6}	Cast
$Ge_{33}As_{12}Se_{55}$	0.8–16	2.49	$+71 \times 10^{-6}/^{\circ}C$	300	$13 \times 10^{-6}/^{\circ}C$	171	3×10^{6}	Cast
Summary	Broad	Moderate	Small	Low	Large	Soft	Weak	Very Large

Table 4. Chalcogenide glasses.

Because marine applications require high structural strength and corrosion resistance above all, the two principal materials that have been considered for the 8–14 μm wavelength atmospheric window are polycrystalline germanium and the amorphous chalcogenide glasses. Others with desirable structural properties, for example ZnS, will be considered in the future. The optical and mechanical properties of germanium and the chalcogenide glass AMTIR-1 (germanium-arsenic-selenium glass) (ref 5) are compared in table 5. The principal structural differences involve the presence of crystalline structure in germanium, whereas the chalcogenide glasses are supercooled liquids in structure, have no inner surface structure, and are therefore termed amorphous.

5. Hilton, A, Infrared Transmitting Glasses as Optical Materials in Passive Systems, Society of Photo-Optical Instrumentation Engineers, Proceedings, vol 131, 1978.

Property	Germanium	AMTIR-1
Composition	Ge	$Ge_{33}As_{12}Se_{55}$
Transmission range (μm)	2-18	1-15
Refractive index (n) at 10μm	4.0025	2.4976
Thermal change in n	400×10^{-6}/°C	72×10^{-6}/°C
Hardness (Knoop)	850	170
Thermal expansion coefficient	6×10^{-6}/°C	12×10^{-6}/°C
Thermal conductivity (cal/cm • s • °C)	1.4×10^{-2}	5.5×10^{-4}
Specific heat (cal/g • °C)	7.4×10^{-2}	7.2×10^{-2}
Density (g/cm^3)	5.33	4.40
Modulus of rupture, annealed (psi)	8000	2500
Glass transition temperature, T_g (°C)	937 (MP)	405
Upper use temperature (°C)	200	310
Dispersion		
3-5 μm	102	194
8-12 μm	970	115
Reflectivity (%)	36	18.3
Transmission maximum, uncoated (%)	53	69
Absorption at 10.6 μm, per cm	0.02	0.01
Poisson's ratio	0.25	0.27
Compressive strength (psi)	30 000	30 000
Modulus of elasticity (psi)	1.49×10^7	0.319×10^7

Table 5. Comparison of physical and optical properties of optical grade germanium and chalcogenide glass.

GERMANIUM

Germanium has long been the material of choice for windows in IR systems because of its superior optical and mechanical properties. It has the highest flexural, tensile, and compressive strength of all the materials transparent to IR signals in both the 3.5-5 and 8-14 μm ranges and a price within reach. With respect to mechanical properties, germanium is stronger, harder, more thermally conductive, and hence more resistant to fracture than the glasses.

Most IR windows currently in use in air, marine, and terrestrial environments are made of germanium. Manufacturers have had nearly 20 years of experience in fabricating germanium lenses and windows for thermal imaging systems. Because of this broad manufacturing technology base, optical-grade germanium is readily available in virtually any size and shape at a lower price than that of many of the other IR materials.

The transmission properties of germanium are favorable for the 3-5 μm and 8-14 μm windows commonly employed by IR systems in the marine environment (fig 8).

But there is a major drawback in using germanium in a marine environment: seawater attacks it, quickly etching the highly polished surface of optical elements and degrading both its optical and structural properties. It also causes fine cracks at germanium window edges, causing further significant weakening.

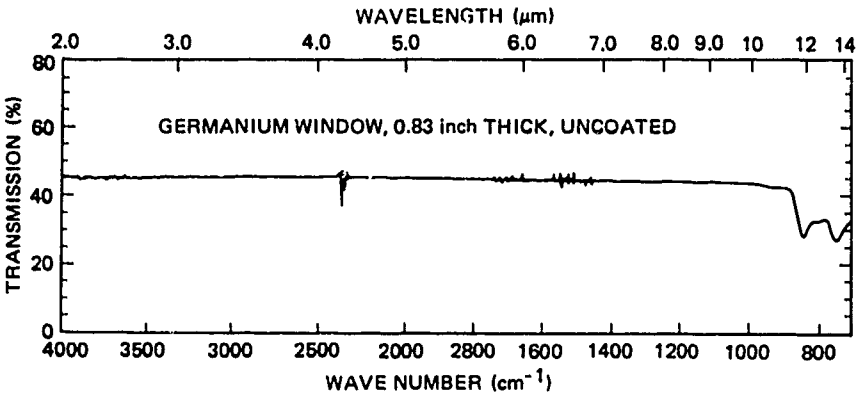

Figure 8. Transmittance of a 0.83-inch thick uncoated germanium disk with polished surfaces.

The primary approach to preventing the corrosion of germanium windows by seawater is through application of a seawater-resistant surface coating. Normally, germanium must have an antireflective coating if it is to be used as a window. Otherwise its transmission of incident thermal radiation is only in the 40–50% range. The antireflection coating can also serve to provide the germanium substrate with protection from seawater corrosion. The degree of protection depends upon three fundamental factors: the composition of the antireflection coating, the method of applying it to the substrate, and the number of layers applied to form the coating. Testing conducted at NOSC from 1978 to 1981 showed that antireflection coatings last from 1 to 6 months in seawater, depending on these parameters (ref 6).

Multilayer carbon-based coatings were as a class the most promising antireflection coatings tested, for several reasons. Carbon is impervious to seawater and hence is corrosion resistant. Carbon coatings have extreme scratch resistance because of their diamond-like hardness. A scratch resistant coating is very desirable, since scratches in coatings can lead to seawater intrusion and localized corrosion. Because the carbon coatings tested were very thick, they had few pinholes. (Pinholes occur during the coating process.) The preference of multilayer coatings over single-layer coatings is due to the elimination of pinholes by the multilayer coating process. Pinholes are thought to be a result of a dendritic coating structure, localized dust particles on the substrate, and/or the presence of minute surface discontinuities on the substrate. These complications prevent the coating from being applied evenly, and pinholes result.

Although each layer of a multilayer coating may contain pinholes, the pinholes tend to be covered when the coating material is applied in several layers. Since superimposed pinholes in consecutive layers are very rare, the pinhole problem is significantly reduced in multilayer coatings. There are drawbacks, however, to even the best available carbon-based coatings for germanium. Studies conducted at NOSC show that carbon-based coatings deteriorate during exposure to seawater for extended periods. Carbon-coated germanium test specimens decreased 5–20% in transmission after about 4 months of seawater exposure, although no corrosion was visible.

6. NOSC TR 633, Resistance of Coated and Uncoated IR Windows to Seawater Corrosion, Phase V – Summary, by JD Stachiw and SL Bertic, 1 February 1981.

From the study conducted, it was estimated that the life span for a germanium window with the best available carbon-based coating is about 6 months. Since the carbon-based coating gave the best results of all the coatings tested, it is reasonable to assume that the typical life span for germanium with other types of multilayer antireflection coatings would be no greater. In fleet applications, 6 months is not an unreasonably long period for a germanium window to be immersed in seawater.

A 6-month estimated life span would imply that at least once or twice a year windows and IR systems on submarines and surface ships would have to be removed and replaced. In terms of the cost of the replaced windows, the cost of the labor needed to replace them, and the fact that an IR system is out of commission while this work is being done, window replacement every 6 to 12 months constitutes a major expenditure. Although a window may be purchased for about $10 000, the cost of the replacement work often exeeds the cost of the window. In fact, the total cost of window replacement is easily a factor of four to five times the cost of the window alone, when installation and reactivation are included. Since there are many IR systems in service in the fleet, the combination of high costs and high replacement frequency for this type of window is unacceptable.

ALTERNATE WINDOW MATERIALS

It would be desirable to locate a new window material and/or a coating material with a life span preferably in excess of 1 year. Over the projected 10- to 20-year life span of an IR system, the high cost of window replacement for all the systems in the fleet would be considerably reduced. Annual dollar savings could run into the many millions.

There are many new window materials that are transparent to 3–5 or 8–14 μm IR radiation and that are resistant to seawater corrosion. Among those of interest are diamond, zinc sulfide, and chalcogenide glasses. Diamond and some other materials are cost prohibitive. Others are more or less desirable for reasons such as the degree of difficulty in fabrication, intrinsic costs, structural properties, and the extent of their transmittance in the 3.5–5 and 8–14 μm wavelength atmospheric windows. Chalcogenide glasses were selected for further investigation because they exhibit many of the optical and mechanical properties desirable in windows for the marine environment. This report is a summary of NOSC exploratory investigations into the applicability of chalcogenide glasses to IR windows for marine service. The study was limited in scope to AMTIR-1 chalcogenide glass, since this particular composition was readily available in large sizes and diverse shapes (fig 9).

CHALCOGENIDE GLASSES AS IR OPTICAL MATERIALS

EARLY STUDIES

The use of chalcogenide glasses as infrared optical materials began over 20 years ago with the rediscovery of As_2S_3 glass by Frerichs (ref 7, 8) and Fraser and Jerger (ref 9). The

7. Frerichs, R, paper on the new As_2S_3 glasses, Physical Review, vol 76, p 643, 1950.
8. Frerichs, R, New Optical Glasses with Good Transparency in the Infrared, Journal of the Optical Society of America, vol 43, p 1153, December 1953.
9. Fraser, WA, and J Jerger Jr, paper 57, Arsenic Trisulfide: A New Infrared Transmitting Glass, reported in Journal of the Optical Society of America, vol 43, p 332, April 1953.

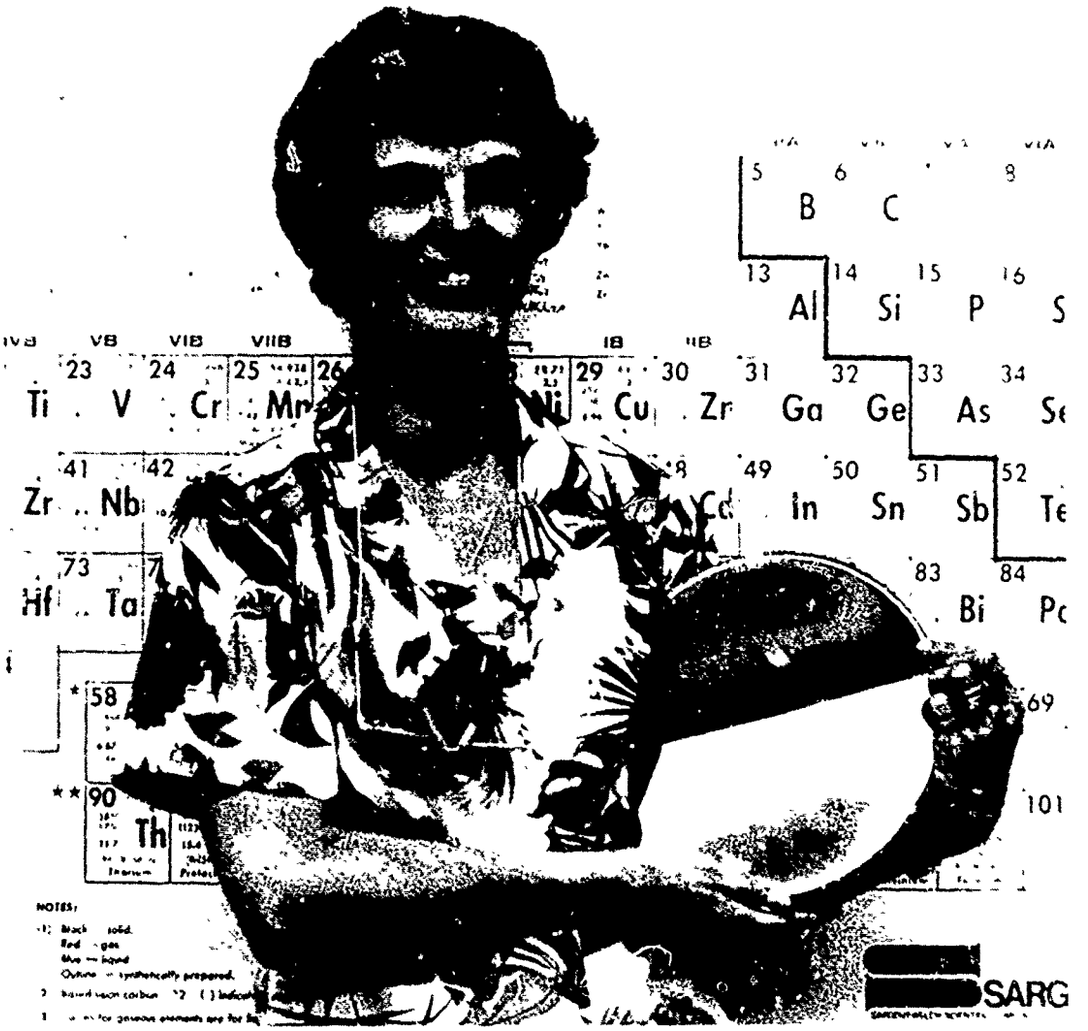

Figure 9. A large sample of massive AMTIR-1 chalcogenide glass cast by Amorphous Materials, Inc, Garland, Texas.

work was continued by Jerger and Billian (ref 10) at Servo Corporation, where glasses were produced for use in infrared systems. Work leading to the development of IR transmitting glasses for 8–12 μm systems began at Texas Instruments in 1961 with the exploratory work of Hilton, Brau and Jones (ref 11–13). The Ge-Sb-Se system from which TI 1173 was

10. Billian, CJ, and J Jerger, Servo Corp of America Contract NONR 3447 (00), 1943, Contract NONR 4212 (00), 1964.
11. Hilton, AR, and M Brau, New High Temperature Infrared Transmitting Glasses, Infrared Physics, vol 3, p 69, July 1963.
12. Hilton, AR, CE Jones, and M Brau, New High Temperature Infrared Transmitting Glasses–II, Infrared Physics, vol 4, p 213, December 1964.
13. Hilton, AR, CE Jones, and M Brau, New High Temperature Infrared Transmitting Glasses–III, Infrared Physics, vol 6, p 183, 1966.

developed was first reported by Patterson (ref 14) prior to the beginning of a glass development program funded by the Air Force (ref 15). References to the Ge-As-Se glass system occur in work at Servo Corporation reported by Jerger (ref 10), work at the Royal Radar Establishment (England) reported by Nielsen and Savage (ref 16), and work reported in Soviet literature (ref 17). The Ge-As-Se system references (10, 16, and 17) predate the decision made at Texas Instruments during the Air Force funded program to develop Ge-As-Se glasses. Neither Texas Instruments nor any other company has a proprietary position relative to glasses containing the elements Ge-As-Se.

The advent of mercury-cadmium telluride detectors in FLIR systems led to the technique of pairing a second infrared optical material with germanium for color correction. The most extensively used second material has been the infrared transmitting glass, TI 1173 (ref 18), which is specified by drawings as the second material in the US Army production systems TOW Night Sight and Tank Thermal Sight (TTS). Since current access to TI 1173 is very limited for other manufacturers of infrared systems for the US Army, a second source of infrared glass was needed.

Amorphous Materials, Inc, of Garland, Texas, was founded in May 1977, with the purpose of serving as the second source for infrared transmitting glass. AR Hilton, the founder of the company, had served for many years as the resident expert for infrared optical materials at Texas Instruments and had managed the TI 1173 production facility. Efforts by Amorphous Materials to obtain a license from Texas Instruments to produce TI 1173 proved fruitless. The decision was made to develop the technology to produce Ge-As-Se glass of the same composition as that developed on Air Force funding at TI. The name given to the composition was AMTIR-1, where AMTIR is an acronym for amorphous materials transmitting infrared.

A comparison of the detailed physical properties of AMTIR-1 with those of TI 1173 (table 6) reveals that the Ge-As-Se glass actually is a better material – harder, stronger, and less susceptible to heat shock. Optically, the two glasses are about the same. Design studies carried out at Martin Marietta indicated that AMTIR-1 may be substituted for TI 1173 in the TOW Night Sight with no measurable difference in performance provided the radii of curvature for the glass elements are slightly changed.* Substitution could then be made with no change in element spacing, lens mount, or appearance of the elements. Evaluation of common module lenses fabricated from AMTIR-1 led the US Army to amend its data packages to allow direct substitution of AMTIR-1 lens elements for TI 1173. Amorphous Materials, Inc, was designated as a second source for infrared glass in the fall of 1978 and received its first production contract order from Kollsman Instruments in March 1979.

*From a private communication with B Coon, Optic Electronic Corp (formerly with Martin Marietta Corp).

14. Paterson, RJ, and M Brau, 129th Meeting of the Electrochemical Society, May 1966.
15. Jones, C and H Hafner, Contract AF33 (615) 3963, October 1963.
16. Savage, JA, and S Nielsen, Preparation of Glasses Transmitting in the Infra-red Between 8 and 15 Microns, Physical Chemistry of Glasses, vol 5, no 3, p 82, June 1964.
17. Myuller, RL, LA Bardokow, and ZV Borisova, Journal of the University of Leningrad, vol 10, p 94, 1962.
18. Hilton, AR, JJ Hayes, and MD Rechtin, Chalcogenide Glasses for High Energy Applications, Texas Instruments Inc Contract N00014-73-C-0367, Technical Report 1, January 1974.

Property	AMTIR-1	TI 1173
Composition	$Ge_{33}As_{12}Se_{55}$	$Ge_{28}Sb_{12}Se_{60}$
Transmission range (μm)	0.9-16	1.0-16
Refractive index (n) at 10 μm	2.4975	2.6036
Thermal change in n	72×10^{-6}/°C	91×10^{-6}/°C
Hardness (Knoop)	170	150
Thermal expansion coefficient	12×10^{-6}/°C	14×10^{-6}/°C
Thermal conductivity (cal/cm · s · °C)	5.5×10^{-4}	5.0×10^{-4}
Specific heat (cal/g · °C)	7.2×10^{-2}	6.6×10^{-2}
Density (g/cm^3)	4.40	4.67
Modulus of rupture (psi)		
Anealed	2500	2500
Tempered	7000	7000
Young's modulus (psi)	3.2×10^6	3.1×10^6
Shear modulus (psi)	1.3×10^6	1.2×10^6
Poisson's ratio	0.26	0.26
Glass transition temp, T_g (°C)	405	295
Upper use temperature (°C)	310	200
Dispersion		
3-5 μm	194	174
8-12 μm	115	110
Reflectivity (%)	18.3	19.8
Transmission max (uncoated) (%)	69	67
Absorption at 10.6 μm, per cm	0.01	0.01

Table 6. Comparison of AMTIR-1 and TI 1173.

CHARACTERISTICS

The salient feature of the chalcogenide family is that the members are amorphous glasses rather than crystalline. In amorphous materials the molecules do not align in the lattice formations characteristic of crystals. As a result there are no intercrystalline boundaries or planes of cleavage that can be attacked by seawater and etched. For this reason glasses normally resist seawater attack better than crystalline materials (ref 19).

Chalcogenide glass material is optimal for infrared systems in a marine environment both because it resists seawater corrosion and because of its superior transmissive properties over the full spectrum of infrared wavelengths. Furthermore its constituent elements can

19. NOSC TR 421, Resistance of Coated and Uncoated IR Windows to Seawater Corrosion, JD Stachiw and SL Bertic, 1979.

be tailored to produce specific optical properties (eg certain color corrections) or structural properties.

AMTIR-1, the chalcogenide glass selected for this investigation by NOSC [illegible] ical in composition to Texas Instruments' TI-20. This particular glass was selected [illegible] cause it was developed with government funding and therefore is not covered by proprietary restrictions imposed by Texas Instruments on some of the other chalcogenide glasses. Also, earlier data pertaining to chalcogenide glass of this composition indicated that a study of the material would be rewarding.

AMTIR-1 material has several desirable aspects. Its transmissive response is flat across the electromagnetic spectrum from the near infrared (about 1 μm) to the very far infrared (about 15 μm). Its transmission rises rapidly at a wavelength of about 0.8 μm and remains constant in the 50–70% transmission range through 15^{+} μm (fig 10). It is therefore useful for all current IR applications, ie the near infrared, 3–5 μm, and 8–14 μm windows. Moreover, its high transmissivity (as a result of its low index of refraction) is characteristic of the material in its uncoated state, whereas germanium must be coated with an AR substance.

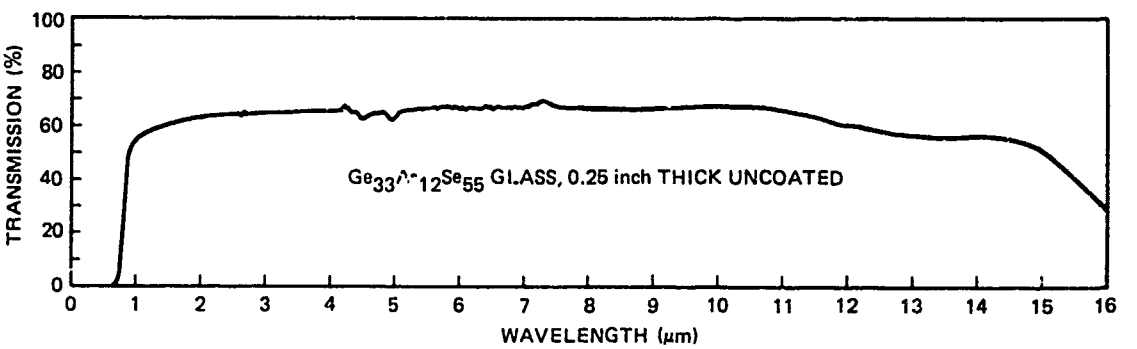

Figure 10. The transmittance of a polished, uncoated, 0.25-inch thick chalcogenide glass AMTIR-1 composition specimen.

Chalcogenide glass has a further advantage in that its transmission properties are not affected by normal ranges of atmospheric temperature. Whereas AMTIR-1 can be used at elevated temperatures, germanium's transmission is a function of temperature and degrades significantly at temperatures above 30–40°C.

A valuable asset of AMTIR-1 is that because the material is transparent in part of the visible spectrum as well as in the infrared spectrum, visual inspection techniques may be used for material fabrication and quality control. Ordinary optical techniques may be used to check both optical and structural quality, eg to detect defects such as striae in the glass, inclusions, cracks, and uneven index of refraction due to improper composition. Visible light at about 0.8 μm and appropriate optical instruments may be used to examine glass blanks prior to final grinding.

Visual inspection is considerably less expensive than contemporary methods of quality inspection by infrared light. IR inspection of germanium, a complicated and expensive procedure, would require an IR energy source and an accompanying optical system that would collimate the IR rays and project them on detectors of some type (fig 11). The inspector would then use visual senses to interpret the date from the detectors. This

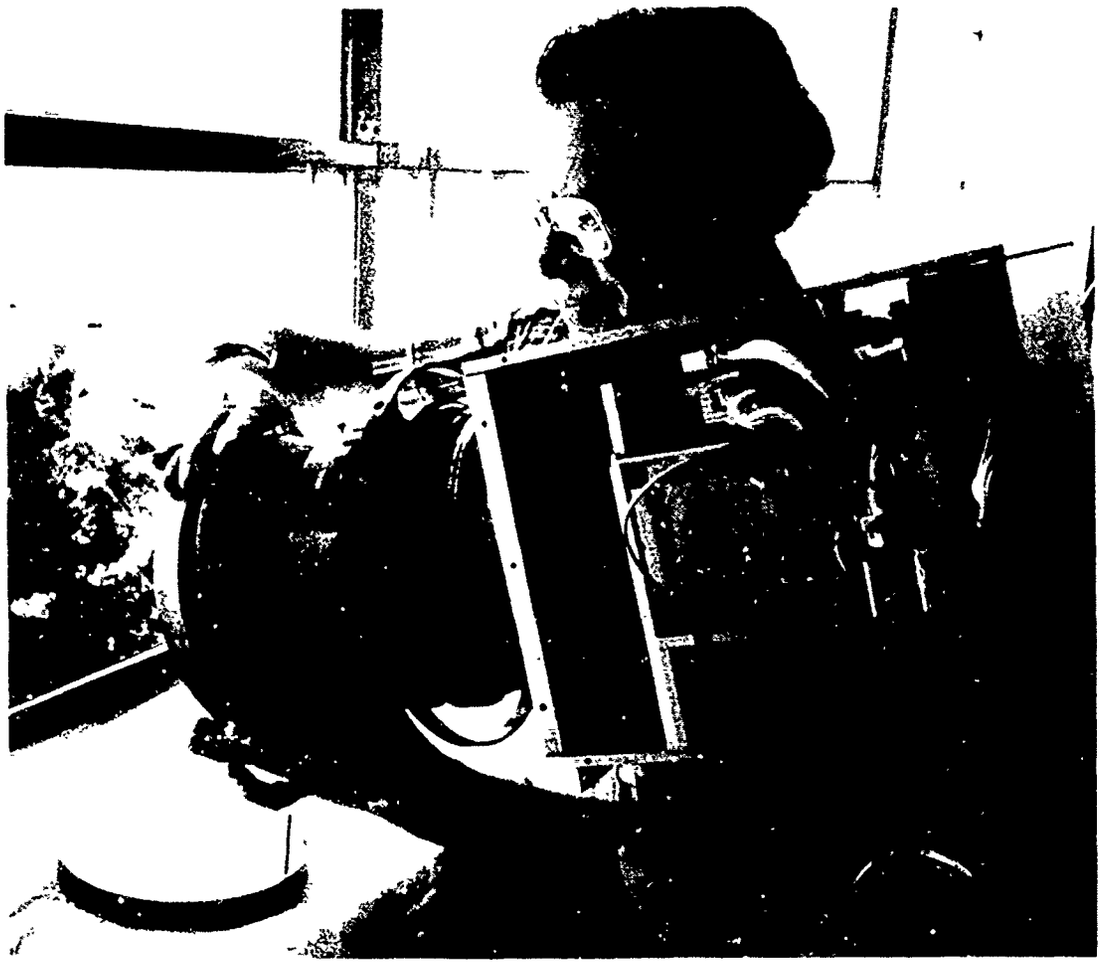

Figure 11. The examination of germanium blank for internal flaws by placing it in front of a thermal imager.

instrumentation is expensive and data interpretation often is imperfect. The advantage of using a material that may be inspected visually is obvious.

Along with their many desirable characteristics, chalcogenide glasses do have some drawbacks. They are softer than materials such as germanium and are scratched fairly easily, even during routine maintenance procedures. They have high coefficients of expansion, making lenses subject to cracking if the application of heat is uneven.

The softness of the glass can be beneficial during some steps of the manufacturing process, however. Glass is easier to shape and grind than a harder material, although grinding rates are limited by the heat rise in the material. The material's high coefficient of expansion causes cracking if there is a substantial temperature differential between the surface layer and the interior of the material. Special precautions must be taken during glass manufacture to prevent glass blank fracturing due to rapid temperature rise or uneven heat application. Local heat generation during grinding must be carefully regulated to avoid fracture. Furthermore, temperature restrictions may be necessary during actual use of the glass window. In the process of heating windows for deicing, for example, special precautions must be taken to prevent large temperature gradients, which might lead to

fracture. Exploratory investigation into the deicing of chalcogenide glass windows has shown that it is feasible to raise the glass surface temperature 35°F (19°C) with 1W/inch^2 power input to electrically conductive indium oxide films, which have only 10% absorptance at 10 μm wavelength (ref 20).

NOSC INVESTIGATION

Early in 1978, test specimens of AMTIR-1 were purchased by NOSC for evaluation of the resistance of this infrared optical material to the corrosive action of seawater. The objective of the study was to explore the possibility that chalcogenide glasses could serve as a corrosion-resistant structural material for optical viewports or as a corrosion-resistant coating on optical viewports fabricated from corrodable materials operating in a marine environment. Past experimental data indicated a potential not only as a primary (ie structural) window material, but also as a protective and antireflective coating material for a structural window substrate such as germanium. It was hoped that the exploration of these two applications could provide optimum engineering solutions for all typical marine applications.

In marine applications where the viewport is not subjected to very high hydrostatic or hydrodynamic loading, for example, economic considerations and corrosion resistance of the viewport material take precedence because the structural requirements are less demanding. Marine applications in which the viewports are subjected to high dynamic and/or static pressures, on the other hand, require materials with premium structural properties, and other properties such as corrosion resistance become secondary. Investigating chalcogenide glass both as a primary material and as a coating material provides the flexibility for adapting applications to different operational modes.

The experimental approach to the study relied largely on previous experimental and analytical work conducted with viewports that used acrylic plastic, glass, ceramic, and germanium windows. Tests included uniaxial and biaxial compressive and flexure loading (both short- and long-term) of test specimens, dynamic impulse loading, corrosion testing, and adherence testing (for the calcogenide coatings).

The NOSC tests showed AMTIR-1 glass to be very successful (in comparison with germanium and zinc selenide); the results were reported in the summer of 1979 (ref 19). Work reported here represents the next step in the evaluation of AMTIR-1 glass as a potential FLIR dome or window material for US Navy systems.

CHALCOGENIDE GLASS FABRICATION PROCESSES

All specimen blanks of chalcogenide glass used in these tests were fabricated by Amorphous Materials, Inc, of Garland, Texas. Specimens were then finished either at Amorphous Materials or at Optic Electronic Corp, of Dallas, Texas. All chalcogenide glass coating of germanium was done by Optic Electronic Corp. Wherever feasible, specimens were fabricated in sufficient number to provide good statistical reliability for the data. Where it was not possible to obtain specimens in sufficiently large number, those available were used as general feasibility indicators of the fabrication and utility of this material.

20. Technical Report AFAL-FR-73-340, Development of Deicing Methods of Chalcogenide Glass Windows for Reconnaissance and Weapon Delivery, SN Rea and RS Wriston, Texas Instruments Inc, 1973.

PRIMARY MATERIAL

Figure 12 is a simplified diagram depicting the glass compounding and casting process developed by Amorphous Materials to produce AMTIR-1. All three glass processes (purification of elements, compounding the glass, and casting the plate) are combined into a single continuous process. Glasses are compounded from the elements in high-purity evacuated quartz containers placed in a dual-zone resistive heat furnace. Zone 1 contains the round empty chamber that serves as the casting mold later in the process. Zone 2 contains the glass compounding chamber.

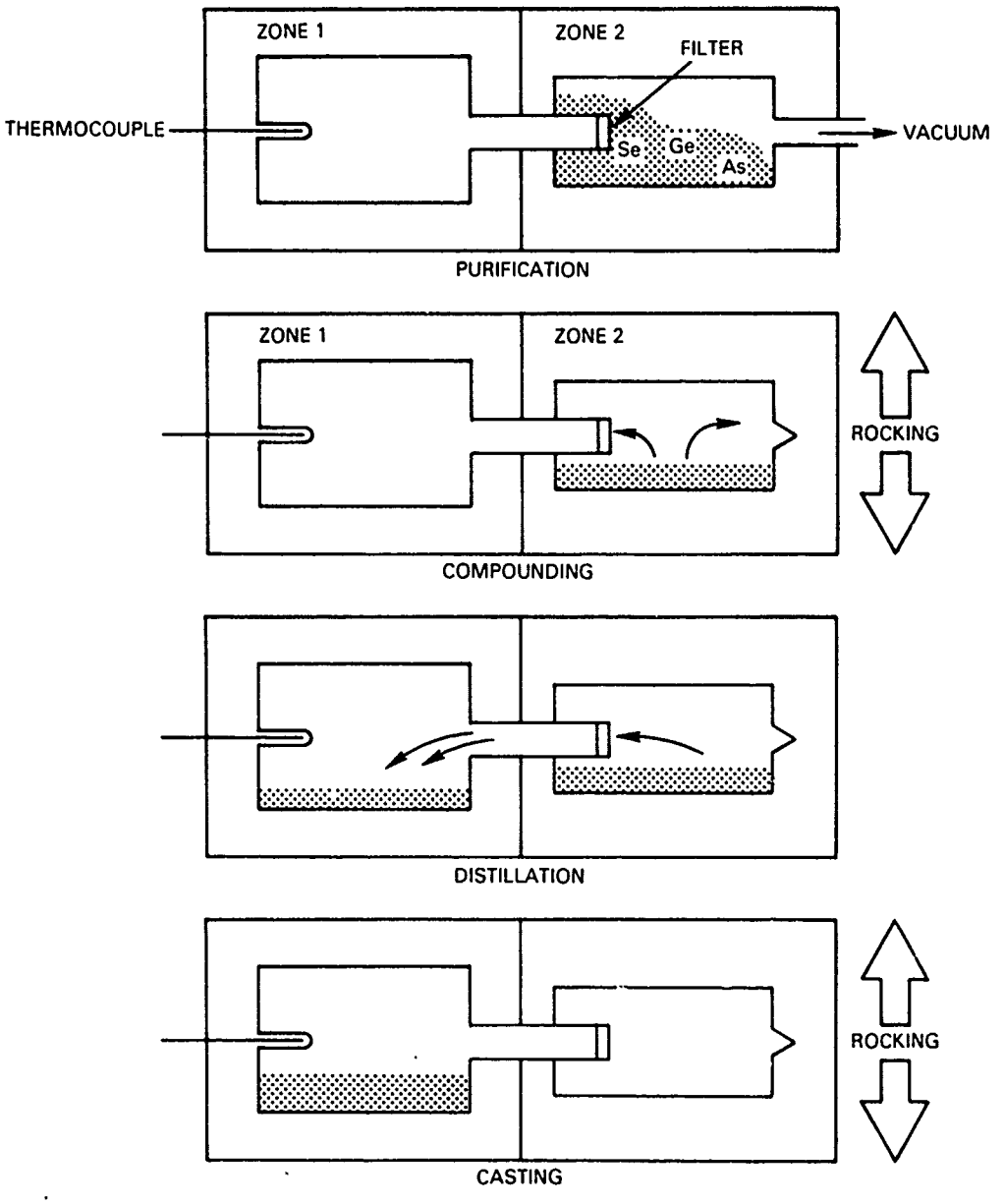

Figure 12. Process diagram for production of AMTIR-1 glass.

Initially both quartz chambers are evacuated and heated to remove moisture. The compounding chamber containing the elements is heated further to melt the selenium and to allow dissolved gases to be removed. After about 3 hours the chamber is sealed off while still under vacuum by heating and collapsing the quartz vacuum pumping tube. The furnace is closed and need not be reopened until the glass is quenched.

The temperature in both chambers is then raised to about 800°C while the furnace is rocked for about ? hours to insure that all the molten elements have reacted properly and are uniformly mixed. The reason for heating the casting chamber is to prevent premature transfer of the elements from the compounding chamber.

The rocking is then stopped and the casting chamber is cooled to transfer the compounded glass into the casting chamber. Distillation occurs through a porous quartz frit selected to filter out all particulate matter. The distillation generally takes 12–15 hours. The amount of material passed through the frit varies, depending upon the diameter and thickness of the casting. A 6-inch diameter plate 2 inches thick requires about 4 kg of glass while an 8-inch diameter plate 2 inches thick weighs about 7 kg.

The casting chamber temperature is increased above the glass melting point after glass transfer is complete. The compounding chamber is left at an elevated temperature to prevent any reverse transfer of material. The molten glass is mixed by rocking for about 2 hours, while the glass is allowed to cool to the casting temperature range (about 600°C). Rocking is then stopped and the furnace is leveled.

The glass is formed when the furnace is opened and air is blown onto the molten material. It is then cooled rapidly to the anneal temperature (~370°C). The furnace is closed and the glass is annealed for 6–8 hours. The furnace is then shut down and allowed to cool to room temperature.

After it has cooled, the chamber is opened to remove the glass plate. Great care must be exercised in this part of the process to avoid damaging the valuable quartz casting chamber. The chamber is opened by cutting above the AMTIR plate with a horizontal diamond saw.

After removal of the glass plate, the quartz container is cleaned and resealed on a glass lathe to prepare it for reuse, which is essential to the economic production of AMTIR glass.

Figure 13 is a photograph of the two types of casting chambers. The chamber used to cast the smaller 6-inch diameter plates is fabricated by ring-sealing two plates into quartz tubing to form a cylinder. The larger 8-inch and 10-inch diameter chambers are formed by sealing a single polished quartz plate into a quartz crucible. The crucibles are used to minimize expense and because their curved surface offers a greater strength when the system (ie the crucible, the casting chamber, and the compounding tube joining them) is evacuated and heated.

The two-zoned furnace used in preparing the glass plates is shown in figure 14. Note the circular zone, which is the casting side. Not shown in the photograph is the rocking platform on which the furnace is mounted. The furnace and platform are housed within a metal enclosure as a safety measure.

The automatic control units used to power the compound and casting furnaces are shown in figures 15 and 16. Figure 15 shows a single Barber-Colman unit with its microprocessor computer unit on the left. Figure 16 is a view of the glass production area at Amorphous Materials, showing all four compounding and casting units. The automation of

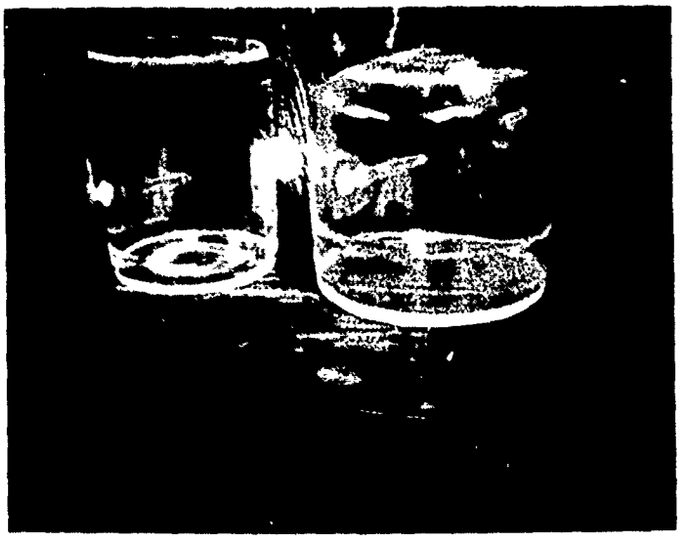

Figure 13. Quartz chambers for casting of 6-inch and 8-inch diameter glass blanks.

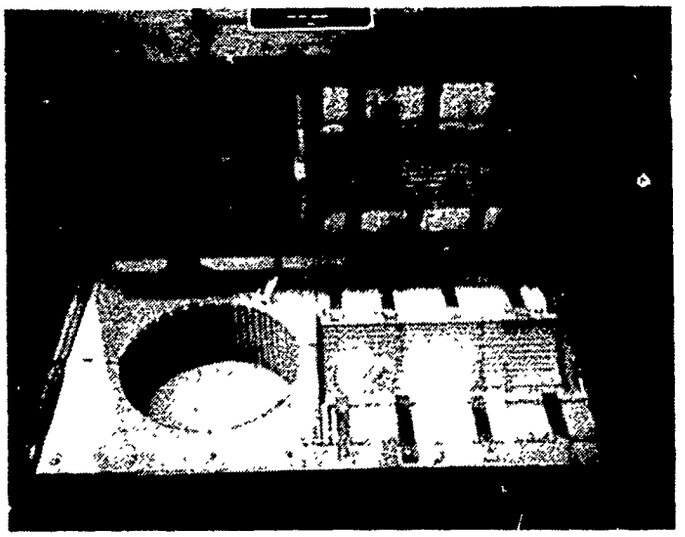

Figure 14. Round chambered compounding and casting furnace

Figure 15. Barber-Colman microprocessor power control unit.

Figure 16. Compounding and casting production area showing all four automatic power control units.

all units has greatly improved batch-to-batch reproducibility. These units may be operated three times per week. Present capacity is about 300 kg of cast plates per month.

Figure 17 is a photograph of AMTIR-1 6-, 8-, and 10-inch cast plates prepared by this process and equipment. Also shown are lens blanks of various sizes that have been core-drilled from the plates. In the center is shown one of the 8-inch diameter test domes prepared for NOSC. The dome was ground and polished by Optic Electronic Corp on a subcontract to Amorphous Materials.

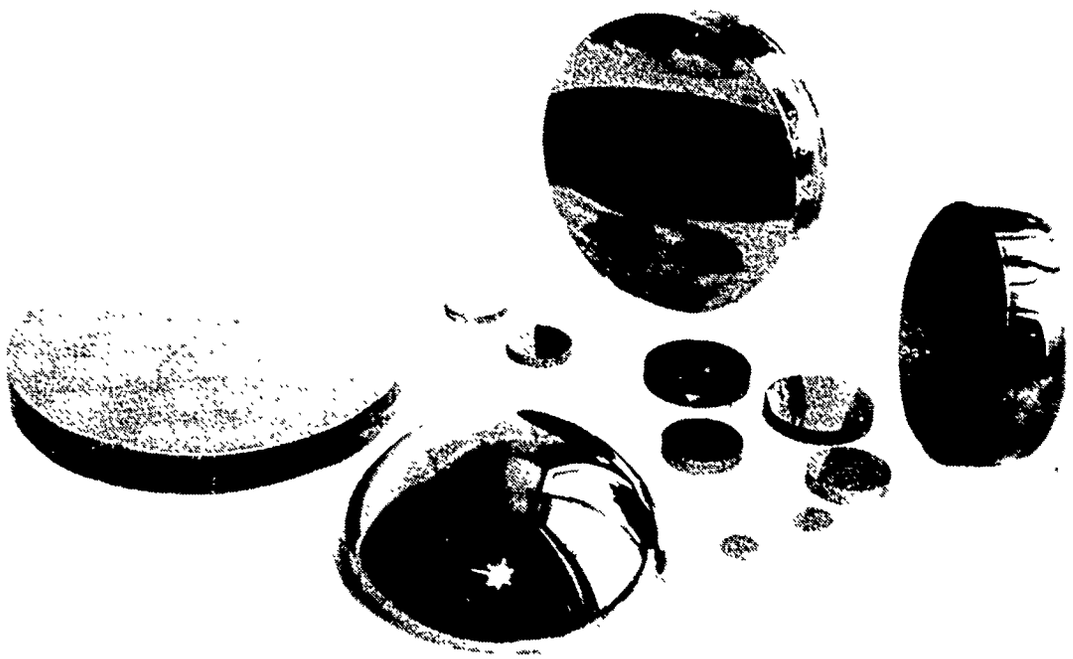

Figure 17. AMTIR-1 cast plates, blanks, and spherical sector window.

COATING FOR GERMANIUM

For many years sputtering techniques have been used to produce good-quality thin coatings of a variety of materials on a variety of substrates. Physical sputtering is a process whereby a solid (usually) is bombarded by a stream of ions, atoms, or molecules. When the kinetic energy of a bombarding particle exceeds the binding energy of a target solid, atoms of the lattice are moved about. If the kinetic energy of the bombarding particle exceeds by about four times the heat of sublimation of the target material, lattice atoms in the target are dislodged and ejected into the gas phase. This ejected or "sputtered" material may then form the desired coating on a substrate material (ref 21).

21. Maissel, LI, and R Glang, Handbook of Thin Film Technology, McGraw-Hill, New York, 1970.

Of the several techniques of sputtering, the use of ion beams has several advantages over other methods. Ions can be accelerated to any desired kinetic energy with electric fields, whereas neutral atoms cannot be so accelerated. And since beam current density and ion energy are largely independently adjustable, greater flexibility exists in ion beam parameter adjustments than in many other sputtering techniques. Further, ion beam sputtering may be conducted under high-vacuum conditions, the target may be bombarded at other than normal incidence, and the target and substrate may be maintained with a "field free" region between the two. Oblique incidence is advantageous in that it can cause an increase in sputtering yield in some materials. A field-free region is an advantage in that either positive or negative ions may be sputtered onto a target. (This is not always possible in plasma sputtering.)

The major drawback to ion-beam sputter deposition is the fairly low deposition rate for most thin coatings. This is a major problem where coatings of uniform thickness are to be applied over large areas of substrate, a process that requires a high deposition rate.

The ion-beam sputtering technique was used to investigate the use of chalcogenide glass AMTIR-1 as a coating material for germanium windows (ref 22). A hybrid deposition technique was employed that combined the advantages of sputter deposition, during the initial stages of film growth, and subsequent thermal generation, to achieve faster deposition rates.

Coating a germanium substrate with chalcogenide glass by this technique is a two-part process. First the substrate surface to be coated is cleaned by ion-beam bombardment, then the chalcogenide glass target material is sputtered onto the germanium substrate. The approximate deposition rate for the sputtering configuration employed in initial testing was 8 Å/s for a 10 mA beam current. Increasing the beam current beyond 10 mA increases the deposition rate dramatically (fig 18) because of ion beam heating of the target. The substrate is rotated during sputtering.

PREPARATION OF TEST SPECIMENS

COMPRESSION CYLINDERS

About 30 or 40 compressive strength test specimens consisting of 1-inch diameter cylinders (fig 19) were core drilled from 2-inch thick AMTIR-1 blanks after first grinding and polishing them to plates with flat and parallel surfaces. During drilling, care was taken to avoid scratching the sides of the cylinders, which were left in the uniform unpolished condition created by the diamond core drill. Past experience has shown that lack of polising on the cylindrical surface has no affect on the compressive strength of the specimens. Great care was taken to see that that the polished surfaces were uniformly flat and that the edges were carefully chamfered to avoid the tendency toward chipping.

22. Herrman, WC Jr, and JR McNeil, Ion Beam Deposited Ge-As-Se Glass for Applications in the 1 μ to 16 μ Wavelength Region, 12th Annual Symposium on Optical Materials for High Powered Lasers, Boulder, Colorado, 30 September 1980.

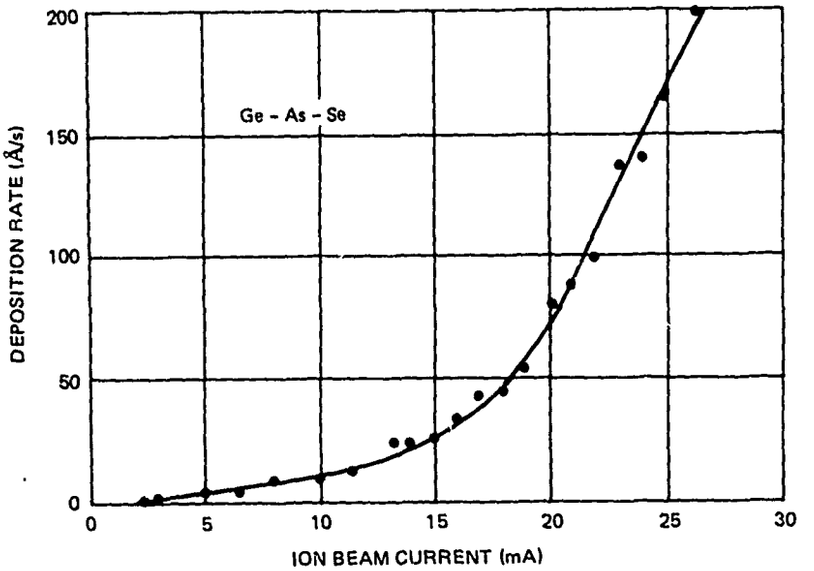

Figure 18. A plot of coating deposition rate as a function of ion beam current for Ge-As-Se composition coatings.

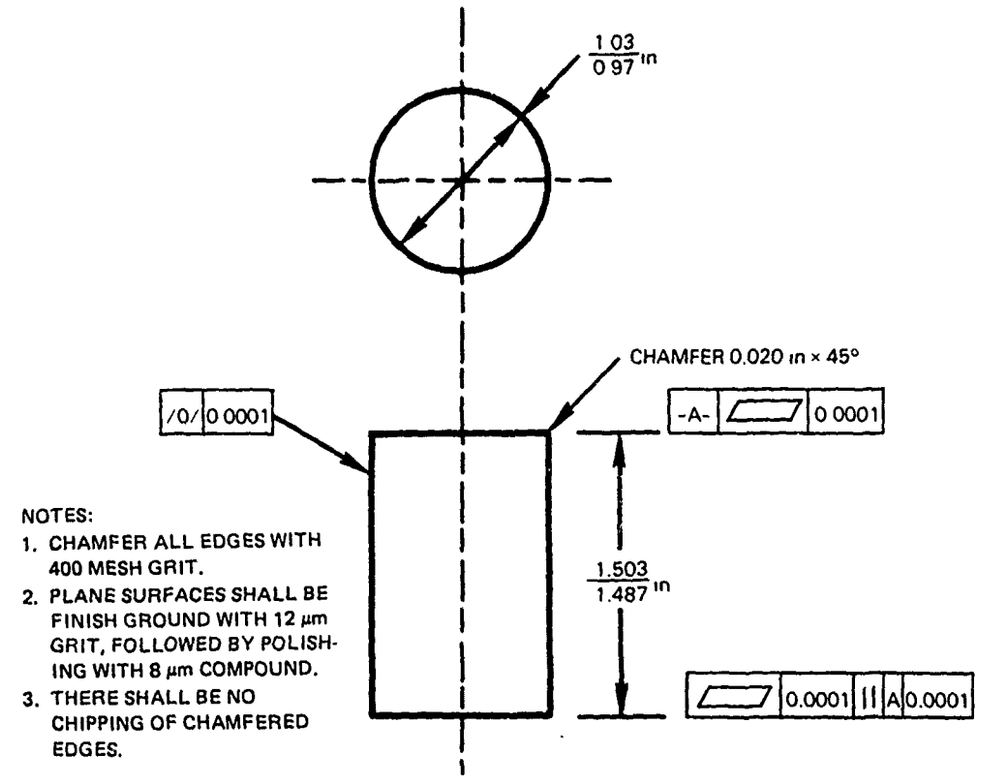

Figure 19. Specifications of the massive chalcogenide glass uniaxial compression test specimens.

FLEXURE BARS

About 30 or 40 flexure specimens were prepared by Amorphous Materials for use in this study. Fabrication began by waxing 8-inch diameter cast AMTIR-1 plates to a base plate and sawing them into long slabs of 1/2- by 2-inch cross section. The ends were cut at right angles to produce 4- and 6-inch slabs. Each slab was then placed flat and sawed again to form 1/2-inch square cross-section bars (fig 20). All the bars were blocked in parallel on the same plate for grinding to uniform dimensions and polishing. Bearing surfaces were made parallel to within 0.0001 inch and chamfered edges were carefully hand polished to insure uniformity. The modulus of rupture, which is determined by flexing the rectangular specimens to destruction, depends to a large extent on the finish of the chamfered surfaces, regardless of the degree of polish on the faces of the specimens. Since the stress at which the specimen fails is governed invariably by the size of the chips in the chamfered surface, all chamfers of the flexure specimens were finished to identical standards. Thus the failure point is representative of the material rather than of the finish.

To evaluate the effect of surface finish on the flexural strength of the material, one set of flexure specimens was left unpolished but simply finely ground and finished with 8 μm powder. It was hoped that comparison of the two sets would show whether polishing after grinding would allow the specimens to reach higher stress levels.

FLEXURE DISKS

The specimens for biaxial tensile loading were 3-inch diameter by 0.25-inch thick cylindrical disks (fig 21), which were also saw-cut from 1-inch thick cast blanks, ground flat, then pitch-polished on both sides. Specimens of this type were also used for corrosion resistance testing in San Diego Bay (discussed under Chalcogenide-Glass-Coated Elements).

SPHERICAL SECTORS

Specimens for biaxial compressive loading were 1-inch thick, 150° spherical sector windows with 4-inch outside radius (fig 22). They were fabricated from AMTIR-1 that was cast into a large solid blank, then hollowed out.

The window design selected for evaluation in this study was a proven one, used previously by Naval Undersea Center (now merged into NOSC) for evaluation of glass ceramic as window material for the near-infrared region of the electromagnetic spectrum. It was based on the following principles validated in other studies of viewports employing glass, acrylic plastic, germanium, or ceramic windows for high-pressure service (ref 23-25).

23. Stachiw, JD, Transparent Structural Materials for Underwater Research and Exploration, Industries Atomiques et Spatiales, vol 18, no 3, p 71-94, 1974.
24. NOSC TR 565, High Pressure Viewports for Infrared Systems, Phase I – Germanium, JD Stachiw, September 1980.
25. NOSC Technical Report NUC TP-393, Glass or Ceramic Spherical Shell Window Assembly for 20,000 psi Operational Pressure, JD Stachiw, May 1974.

NOTES:

1. CHAMFER ALL EDGES 0.020 in x 45° WITH 400 MESH GRIT FOLLOWED BY POLISHING WITH 20 μm COMPOUND.
2. FINISH GRIND ALL SURFACES WITH 12 μm GRIT, FOLLOWED BY POLISHING WITH 8 μm COMPOUND.
3. THERE SHALL BE NO CHIPPING OF CHAMFERED EDGES.

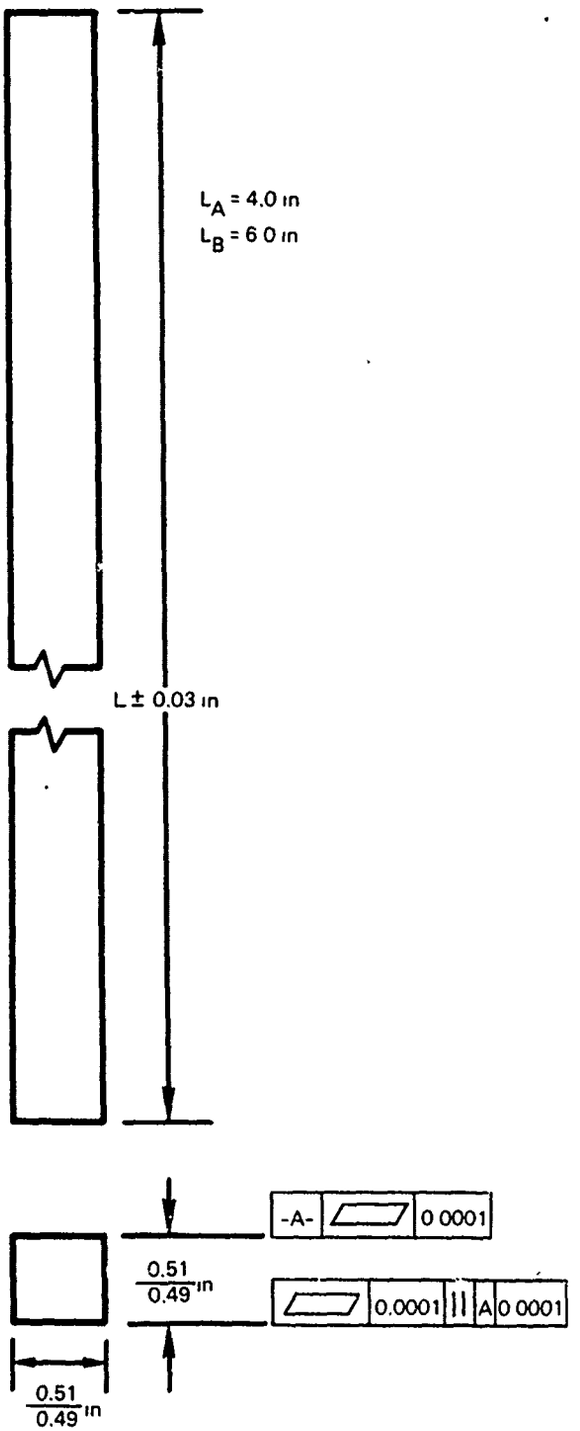

Figure 20. Specifications of the massive chalcogenide glass uniaxial flexure test specimens.

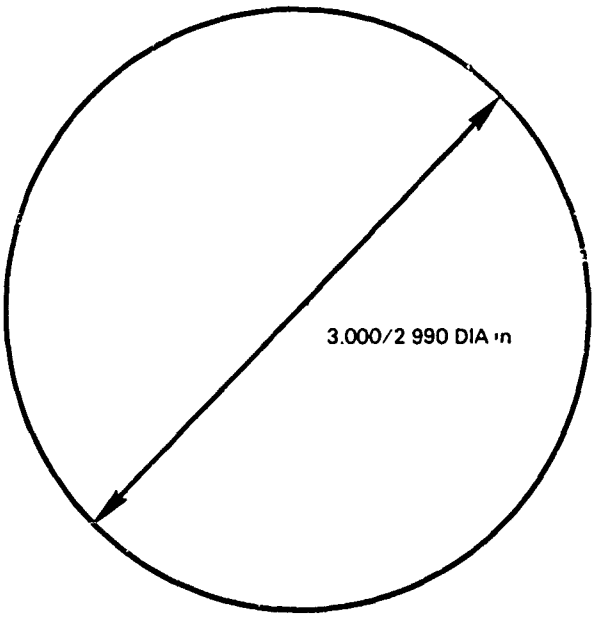

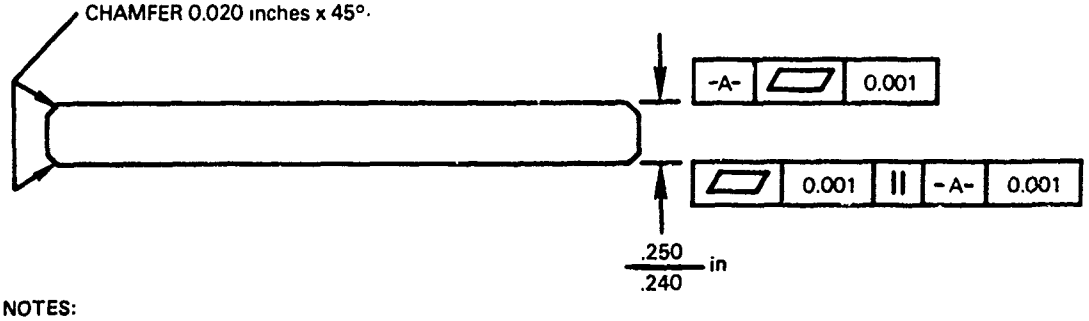

NOTES:

1. CHAMFER ALL EDGES WITH 400 μm MESH GRIT.
2. PLANE SURFACES SHALL BE FINISH GROUND WITH 12 μm GRIT, FOLLOWED BY POLISHING WITH 8 μm COMPOUND.
3. THERE SHALL BE NO CHIPPING OF CHAMFERED EDGES.

Figure 21. Specifications of the 3-inch cylindrical disks of AMTIR-1 glass used for biaxial tensile loading and corrosion testing.

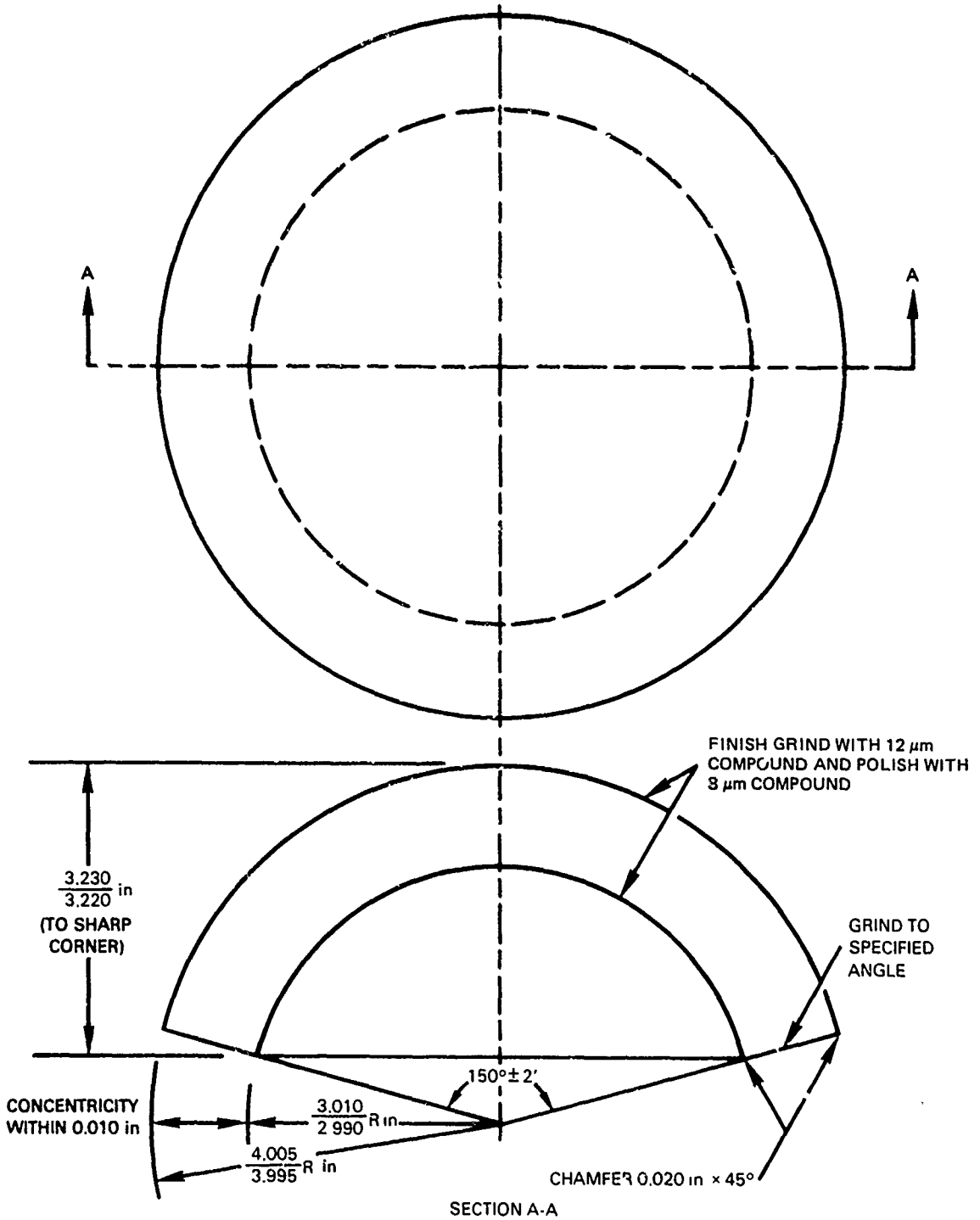

Figure 22. Specifications of the 150° spherical sector massive chalcogenide glass specimens used for biaxial compressive load testing.

1. Spherical sectors see only compressive stresses under external pressure loading. This shape thus is best suited for windows made of materials with low tensile but high compressive strength (ref 24, 25).

2. A spherical sector with a 150° included spherical angle appears to generate the least number of shear cracks in the conical bearing surface of the sector under a given bearing stress.

3. A plane conical bearing surface on a spherical sector window generates the least concentration of stresses in a window mated to a seat whose radial and angular displacements differ from that of the window.

4. The included angles of the window seat must match within 1 to 2 minutes of arc the included angles of the window bearing surface.

5. Bearing gaskets made of compliant elastic material must be interposed between the mating surfaces of the window and the seat (fig 23).

6. The radial and angular displacements of the window seat should match as closely as possible the radial and angular displacements of the window.

7. The retaining ring should generate only compressive stresses inside the window.

8. The bearing surface on the window must be either pitch-polished or finished with an 8–10 μm grinding compound.

9. The edges of the bearing surface of the window must be provided with a 0.010- to 0.020-inch chamfer whose finish matches that of the bearing surface. No chips are to be allowed on the chamfered surfaces. Chips of up to 0.020 inch can be removed with a stone of appropriate roughness.

On the basis of the above criteria, a 150° spherical sector viewport was designed (fig 22 and 24–27). The dimensions chosen were the same as those of previous successful NOSC spherical deep-submergence germanium window assemblies (ref 24). To improve the chances of successfully casting a large solid piece of AMTIR-1, a curved casting mold was chosen. Two 8-inch diameter crucibles were used as the basis for the mold. One crucible served as the curved, semispherical bottom casting surface. A curved bottom insured the glass release from the quartz surface with minimum of stress. The top crucible served to provide added strength to the mold. Figure 28 shows the mold and quartz chamber after removal from the furnace. The amount of material used in each casting was 13 kg (28.6 lb) – a large mass to be supported by a thin-walled quartz chamber that is also evacuated. The second crucible provided only curved surfaces so as to utilize atmospheric pressure to add strength to the mold.

Figure 29 is a photograph of a mold containing a blank. The mold has just been removed from the furnace after undergoing a 6-hour anneal. Note the appendage on the side, which was used to evacuate the mold. The material was added in the form of glass pieces through the tube on top. After all 13 kg of glass pieces were loaded, the top was sealed with a small quartz cap. Glass pieces were used both because there was doubt that the spherical shaped bottom would provide enough agitation during the compounding cycle and because the use of precompounded glass allowed the operation to be carried out at a lower temperature (750°C), reducing the possibility of mold failure. Figure 30 shows a dome blank as it appears on removal from its container. The as-cast surface is bright and shiny. In the next step the blanks are placed in a standard anneal furnace, annealed for 30 hours at 370°C, and returned slowly to room temperature. The total anneal cycle time is 72 hours.

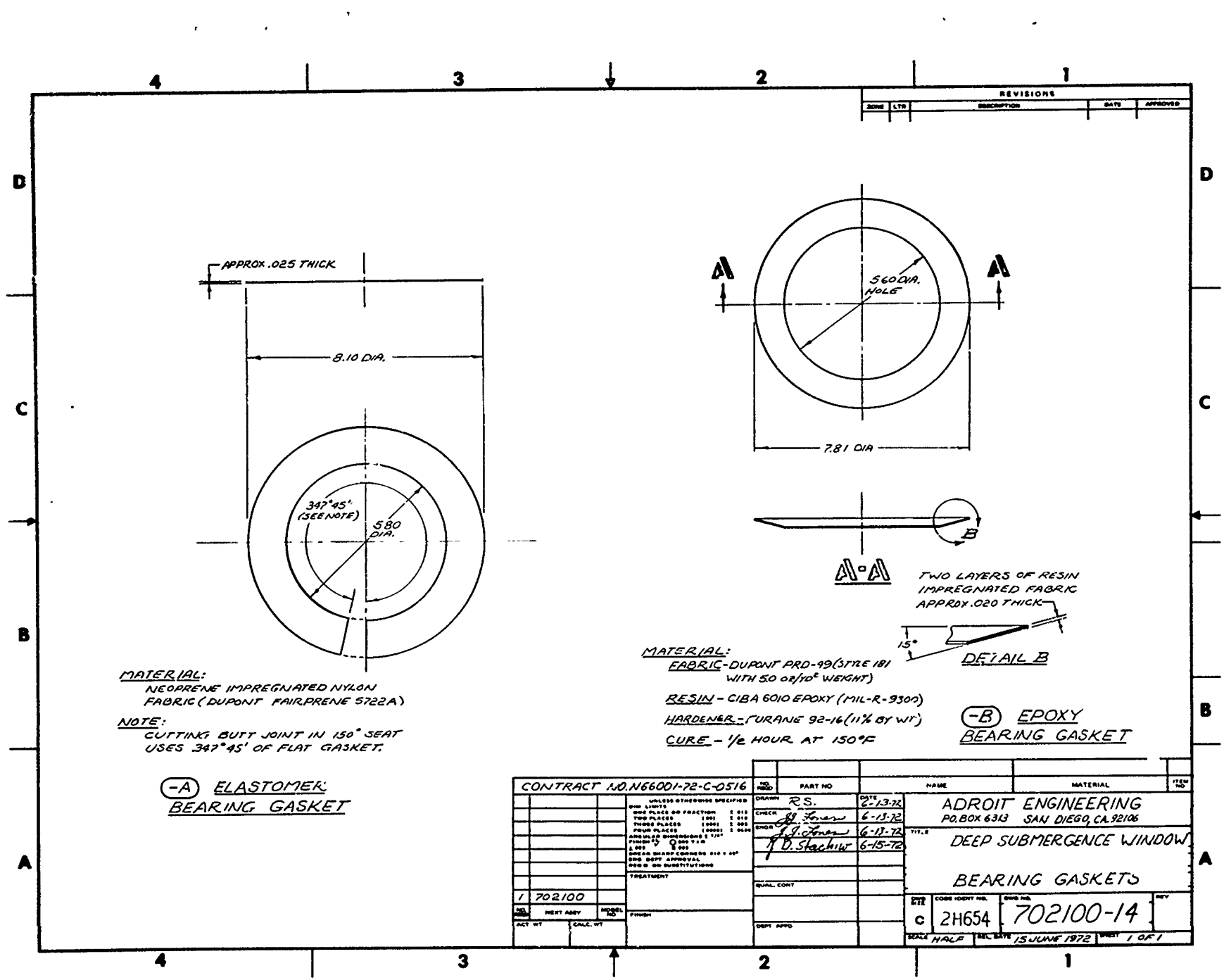

Figure 23. Specifications of the specialized bearing gaskets used with the 150° spherical sector windows.

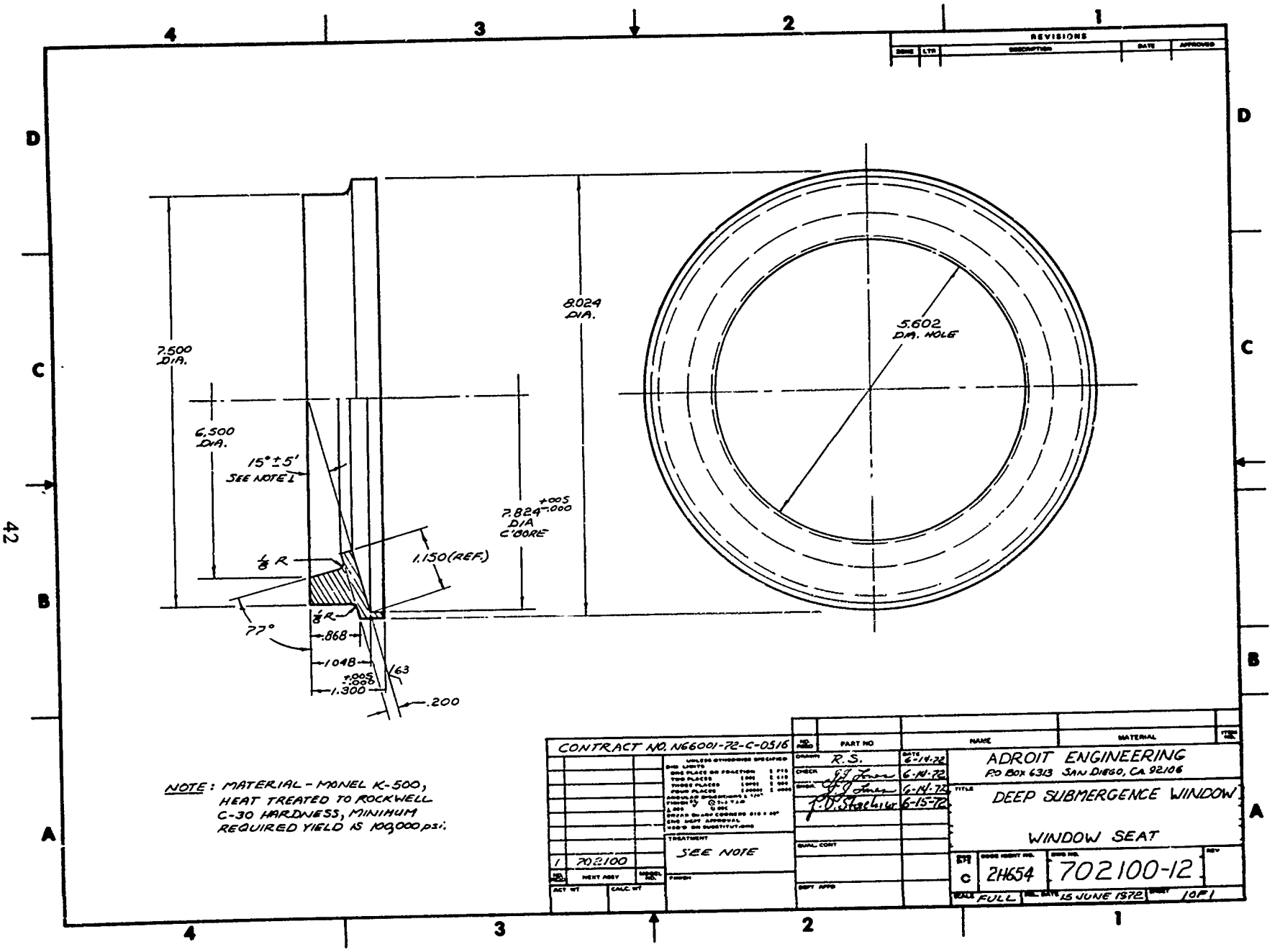

Figure 24. Specifications of the K-500 Monel seat for the 150° spherical sector window.

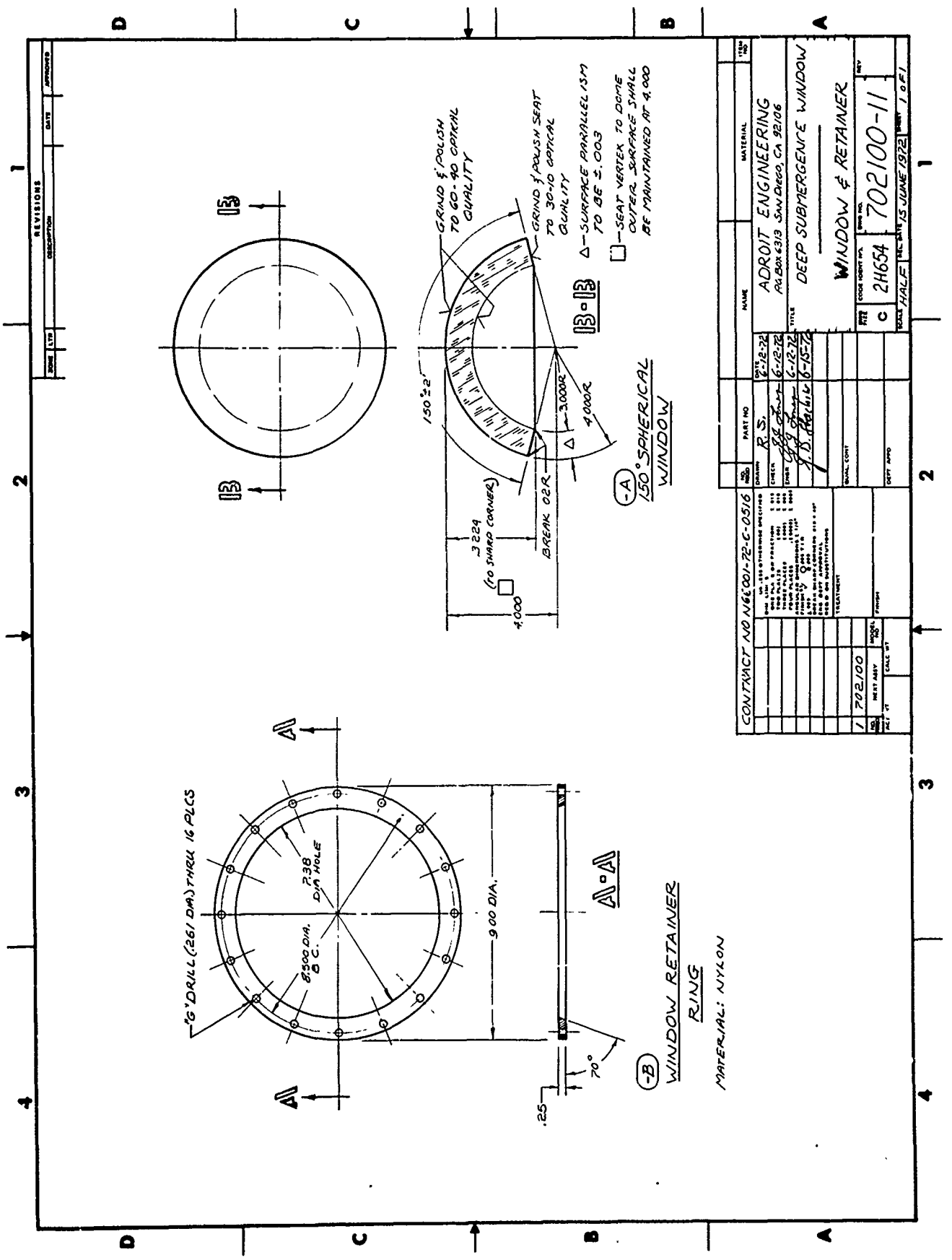

Figure 25. Dimensions of the 150° spherical sector window and retainer.

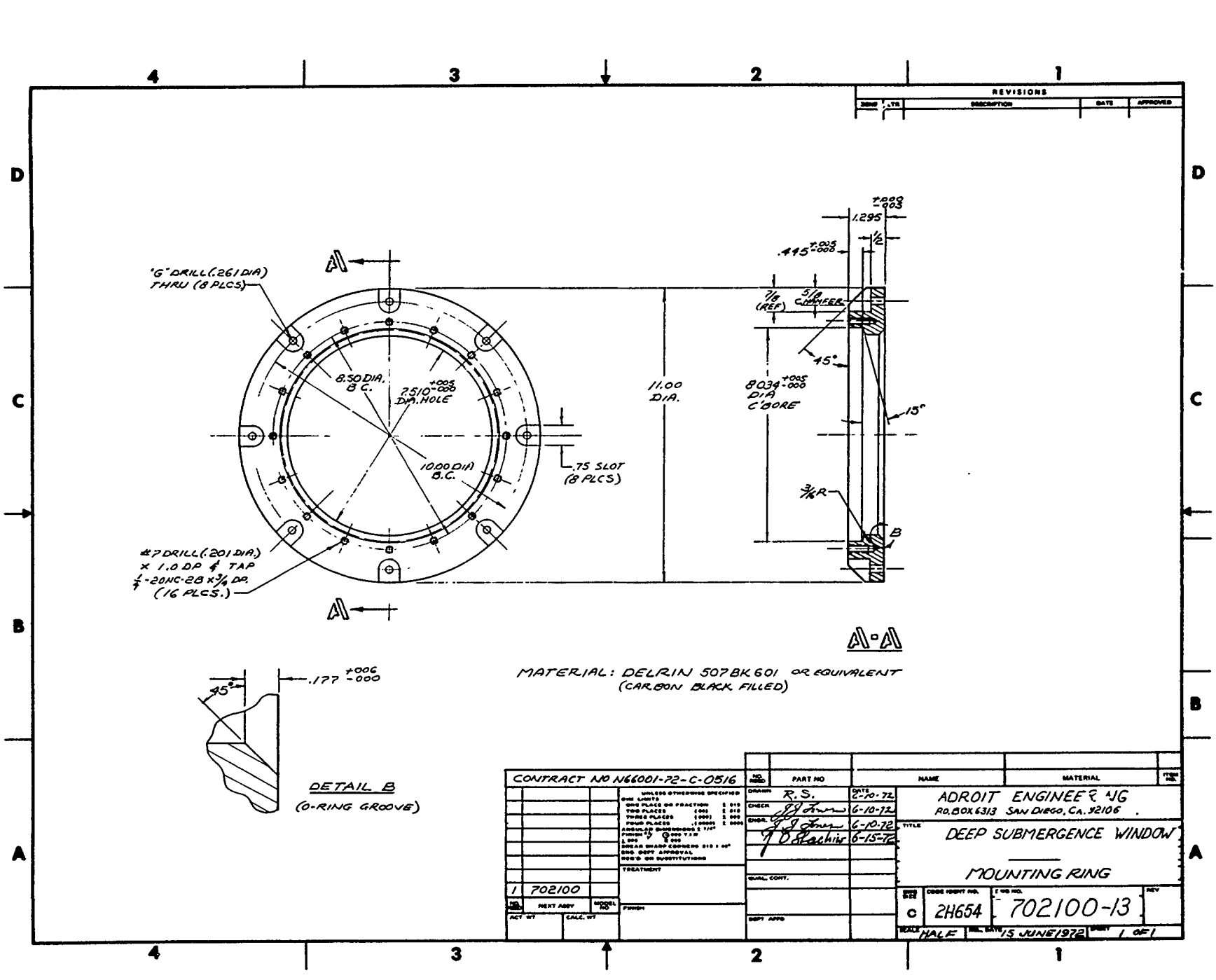

Figure 26. Specifications of the mounting ring for the 150° spherical sector window.

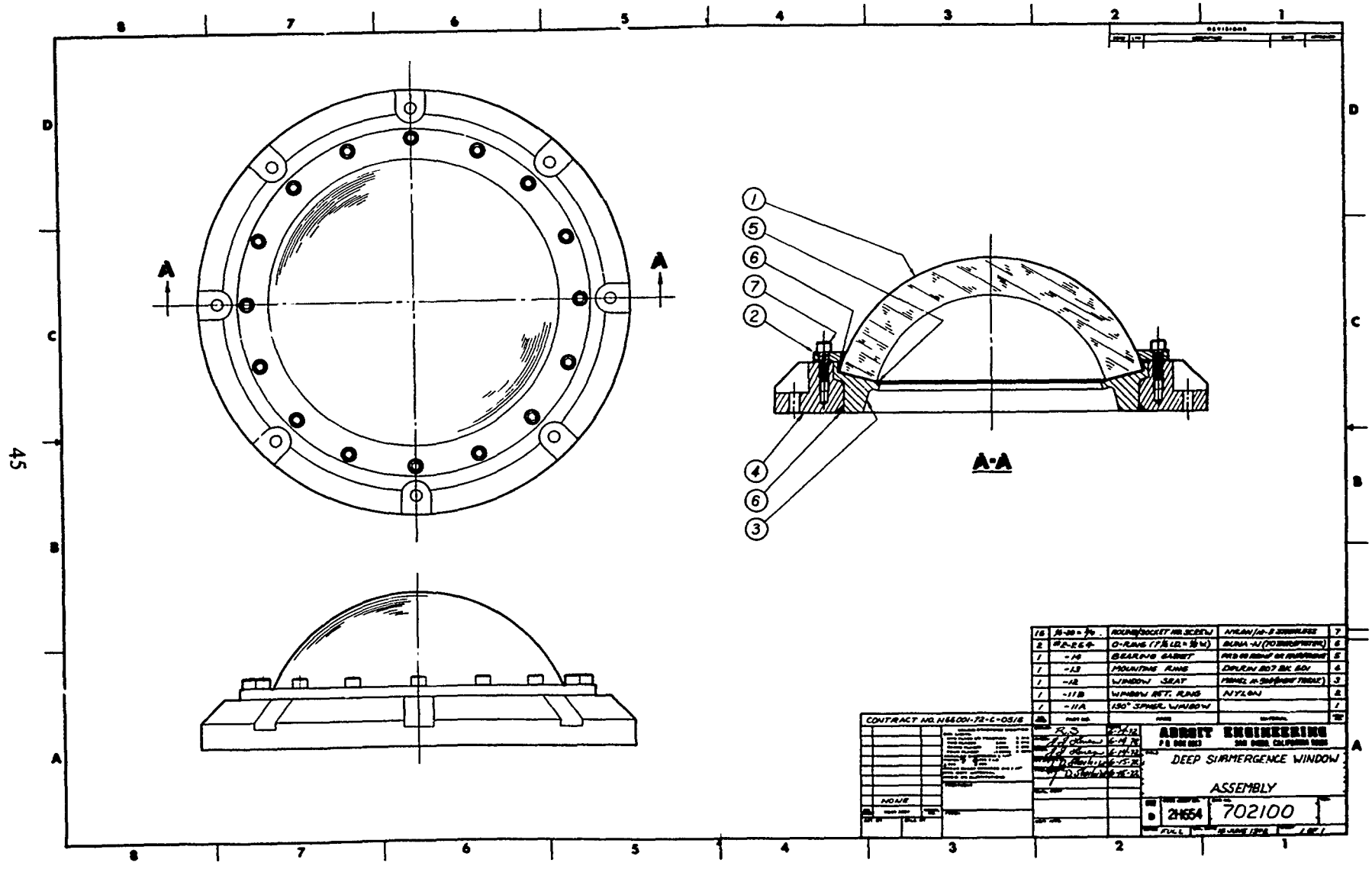

Figure 27. Overall view of the assembled 150° spherical sector window and mounting.

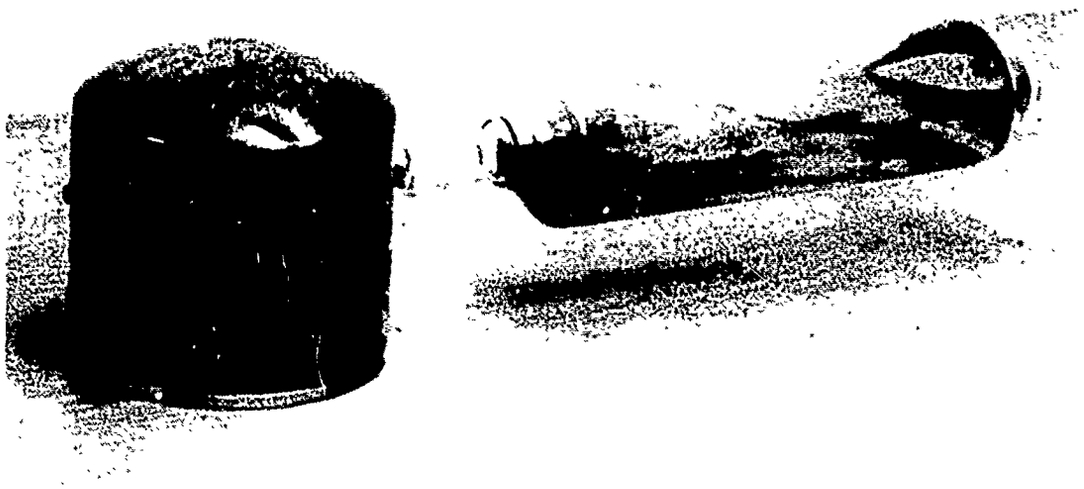

Figure 28. The large mold and quartz chamber used for fabricating AMTIR-1 test domes, after removal from the casting furnace. The horizontal chamber is used for compounding and melting the glass.

Figure 29. The casting mold for an AMTIR-1 spherical sector blank. Note that the mold has already been detached from the compounding chamber.

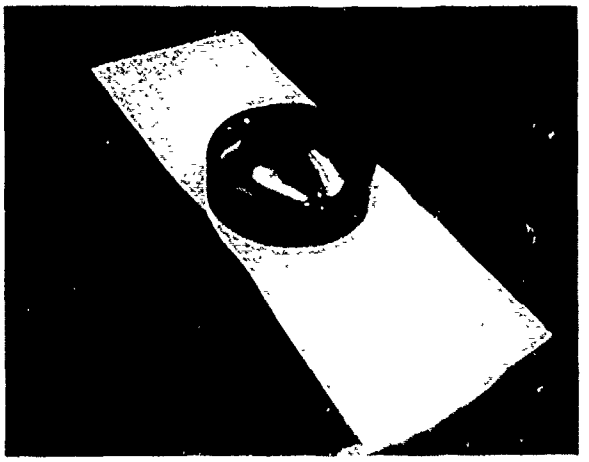

Figure 30. An AMTIR-1 spherical sector blank weighing about 13 kg.

After undergoing the anneal cycle, the AMTIR-1 blanks are transfered to Optic Electronic for fabrication.

Fabrication begins with generation of the outside surface of the spherical sector on a Strasbaugh glass grinder. Any cracks present in the blank become apparent at this step. If cracks are detected, the blank is removed for remelting and recasting.

Generation of the inner surface requires blocking and deblocking of the AMTIR-1 blank onto support plates. As AMTIR-1 is very susceptible to heat shock, this step must be carried out with extreme care to avoid fracturing the glass.

The final finish on the concave and convex surfaces of the spherical sectors is achieved by using 8 μm grinding powder, then pitch polishing. Figures 31 and 32 show the convex and concave polished surfaces, respectively. Special tooling had to be prepared to generate the proper angle for the mounting flange. Flatness of the flange (fig 33) and nickfree precise chamfers (fig 34) are of utmost importance in the preparation of the spherical sectors. The chamfered edges were finished with 8 μm grinding powder to the specifications indicated in figure 22.

The specimens used for dynamic impulse loading are identical to those for biaxial compression loading and use the same test mounting as that for the spherical sector windows. The common shape and mounting permits a direct comparison between the magnitudes of the static and dynamic pressures required to implode the window.

BEARING GASKETS

The bearing gaskets used in specimen testing under biaxial compressive loading play a significant role in obtaining biaxial compression strength values untainted by point or line contacts between the specimen and its seat. The specialized gaskets (fig 23) are constructed for use between the spherical sector windows of chalcogenide glass and the K-500 Monel alloy window seat Actually they are a composite of two types of gaskets: a top gasket in contact with the window, made of two layers of Kevlar-49 cloth impregnated with epoxy; this bonded with rubber contact cement to a lower gasket in contact with the Monel window seat, consisting of one layer of nylon cloth impregnated with neoprene. The overall thickness of the composite gasket is 0.040 inch (~1 mm).

Figure 31. The convex, polished surface of the AMTIR-1 150° spherical sector used as a test specimen in biaxial compression testing.

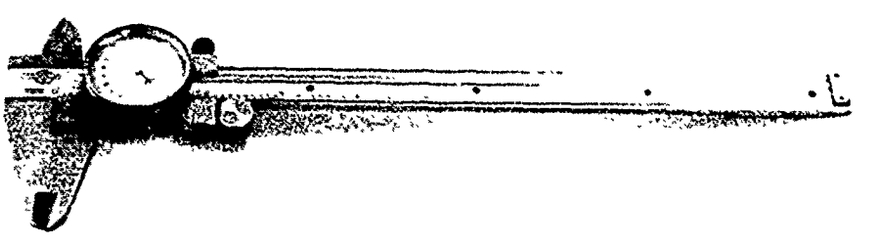

Figure 32. The concave, polished surface of the AMTIR-1 150° spherical sector shown in figure 31. Note that the bearing surface of the spherical sector is left unpolished.

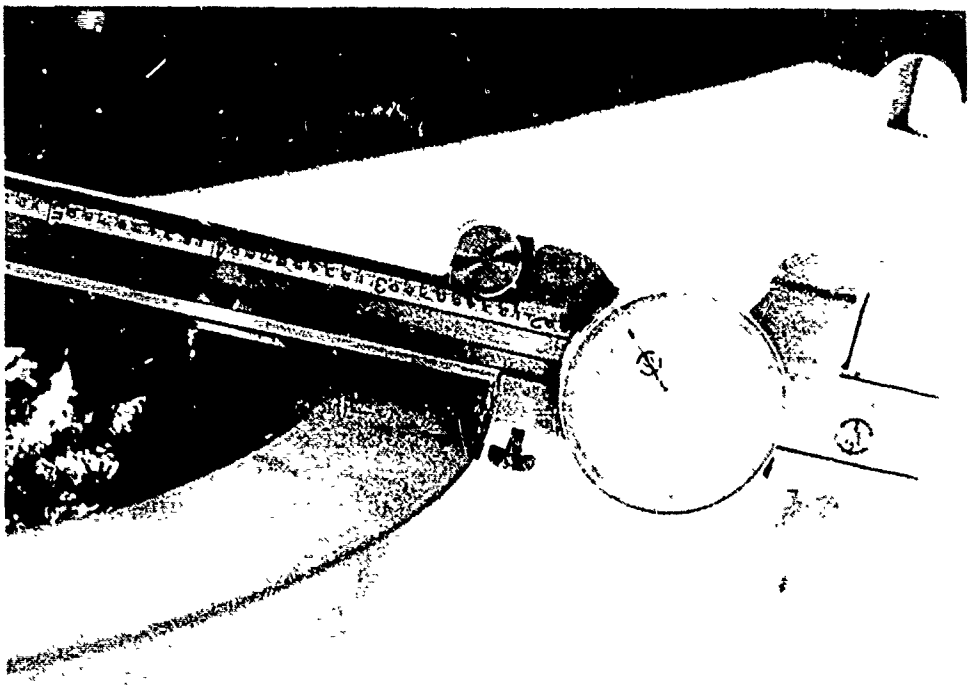

Figure 33. Checking the flatness of the AMTIR-1 150° spherical sector. The quality assurance specification requires that no light be visible between the straight edge of the caliper and the bearing surface of the sector.

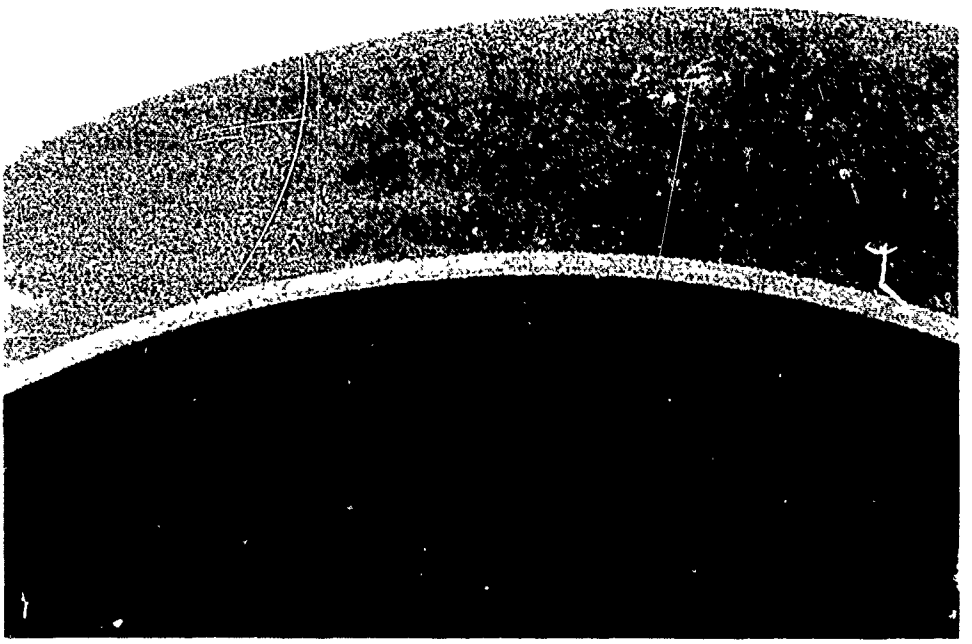

Figure 34. Close-up view of the chamfered inside edge of a spherical sector specimen showing a precise nickfree surface. Small nicks or chips can be smoothed out with a stone or Cratex abrasive elastomeric file.

Selection of this unique gasket construction was based on the necessity to find a combination of materials suitable to bridge the gap between the very soft, brittle window material and the very hard, tough Monel window seat. The Kevlar/epoxy gasket in contact with the chalcogenide window provides a smooth, slick surface for the window to slide on, minimizing shear stresses between the gasket and the window as well as gasket damage due to expansion and contraction of the window.

The nylon/neoprene gasket serves as a compliant bearing surface for the stiff Kevlar/epoxy gasket, thus compensating for slight irregularities in the bearing surface of the window as well as for a slight mismatch in the conical angles between the bearing surface of the window and the Monel seat. The chalcogenide glass window is not bonded to the composite gasket; research has shown that the life of a gasket is significantly extended by allowing it free movement between two mating surfaces.

Since the chalcogenide window and the Monel seat expand, contract, and deflect at different rates under the same pressure and temperature conditions, the 0.040-inch thickness of the gasket is needed to provide sufficient compliance between the dissimilar window and seat materials. The gasket could be eliminated if the window bearing surface and the Monel seat could be made to match perfectly and the radial contraction and expansion of the window and seat also coincided perfectly. On the basis of experimental data showing that any brittle material fails at a lower stress level if a gasket is interposed between it and the seat and that the use of a soft gasket between a brittle surface and a metallic seat causes cracking to be initiated sooner in the brittle material than were the gasket absent, it might seem prudent to eliminate the gasket. But since it is impossible to fabricate perfectly mating surfaces and since there is no way to match the radial expansion and contraction of the window and the window seat, a compliant gasket was selected as the engineering solution to the very difficult mounting problem.

CHALCOGENIDE-GLASS-COATED ELEMENTS

Specimens used in the testing of chalcogenide glass AMTIR-1 as a coating included one 3-inch diameter by 0.25-inch thick germanium disk (a cylindrical section of the same dimensions as the specimen in figure 21), three 8-inch diameter by 0.83-inch thick germanium disks (fig 35), and a 10-inch diameter by 5/8-inch thick germanium hyperhemispherical shell (fig 36). (For details of the fabrication of the 10-inch diameter germanium hyperhemisphere, see references 26 and 27).

The 3-inch specimen was used for an exploratory evaluation of chalcogenide glass coatings in seawater to demonstrate the advisability of proceeding with the study of chalcogenide glass coatings on germanium. The 8-inch diameter flat specimens were used to evaluate the chalcogenide coatings on a "window sized" specimen. While the 3-inch diameter specimen is actually too small to approach the size of an actual in-service window, the 8-inch diameter specimen reasonably approximates many IR windows in service. From it can be evaluated coating nonuniformity and other problems that are likely to occur when a large area of substrate is coated with chalcogenide glass.

---

26. Stachiw, JD, Hyperhemispherical Viewports for Undersea Applications, Journal of Engineering for Industry/ASME Transactions, vol 101, no 3, 1979.
27. Stachiw, JD, and WL Loucks, Design Parameters for Germanium Windows Under Uniform Pressure Loading, Society of Photo-Optical Instrumentation Engineers, Proceedings, vol 131, 1978.

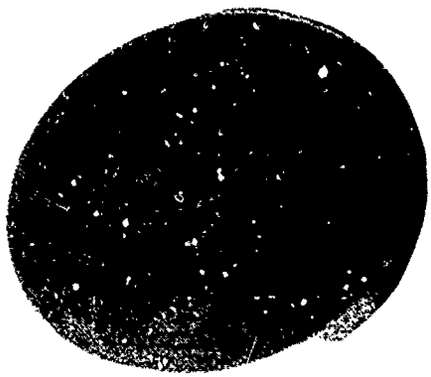

Figure 35 One of the 8-inch diameter 0.83-inch thick germanium disks used in the testing of chalcogenide glass coatings. The plane surfaces were pitch polished prior to coating with glass

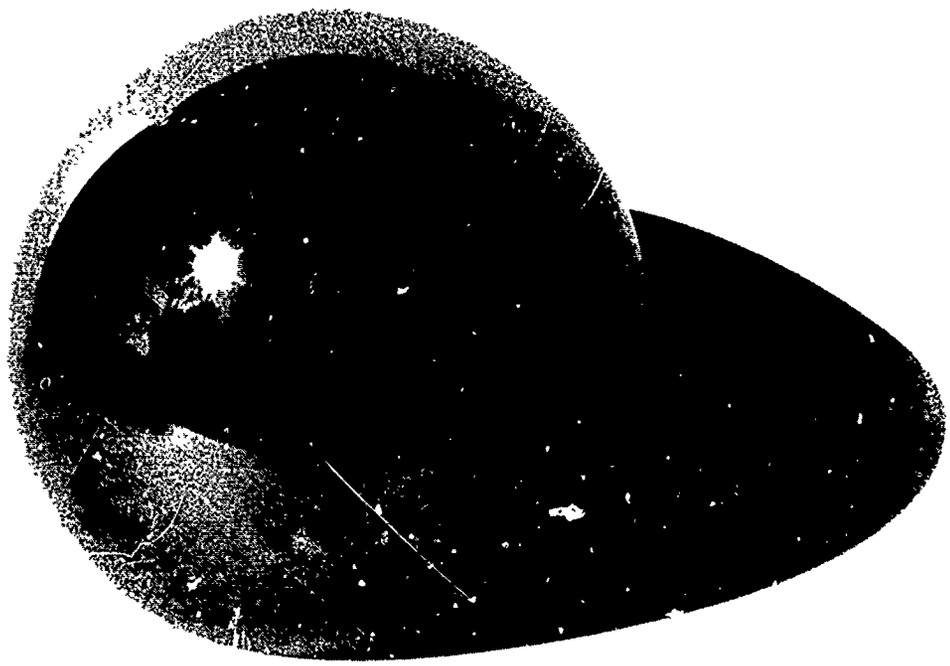

Figure 36. Free-standing hyperhemispherical germanium shell coated with chalcogenide glass. Its dimensions. R_o = 4.967 inches; R_i = 4.318 inches; α = 260° 15′.

The hyperhemispherical specimen served as a means of determining whether chalcogenide glass could be applied to a very sophisticated lens shape. It is known that a hyperhemisphere is the most difficult of lens shapes to coat. If a hyperhemispherical specimen can be given a reasonably uniform chalcogenide glass coating that will not peel off or separate, any window shape can be so coated. Prior to immersion, the average transmissibility of this specimen was measured at several places along the surface (table 7).

Elevation Angle (°)	Transmittance			
	Average (%)	Maximum (%)	Minimum (%)	Standard Deviation (%)
+45	70.44	71.67	69.21	1.10
+30	69.73	71.26	68.20	0.81
+15	71.06	72.13	69.99	1.00
0*	70.45	71.16	69.74	0.90
-15	69.83	70.34	69.32	0.50
-30	69.83	70.96	68.70	0.78

*Equator of the hyperhemisphere.

Table 7. Transmission measurements of the glass-coated germanium hyperhemispherical shell. Concave surface coated with monolayer AR composition XF 751; convex surface with 0.7-μm thick layer of AMTIR-1 chalcogenide glass. (Coatings by Optic Electronic)

The surfaces of the 3-inch and 8-inch specimens were fine ground with 8 μm grinding powder, then the flat surfaces were pitch polished so that the coating could adhere properly. On the 10-inch hyperhemisphere all surfaces were finished with 8 μm grinding powder, then the convex and concave surfaces were pitch polished so that the coating could adhere properly.

Chalcogenide glass was ion beam sputtered onto one surface of the 3-inch specimen, the convex surface of the hyperhemisphere, and one surface each of two of the three 8-inch specimens. One of the latter was coated with Optic Electronic multilayer antireflection coating XF 457 (monolayer zinc sulfide) on the surface opposite the chalcogenide glass coating (fig 37). The other was coated with XF 457 on that surface and with Optic Electronic multilayer antireflection coating XF 508 over the chalcogenide glass coating (fig 38). The third 8-inch germanium specimen (with no chalcogenide glass coating was coated on both faces with Exotic Materials 40100 (fig 39). This specimen was used in the test as a control or comparison standard, since the EM 40100 had been shown in previous experiments to be the most seawater-resistant standard AR multilayer coating.

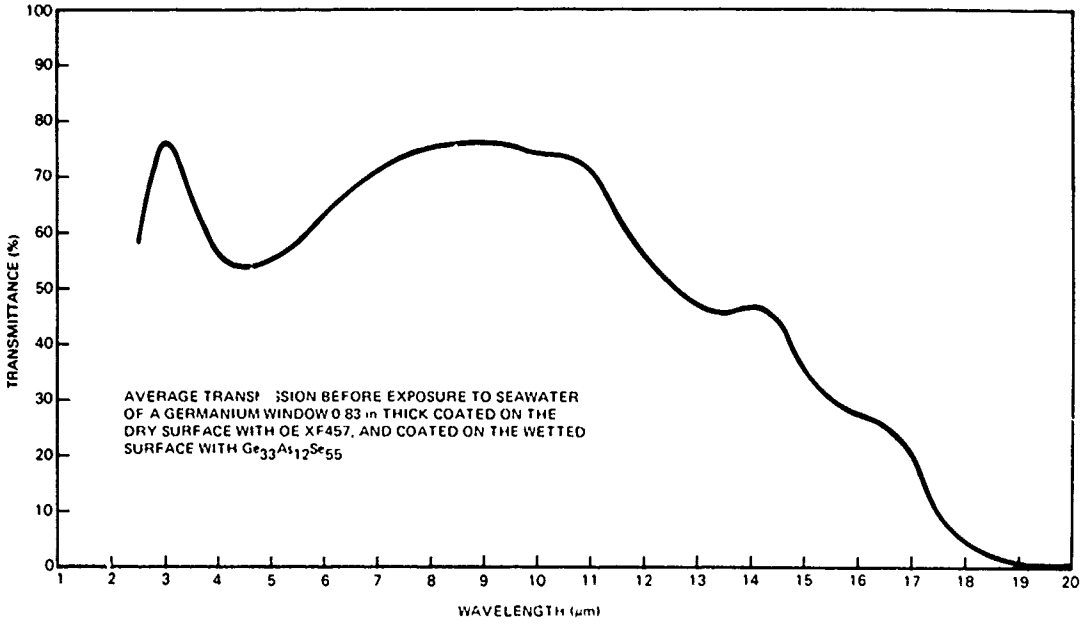

Figure 37. The average transmittance before exposure to seawater of a germanium disk 0.83-inch thick, coated on the dry surface with Optic Electronic multilayer antireflective composition XF457 and on the wetted surface with chalcogenide glass AMTIR-1 composition.

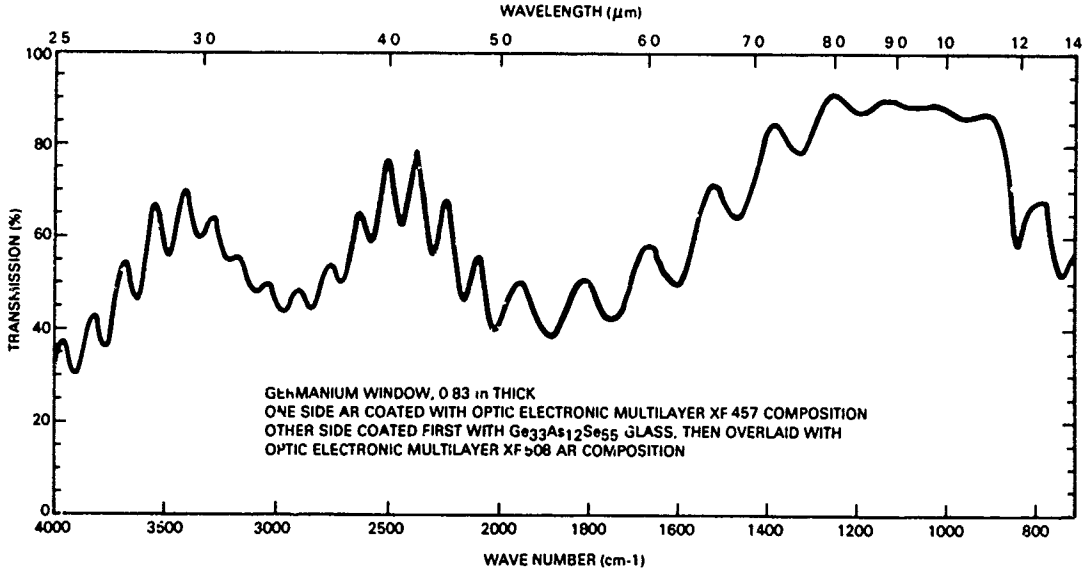

Figure 38. The transmittance, before exposure to seawater, of a germanium disk 0.83-inch thick, coated on the dry side with the Optic Electronic multilayer antireflective composition XF457 and on the wetted surface with chalcogenide glass AMTIR-1 composition overlaid with Optic Electronic Multilayer antireflective composition XF508.

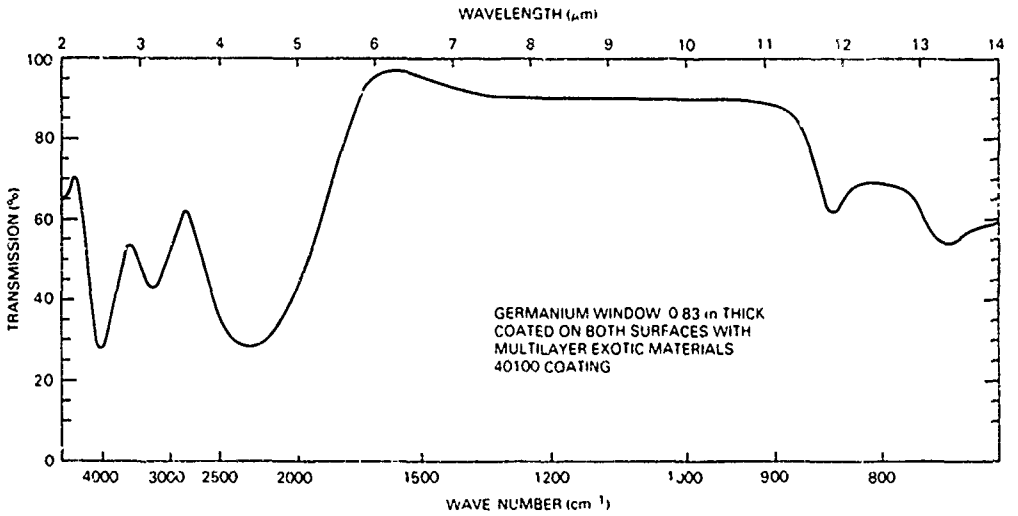

Figure 39. The transmittance of a 0.83-inch thick germanium disk coated on both surfaces with multilayer Exotic Materials 40100 antireflection compound prior to immersion in seawater. This specimen served as standard of comparison for the chalcogenide glass coatings since Exotic Materials 40100 composition has been found in past studies to protect germanium longer against corrosion than any other commercial antireflective coating.

TEST SETUP

INSTRUMENTATION

The only instrumentation used in the testing of material test specimens were load cells, which accurately indicated the magnitude of force applied during testing.

TEST FIXTURES FOR STRUCTURAL STRENGTH TESTS

Standard load application fixtures were used in the short-term uniaxial compression (fig 40) and flexure (fig 41) testing. The sole components that were custom-made for the test fixtures consisted of truncated conical steel anvils with minor diameter matching the diameter of the chalcogenide glass compression-test cylinders. Both the 20° included angle and the Rockwell C60 hardness of the anvil were based on experience with compression testing of glass, ceramic, and other brittle material specimens. It was found that the anvil configuration, anvil material, quality of bearing surfaces, and absence of gaskets were conducive to the generation of high test values during compression testing.

A special load-application fixture was designed and used for long-term flexure testing in seawater environments (fig 42). It consisted of an acrylic plastic compartmented tank with integral specimen holders and removable Monel rods. The rods served as sliding surfaces for nylon strings, which were used to suspend deadweights. By filling half the compartments with water, some of the test specimens were submerged in seawater during the test while the others were tested under atmospheric conditions. In this manner the comparison of test data from the wet and dry test specimens would not be contaminated by other test variables such as differences in temperature, load application procedure, and specimen holder design.

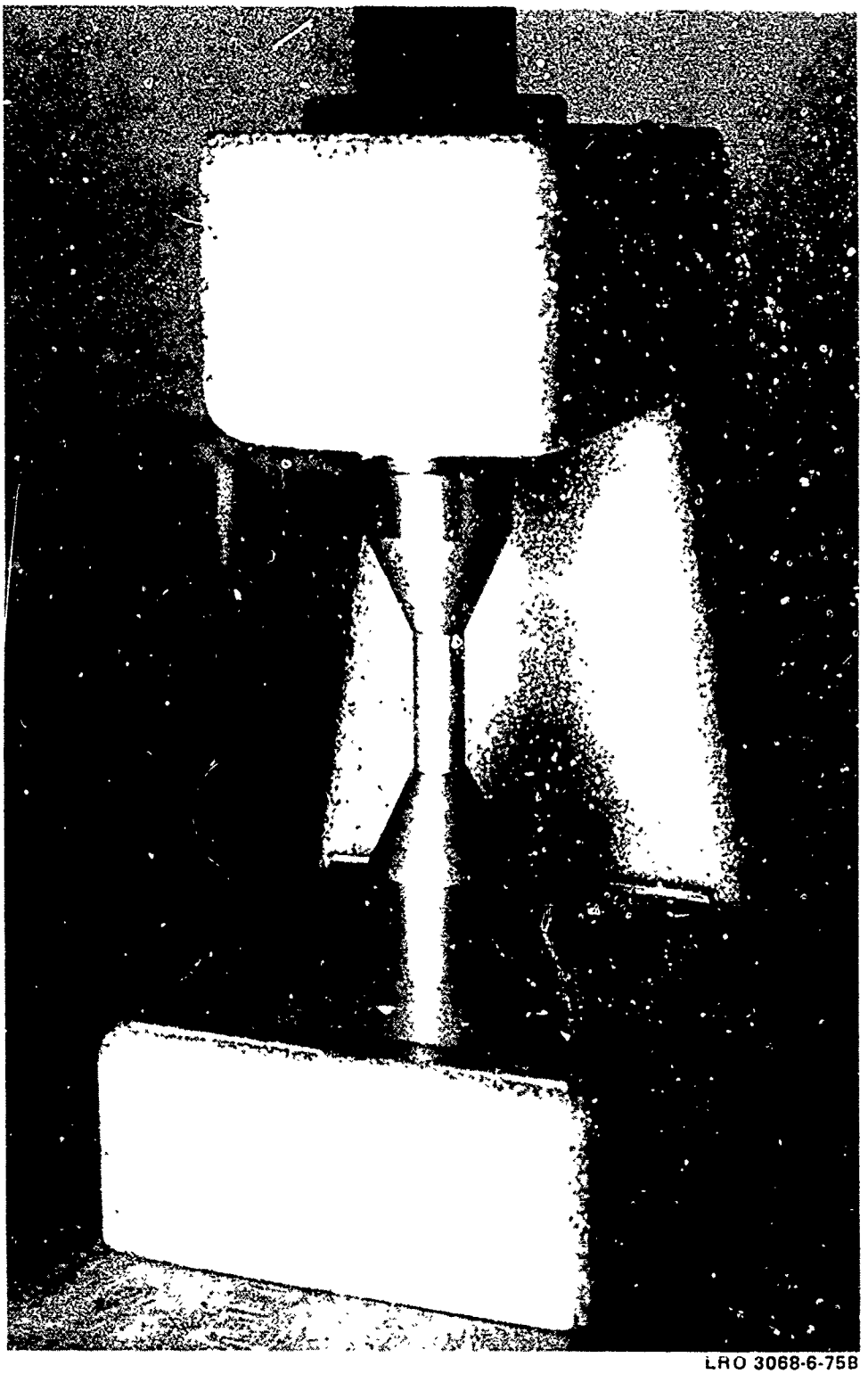

LRO 3068-6-75B

Figure 40. Test fixture for applying compressive load to the chalcogenide glass test specimens. Note that the diameter of the anvils matches the diameter of the test cylinder.

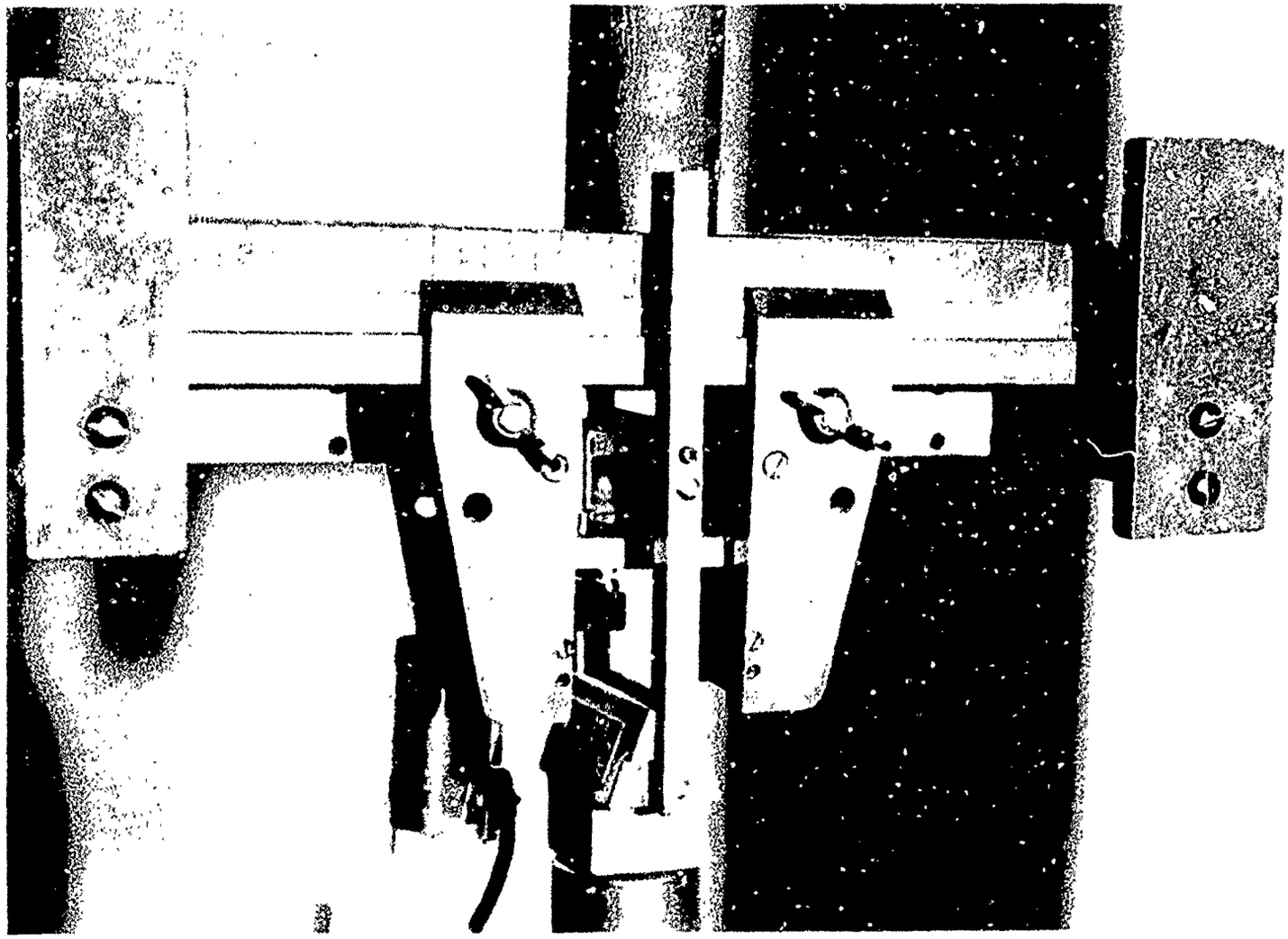

Figure 41. The short-term uniaxial flexure test fixture, used for applying a three-point bending moment to the chalcogenide test specimens.

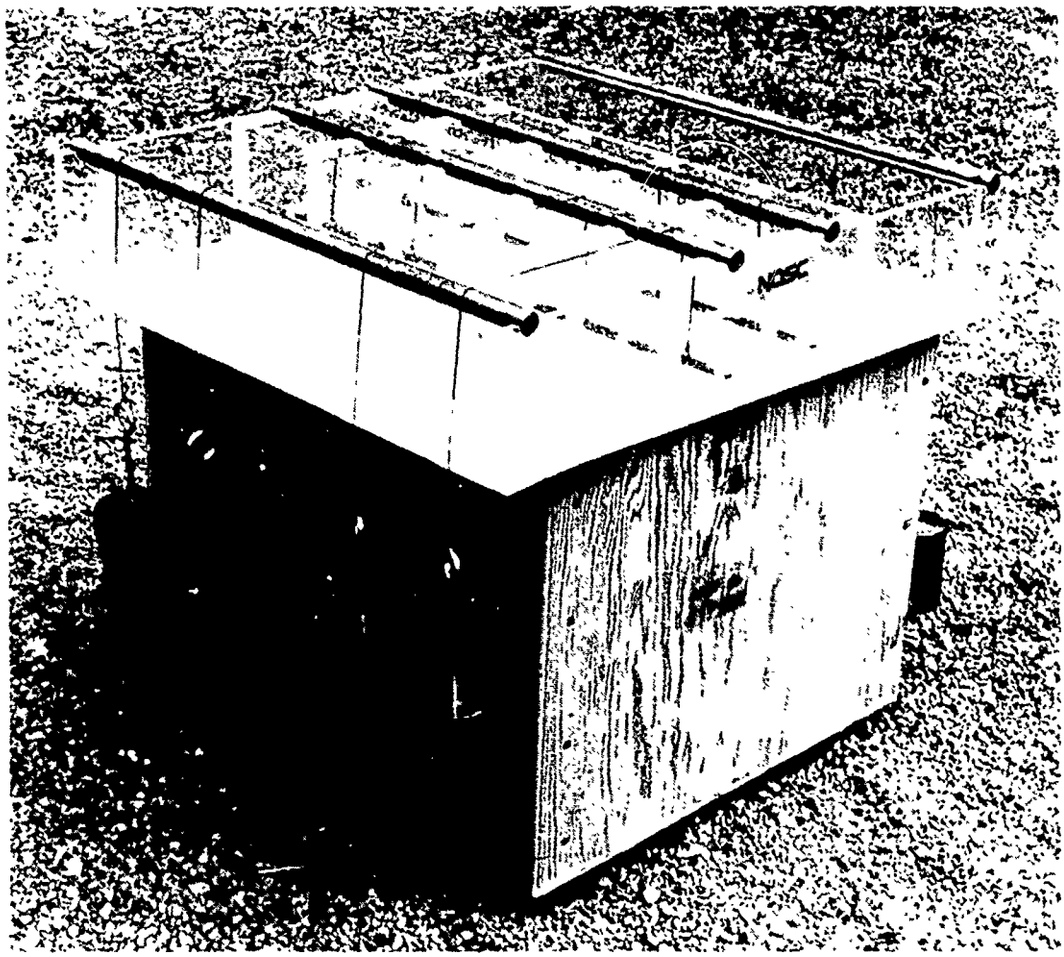

Figure 42. Test fixture for applying three-point bending moment over a period of time to chalcogenide glass test specimens.

For short-term biaxial flexure tests, a special fixture was used that supported a single 3-inch diameter test specimen at its periphery only (fig 43). A thin neoprene-coated nylon gasket is used between the specimen and the seat to take care of any unevenness between the two and as a hydraulic seal. The fixture fits inside a pressure vessel (fig 44) for applying hydrostatic pressure to one face of the 3-inch diameter disk under test.

Each spherical sector window used for hydrostatic and hydrodynamic biaxial testing was placed into a test fixture that simulated an operational window assembly mounted on an instrumentation housing (fig 45). The major departures from an operational configuration consisted of two simple, inexpensive substitutions: (1) a mounting ring of PVC plastic for the Delrin mounting ring and (2) a steel bulkhead for a large instrumentation housing. These substitutions allowed compression testing of the window assemblies in an available 10-inch diameter pressure vessel.

Figure 43. A 3-inch diameter disk test specimen being fitted into the biaxial flexure testing apparatus.

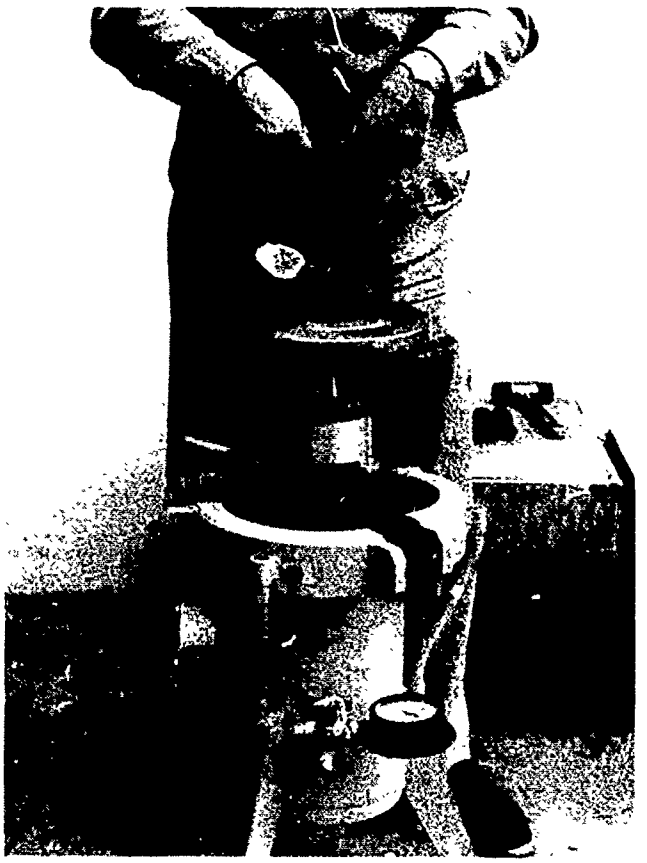

Figure 44. The biaxial flexure test fixture being lowered into the pressure vessel. Hydrostatic pressure applied against the face of the disk specimen causes it to flex. The interior of the test fixture is open to atmospheric pressure via the threaded pipe penetrating the vessel closure.

Figure 45. Spherical sector window in its mounting ring.

Composite gaskets (described under Preparation of Test Specimens) were used in the window assembly. The test fixture, developed by NOSC, was assembled by the following procedure:

1. Clean the bearing surfaces on the window with acetone.
2. Place the neoprene gasket on the window seat.
3. Cut off surplus gasket length with a razor blade without nicking the bearing surface. Take great care to cut the gasket in such a manner that the two ends of the gasket butt together with no overlap or gap.

4. Brush Pliobond contact cement on the top surface of the neoprene gasket and the bottom surface of the Kevlar epoxy gasket and press them together without creating wrinkles in the neoprene gasket. After the cement has set, remove the composite gasket from the mounting and inspect it.

5. Place the gasket on the window seat (fig 46). Pay particular attention to centering the gasket on the bearing surface (fig 47).

6. Place the window on its gasketed steel seat, which has already been inserted into the PVC mounting ring bolted to the top of the steel bulkhead (fig 48 and 49).

7. Insert the O-ring seal into the annular space between the outside diameter of the window and the lip of the window seat (fig 50 and 51).

8. Place the window retainer on top of the mounting ring (fig 52) and bolt it down securely with stainless steel screws to the mounting ring (fig 53). Tighten the screws to secure the window in its seat and to compress the O-ring for a secure seal.

9. Attach the window test fixture to the end closure of a pressure vessel (deep ocean simulator) by means of a threaded pipe that serves as a feedthrough for the instrumentation wires (fig 54).

Figure 46. Placing the composite gasket on the window seat.

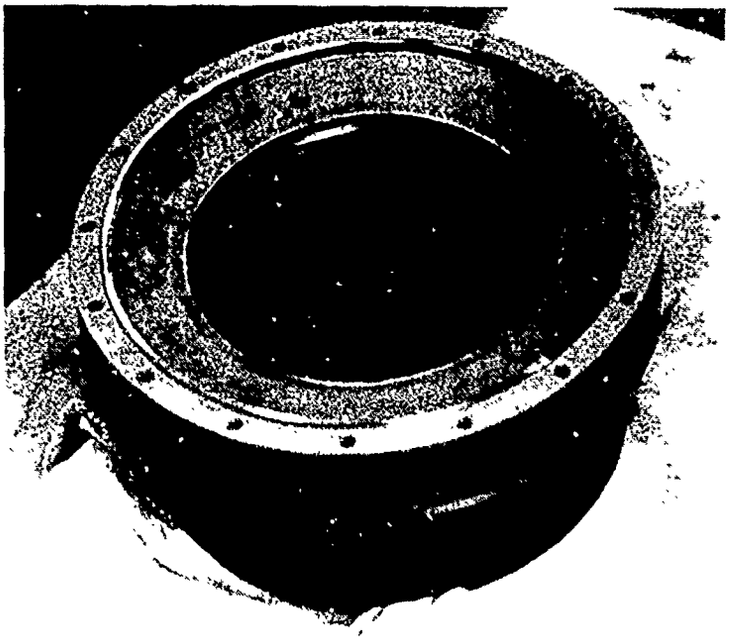

Figure 47. Gasket in place.

Figure 48. In placing the window in its gasketed metal seat, extra care must be taken to center the window prior to contact with the seat; otherwise the edge of the window may strike the metallic seat lip and become chipped.

Figure 49. After the window is seated, its position is adjusted until the annular space between its edge and the seat lip is uniform.

Figure 50. The O-ring seal for the window is lowered into the annular space between the edge of the window and the seat lip.

Figure 51. A wooden spatula is used to seat the O-ring into the annular space between the edge of the window and the seat lip.

Figure 52. The window retainer is placed on top of the mounting ring.

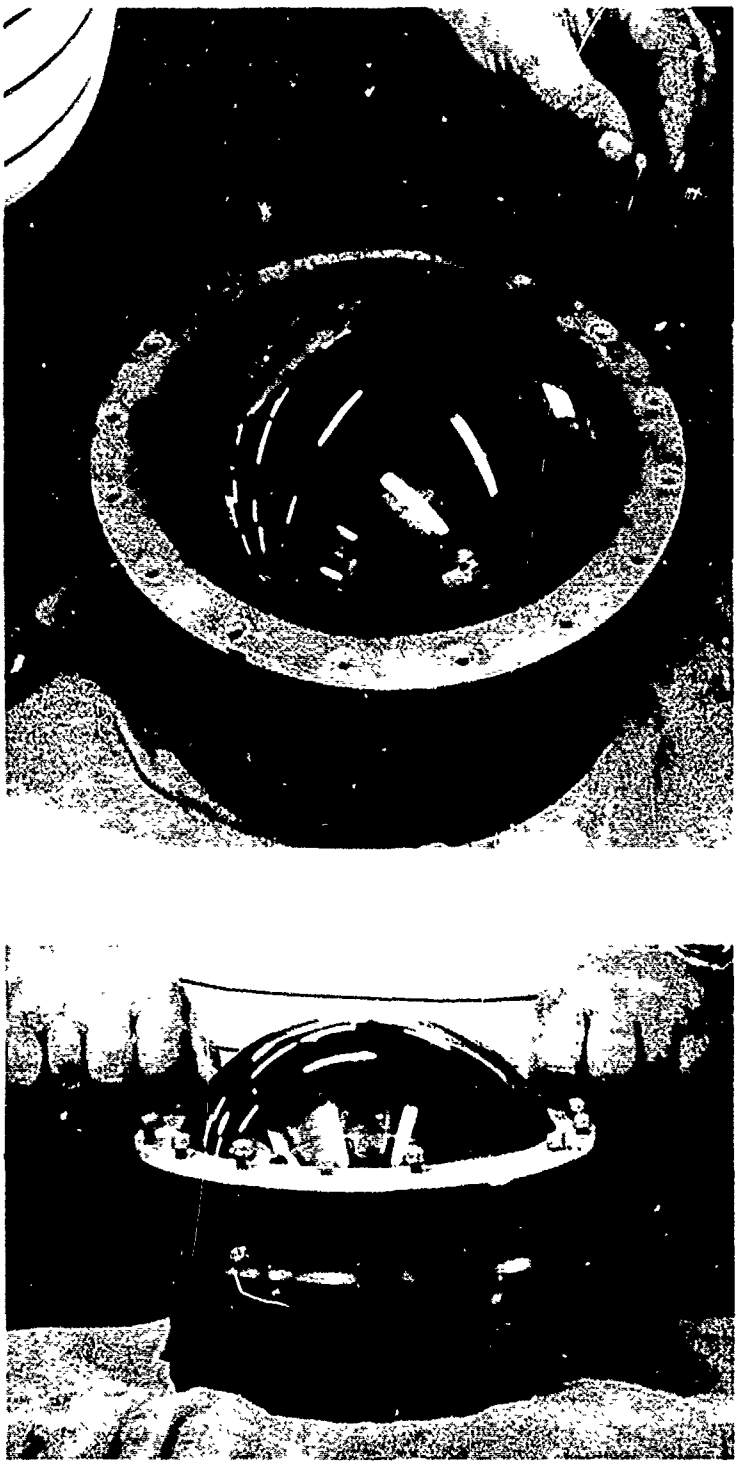

Figure 53. The bolt holes are lined up and screws are inserted through the window retainer into the mounting ring.

Figure 54. The window test fixture, consisting of the window mounting, mounting ring, window retainer, and bulkhead, is attached to the pressure vessel end closure by means of a threaded pipe nipple.

The flange and the mounting of the spherical test specimen have been evaluated in previous studies (ref 25) and found to be well-suited for high-pressure service. Spherical sector test specimens previously evaluated in this test fixture included specimens of quartz, glass, transparent ceramic, and germanium. All were found to perform satisfactorily in this particular mounting. Thus there was no doubt that the critical pressure of the spherical sector, when tested in this flange, would not be a function of the mounting but would represent only the structural performance of the chalcogenide glass.

The test fixture for dynamic impulse loading of spherical sector windows was a 10-foot diameter, 100-foot deep well at Southwest Research Institute, in San Antonio, Texas. The windows under test are mounted into the same K-500 Monel seat used for the short-term biaxial compression tests in the deep ocean simulator. The window test assembly is bolted to a steel frame that can be lowered to any desired depth in the well by means of a cable and winch (fig 55). Dynamic impulse loading is applied to the window by setting off underwater explosive charges near it.

TEST FIXTURES FOR CORROSION-RESISTANCE TESTS

The test fixtures for the corrosion testing of the 3-inch massive chalcogenide glass disks were multiple-specimen holders made of polyvinyl chloride (PVC). Each specimen holder had recesses into which the specimens were sealed by titanium ring clamps and rubber O-rings affixed by nylon bolts (fig 56). The assembled fixtures also had protective acrylic plates, which were held above the PVC baseplate by PVC studs and spacers (fig 57).

The chalcogenide specimens were tested in these fixtures alongside AR-coated germanium specimens in a comparison of performance. Three of the massive chalcogenide glass specimens were tested under natural circulation conditions in the fixture shown in figure 54. The other four massive chalcogenide glass specimens were tested in a fixture of the same basic type modified to have a 6-ft/s stream of water impinge upon each of the specimens (fig 58). The impinging stream of water had a twofold purpose. First, it was to be evaluated as an antifouling measure. Secondly, the effect of water impingement upon specimen surfaces was to be studied as a simulation of a window extended for use on a moving submarine.

The 3-inch disk of germanium coated with chalcogenide glass was also tested in the natural circulation multiple-specimen test fixture (fig 57).

Two test fixtures were built for testing the larger 8-inch disks of germanium coated with various AR and glass combinations. One was a dual-specimen fixture which had a hollow PVC base plate and a recessed seat on each side for the specimens. The two specimens were held in place by stainless steel ring-clamps secured by stainless steel bolts. An acrylic protective plate covered each specimen (fig 59 and 60). The other was a single-specimen test fixture similar to the dual fixture but with only one recessed seat for a specimen and having solid PVC on the reverse side (fig 61 and 62).

The chalcogenide-glass-coated germanium hyperhemisphere was mounted (fig 63) and sealed to a titanium base (fig 64). The base plate held three apertures for threaded stainless steel bolts connecting the base with a titanium top plate, which served as protection for the hyperhemisphere as well as a fastening bulkhead for transportation handles. The top plate was affixed to the three threaded bolts by stainless steel hex and wing nuts.

The corrosion-resistance test fixtures are submerged in seawater by attaching them to a hydraulic hoist that can be lowered to a 35-foot depth (fig 65). The hoist is located in San Diego Bay off Berthing Pier 160, NOSC Bayside.

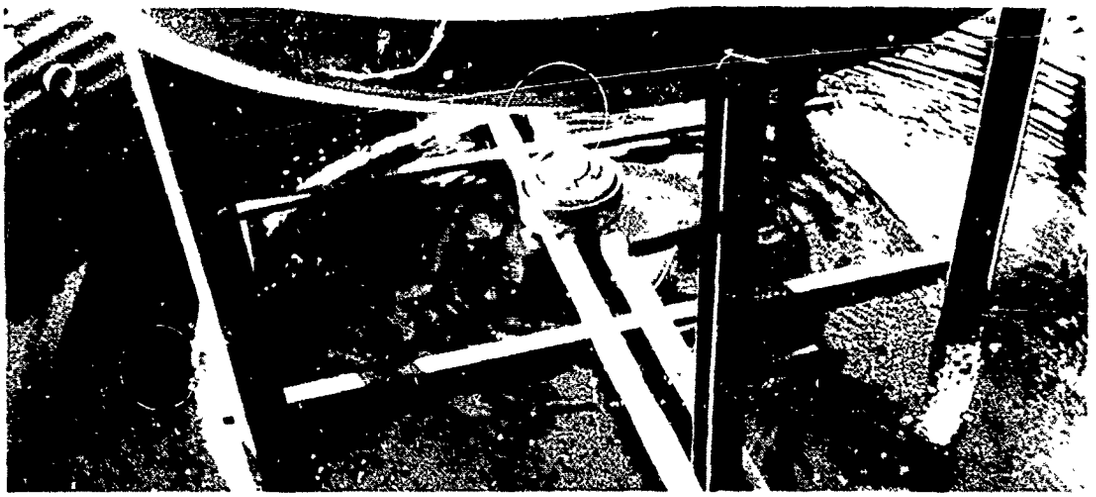

Figure 55. Fixture used for lowering the glass spherical sector assembly into the 100-foot well for underwater explosion tests. The spherical sector faces the explosive suspended above it.

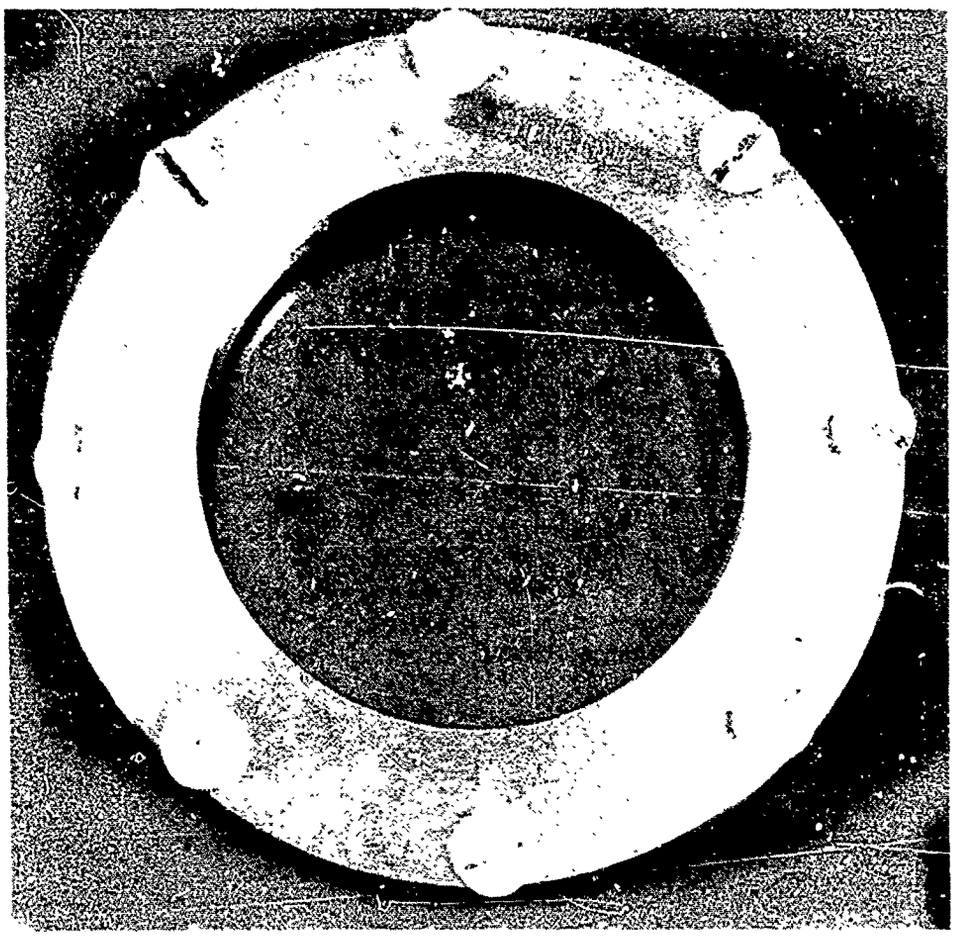

Figure 56. The 3-inch diameter germanium cylindrical disk coated with chalcogenide glass after placement in mounting.

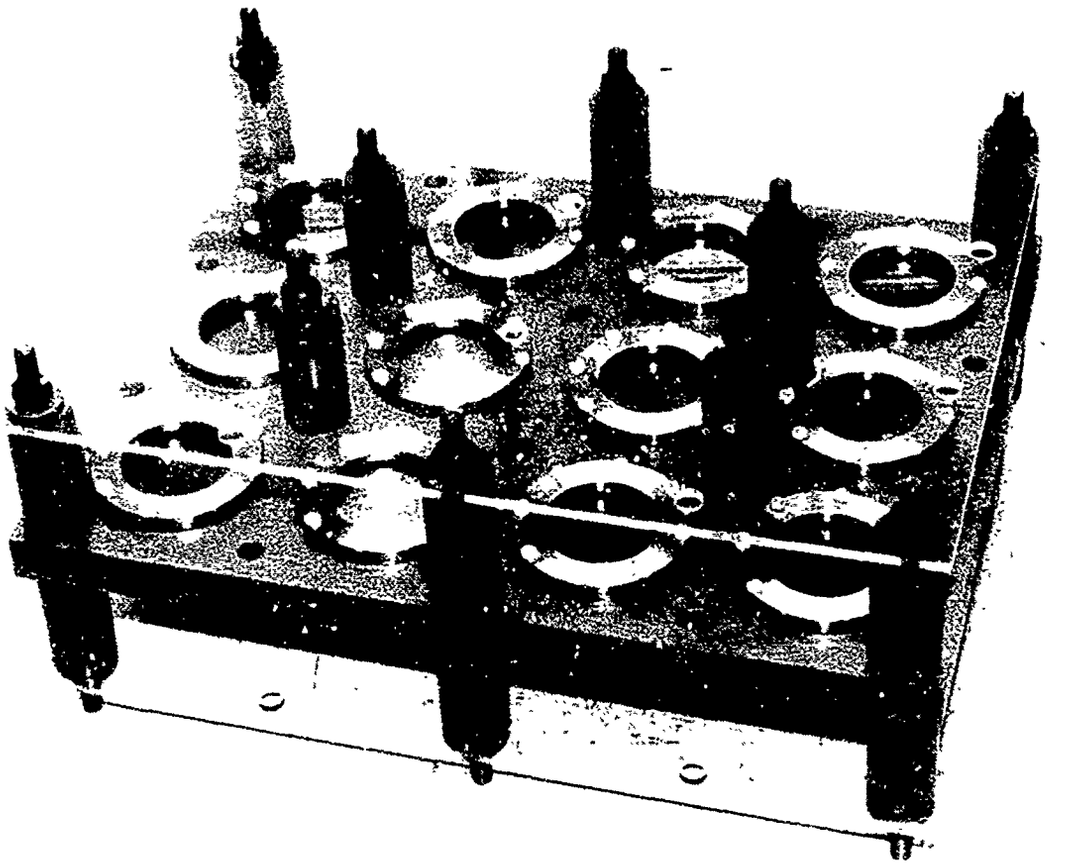

LRO 2675-7-78B

Figure 57. A multiple-specimen test fixture used for seawater resistance testing of 3-inch diameter germanium and chalcogenide glass specimens. The specimens in this test fixture are subjected only to natural circulation provided by tidal currents.

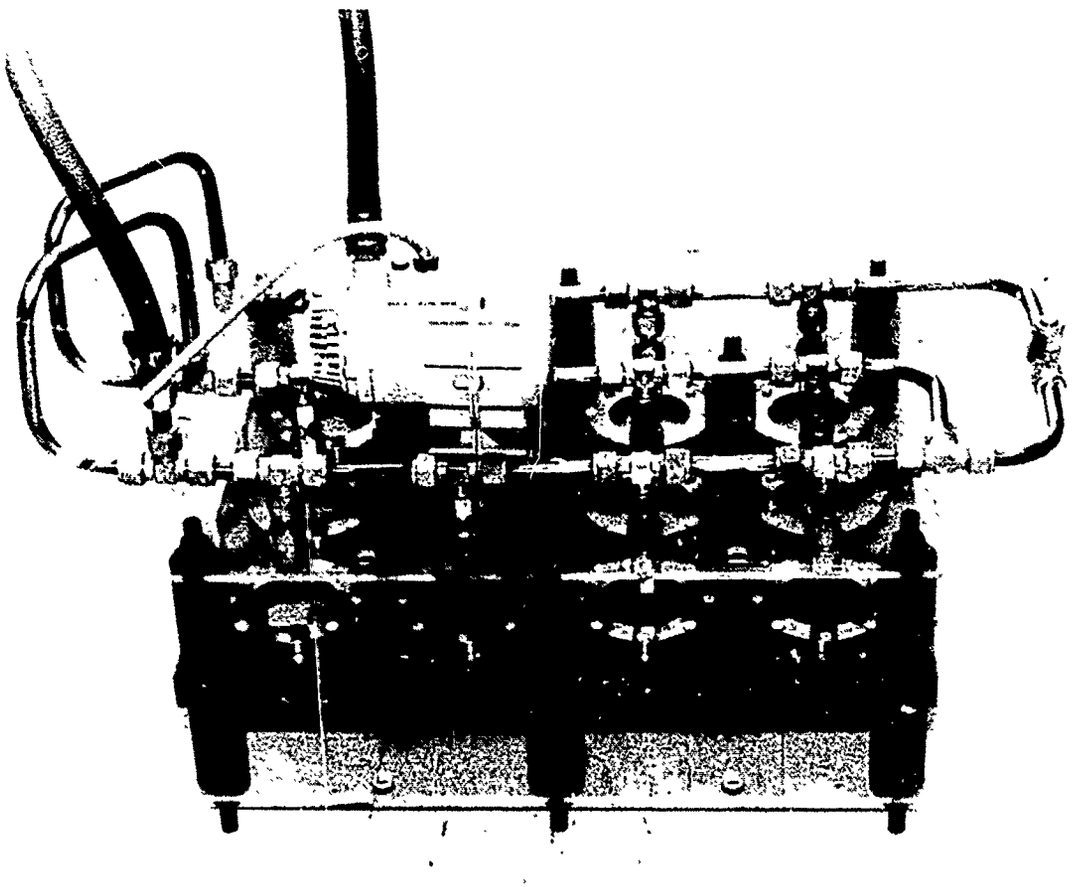

LRO 2676-7-78

Figure 58. The multiple-specimen test fixture used for seawater resistance testing of 3-inch diameter germanium and chalcogenide glass specimens. The submersible pump supplies water to individual jets above each specimen. The acrylic protector plate centers individual jets above each specimen and maintains a fixed distance between the tips of the jets and the surface of the specimens.

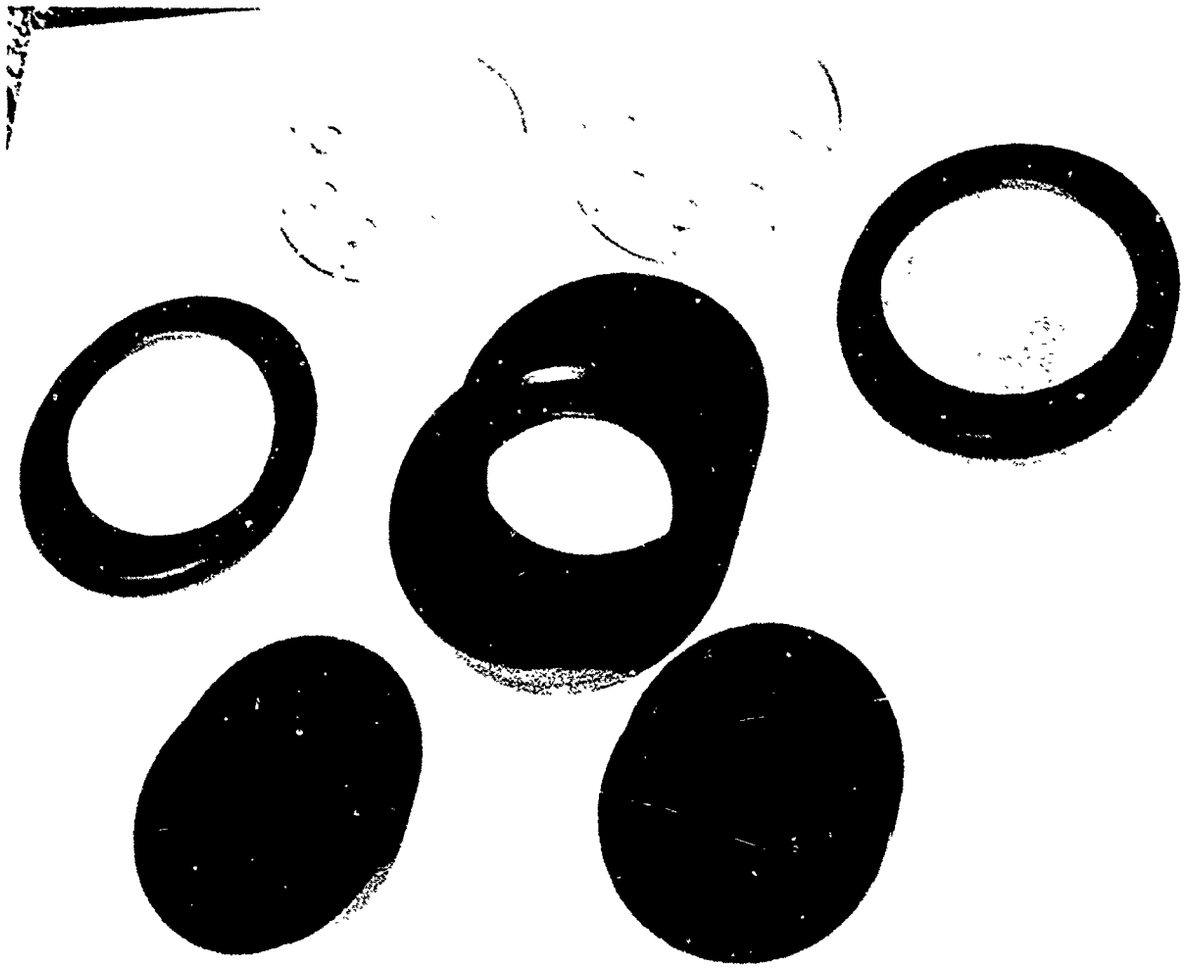

Figure 59. Disassembled test fixture, including two specimens, used for corrosion testing of two of the 8-inch coated germanium specimens. Note the acrylic protector for preventing physical surface damage to specimens.

Figure 60. The assembled two-specimen test fixtures used for the testing of the 8-inch coated germanium specimens.

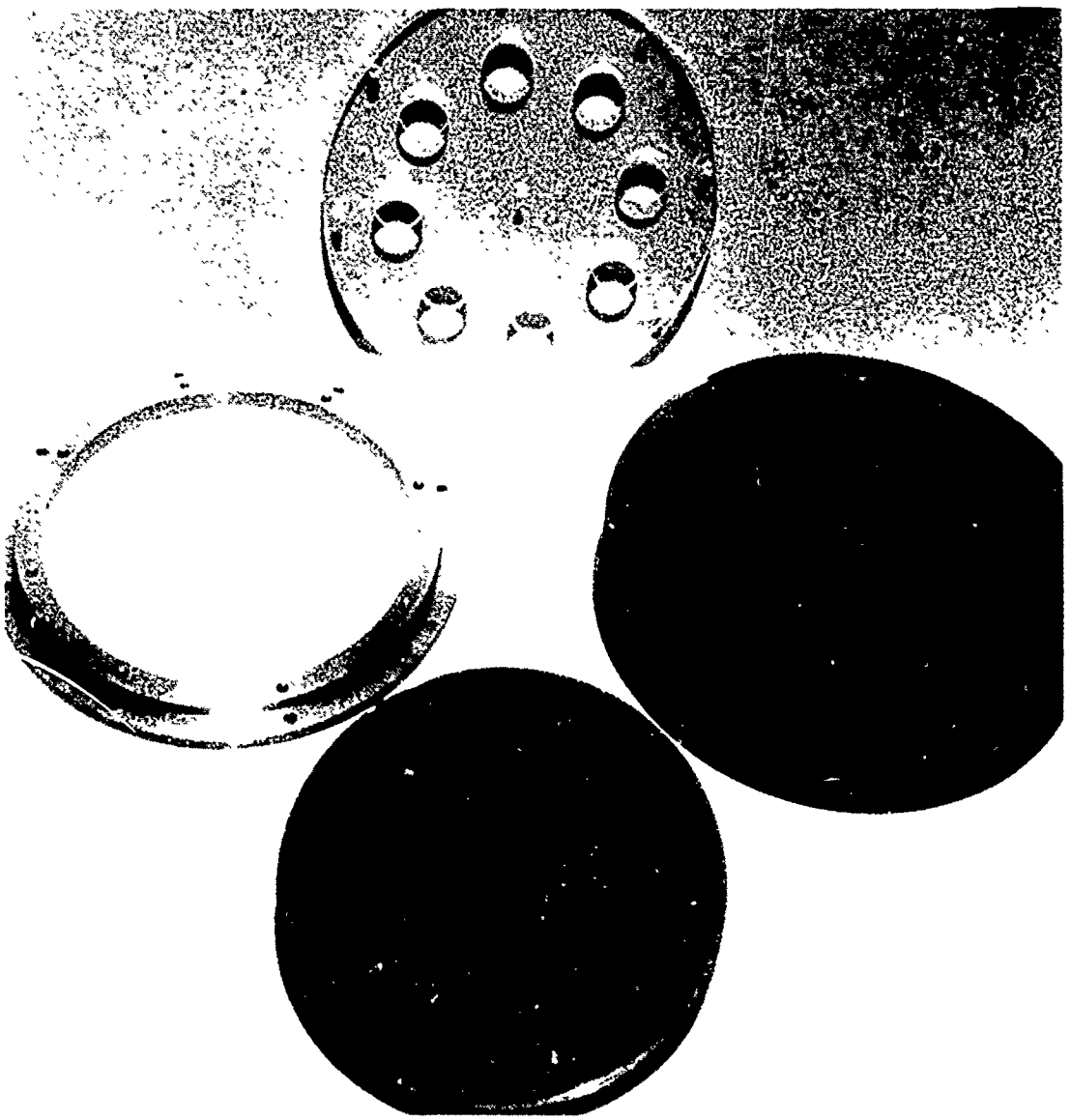

Figure 61. The single-specimen test fixture for an 8-inch coated germanium specimen, shown disassembled with the single specimen.

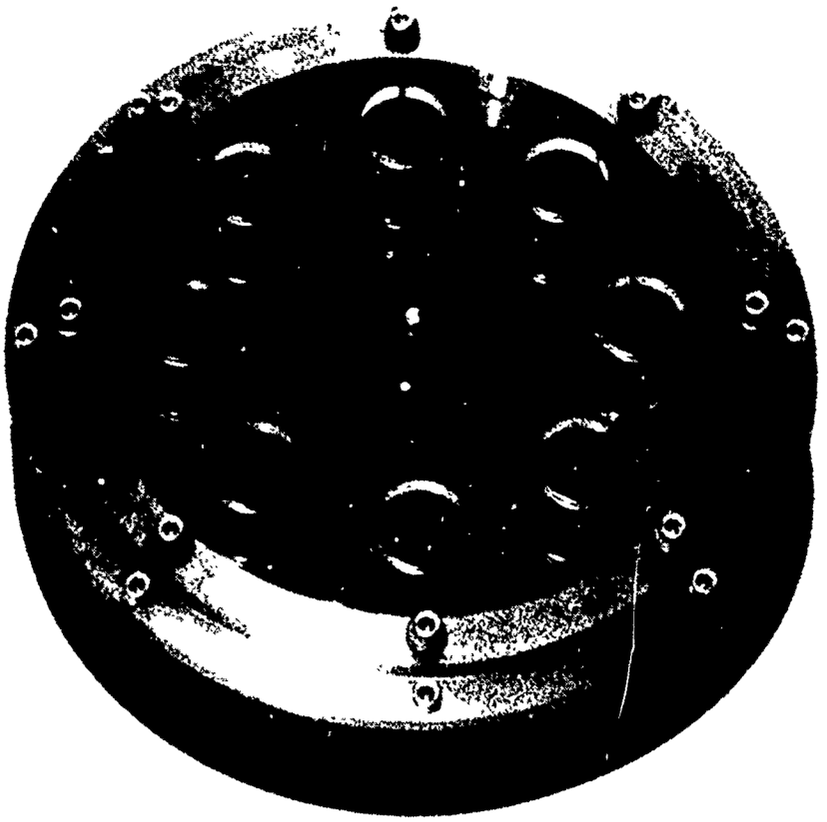

Figure 62. Close-up of the assembled 8-inch single-specimen test fixture.

Figure 63. Hyperhemispherical germanium shell, coated with chalcogenide glass, assembled in its mounting flange.

Figure 64. The chalcogenide glass coated germanium hyperhemisphere in its test fixture prior to mounting on the underwater elevator carriage.

Figure 65. The testing fixtures with corrosion test specimens attached to the submersible platform on inclined underwater railway.

TEST PROCEDURES

SHORT-TERM UNIAXIAL COMPRESSION

Short-term uniaxial compression loading was performed by carefully centering a compression test specimen on the bare anvils in a hydraulically operated loading machine (fig 40) and applying compression at 0.05-inch/minute crosshead speed (1000 psi/minute) until fracture of the specimen took place.

SHORT-TERM UNIAXIAL FLEXURE

Short-term uniaxial flexure loading was performed with a standard three-point load application fixture that bore directly against the test specimen (fig 41). The fixture was attached to a hydraulically operated testing machine. Testing was conducted in a laboratory environment under standard laboratory temperature, pressure, and humidity. The load was applied at 0.02-inch/minute until fracture of the specimen took place.

LONG-TERM UNIAXIAL FLEXURE

Long-term uniaxial flexure loading was performed by placing the test specimens inside the acrylic plastic test fixture (fig 42) and filling half the test-specimen compartments with seawater. The deadweights were chosen to apply flexure stress in the range of 1000 to 4000 psi. The reason for selecting this particular range of flexure stress was to approach (but not too closely) the ultimate modulus of rupture for specimens under short-term loading. By selecting a long-term stress level about 15 to 50% lower than the average value of short-term flexure strength, the premature failure of test specimens during the application of dead loads could be minimized, but the stress level would be high enough that the effect of static fatigue would become apparent in a matter of days rather than months. The long-term testing was executed outdoors in a diurnal temperature range of 50–100°F and relative humidity fluctuation of 40–90%, under about standard atmospheric pressure.

SHORT-TERM BIAXIAL FLEXURE

Short-term biaxial flexure loading was accomplished by placing a 3-inch diameter, 1/4-inch thick specimen of either chalcogenide glass or germanium into the test fixture (fig 43), inserting it into the pressure vessel (fig 44), and applying unidirectional hydrostatic loading from one side until failure of the specimen took place. Specimens of both types were used to obtain a direct comparison between the two materials.

SHORT-TERM BIAXIAL COMPRESSION

Hydrostatic loading was applied to the spherical sector from the convex side in a deep ocean simulator at the Southwest Research Institute in San Antonio, Texas (fig 54). Loading consisted of pressurizing the test specimen at 1000 psi/minute to failure. The objective was to determine the optical pressure of the specimen (ie, the highest value of pressure that it could survive) under a rapid pressure rise.

CYCLIC BIAXIAL COMPRESSION

Cyclic biaxial compression loading was performed in the deep ocean simulator of the Southwest Research Institute to determine the resistance of chalcogenide glass to

fatigue cracks generated by repeated pressure loading and unloading of the specimen. Cyclic pressure was applied by hydraulically loading to the required pressure at 1000 psi/minute holding the pressure at that point for 4 hours, then relieving the pressure at 1000 psi/minute to 0 psi (gage). The specimen was then allowed to relax at 0 psi gage for 4 hours, and the cycle was repeated.

Cyclic pressure loading was applied to a given window until the window failed. Failure was defined either as catastrophic specimen failure or as the presence of any sign of damage that rendered the specimen useless for its intended application. Each specimen was tested to a different maximum cyclic hydraulic pressure. One was cycled to 9000 psi, one to 4500 psi, and one to 2250 psi.

DYNAMIC IMPULSE

Dynamic impulse loading, performed in the 10-foot diameter, 100-foot deep well at Southwest Research Institute (fig 55), was applied to the window by setting off 9-g charges of pentolite suspended a given distance above it. After every explosion, the window assembly was retrieved from the well and inspected for damage. If no damage was detected, the window was then reimmersed in the well and the charge set off a little closer to the window. This process was repeated until the window fractured.

CORROSION

Corrosion testing was done in the San Diego Bay test fixture (fig 65). Specimens were raised once per week to be inspected and hosed off with tap water. Specimens were submerged for periods of 4 months. Photographic and qualitative observational data were taken at regular intervals.

TEST RESULTS – MASSIVE CHALCOGENIDE GLASS SPECIMENS

SHORT-TERM UNIAXIAL COMPRESSIVE STRENGTH

The test specimens failed in a stress range of 18 335–25 147 psi, with an average ultimate compressive strength of 20 924 psi. Catastrophic failure of the specimen (fig 66) was in most cases preceded by audible cracking of the material, which occurred at between 17 and 91% of the ultimate stress (table 8), averaging 73% (median 81%). Only one of the 20 specimens fractured without prior audible cracking. Thus there was usually adequate warning prior to failure. The fracture planes ran parallel to the axis of load application, indicating that the material failed in tension even though the load was compressive. The stresses at which failure occurred in the various specimens indicate that the material was fairly uniform; the deviation from the average of failure stresses was less than 25%.

SHORT-TERM UNIAXIAL FLEXURAL STRENGTH

The specimens failed catastrophically, without prior warning by audible cracking (fig 67). The variation in stresses between individual specimens was very small, ranging from 1620 to 4036 psi, with an average of 2528 psi (tables 9 and 10). Note that the stresses recorded during the flexure testing of specimens that were left unpolished are not much lower than the stresses of the polished test specimens. The average modulus of rupture (flexural strength) for unpolished flexure specimens was 2620 psi, while that for polished specimens was 2511 psi.

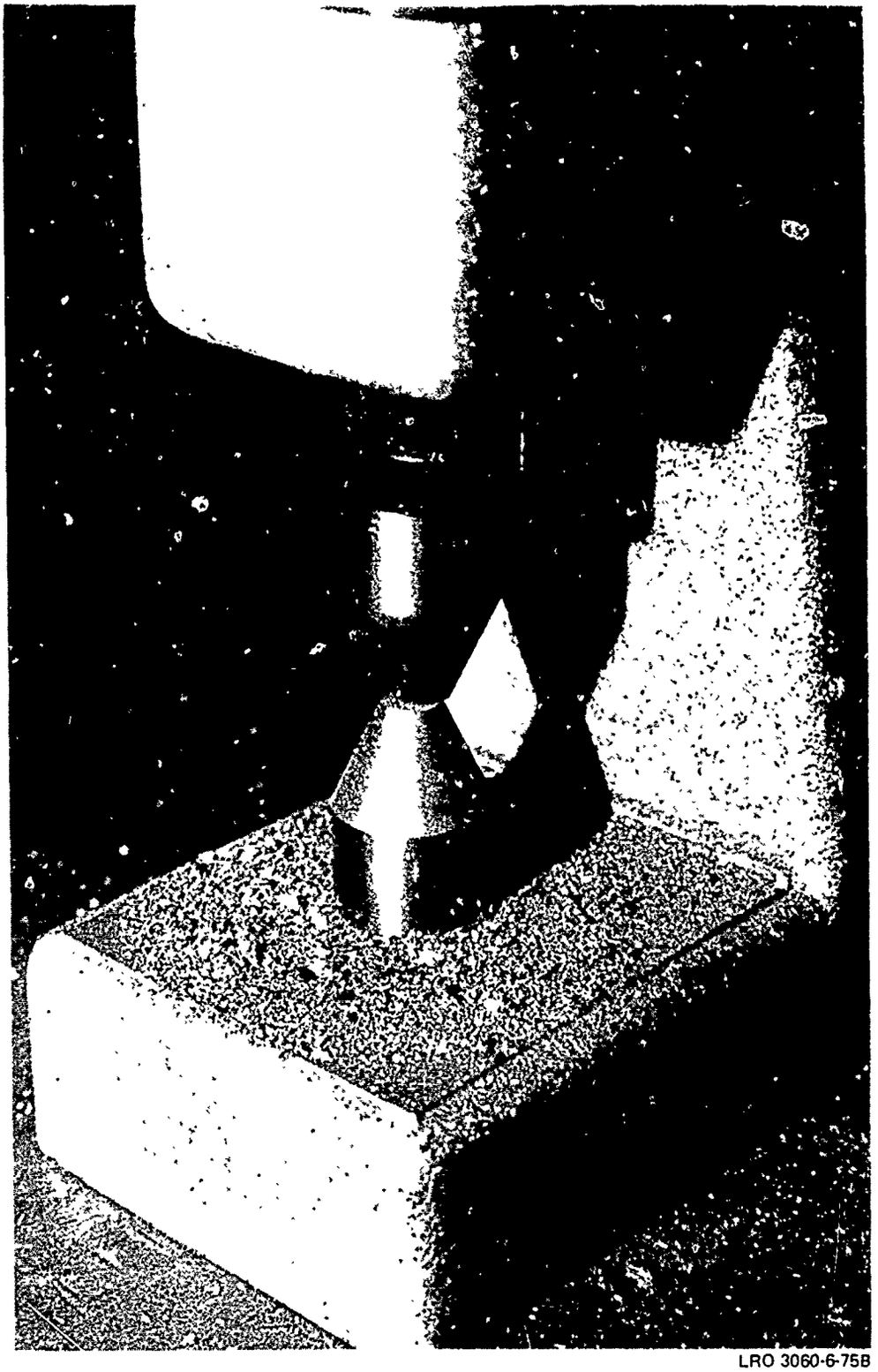

LRO 3060-6-75B

Figure 66. Fragments of a glass specimen that failed catastrophically under short-term compressive loading.

Specimen No	Diameter (inches)	Length (inches)	Load Cracking (lbf)	Load Failure (lbf)	Stress Cracking (psi)	Stress Failure (psi)
1	1.000	1.80	13 000	15 300	16 553	19 481
2	1.000	1.80	14 500	16 000	18 462	20 372
3	1.000	1.80	–	14 400	–	18 335
4	1.000	1.80	16 500	18 900	21 009	24 065
5	1.000	1.80	14 800	16 500	18 844	21 009
6	1.000	1.80	15 000	16 500	19 099	21 009
7	1.000	1.80	13 000	16 100	16 553	20 500
8	1.000	1.80	14 000	15 600	17 826	19 863
9	1.000	1.80	3 000	17 500	3 820	22 282
10	1.000	1.80	13 500	15 700	17 189	19 990
11	1.000	1.80	4 500	13 000	5 730	16 553
12	1.000	1.80	12 700	16 400	16 171	20 882
13	1.000	1.80	13 000	15 650	16 553	19 927
14	1.000	1.80	14 800	18 900	18 844	24 065
15	1.000	1.80	15 500	17 700	19 736	22 537
16	1.000	1.80	13 000	16 500	16 553	21 009
17	1.000	1.550	18 000	19 750	22 919	25 147
18	1.000	1.550	9 000	16 500	11 459	21 009
19	1.000	1.550	10 000	17 000	12 733	21 646
20	1.000	1.550	5 000	15 000	6 366	19 009

Crack initiation stress: Min = 3 820 Avg = 14 820 Max = 22 919
Ultimate compressive strength: Min = 18 335 Avg = 20 934 Max = 25 147

Notes:
1. The testing rate was about 1000 psi/second
2. The specimens were tested on bare steel a[illegible]s 1.0 inch in diameter.

Table 8. Compressive strength of AMTIR-1 short-term loading.

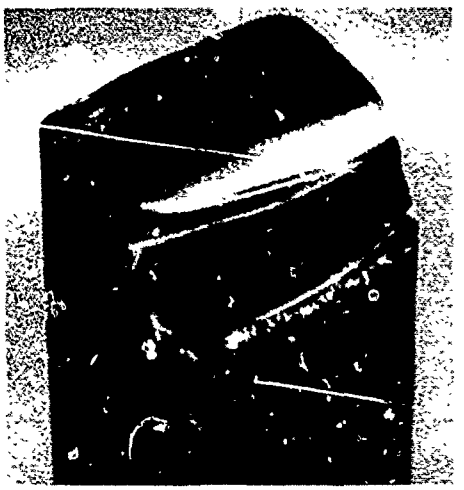

Figure 67. The fractured surface of a glass specimen that was subjected to short-term un axial flexure loading. Note smooth fracture plane typical of amorphous materials.

Specimen No	Thickness (inches)	Width (inches)	Maximum Load (lbf)	Type of Failure	Flexural Strength (psi)
Ground bars					
1	0.356	0.382	24.5	Fracture	2660
2	0.357	0.384	22.8	Fracture	2450
3	0.357	0.384	20.8	Fracture	2230
4	0.356	0.384	24.4	Fracture	2630
5	0.356	0.383	26.8	Fracture	2900
6	0.356	0.384	23.7	Fracture	2560
7	0.356	0.384	25.0	Fracture	2700
8	0.355	0.383	25.7	Fracture	2800
	Minimum: 2230 psi	Average: 2620 psi		Maximum: 2900 psi	
Polished bars					
9	0.578	0.623	77.5	Fracture	2090
10	0.576	0.624	111.1	Fracture	3020
11	0.578	0.624	88.7	Fracture	2390
12	0.578	0.624	77.0	Fracture	2080
13	0.578	0.624	60.4	Fracture	1620
14	0.578	0.624	79.3	Fracture	2140
15	0.577	0.623	63.8	Fracture	1730
16	0.576	0.623	78.3	Fracture	2130
17	0.577	0.623	102.9	Fracture	2790
	Minimum: 1620 psi	Average: 2220 psi		Maximum: 3020 psi	

Notes:

1. Test Method ASTM-C-674 at 0.05 inch/minute rate.
2. Ground bars were lapped with 12 μm grit on sides and 400 μm mesh on bevels.
3. Polished bars were lapped with 12 μm grit and polished with 6 μm grit in suspension on sides. Bevels were made with 400 μm mesh and polished with 20 μm compound.
4. All bars were 4.0 inches long.

Table 9. Comparison of flexure strengths for AMTIR-1 bars with ground and polished surfaces under short-term loading.

Specimen No	Dimensions (inches)	Loading (lbf)	Span (inches)	Moment (lbf-in)	Maximum Stress (psi)	Time Duration
Short -term loading						(seconds)
1	0.490 X 0.436H	39	4.955	48.31	3111.85	<1
2	0.477 X 0.392H	22	4.955	27.25	2230.62	<1
3	0.473 X 0.382H	19	4.955	23.53	2045.43	<1
4	0.480 X 0.383H	17	4.955	21.05	1793.76	<1
5	0.478 X 0.382H	25	4.955	30.96	2663.16	<1
6	0.483 X 0.384H	23	4.955	28.49	2400.12	<1
7	0.478 X 0.381H	18	4.955	22.29	1927.45	<1
8	0.476 X 0.381H	36	4.955	44.59	3871.75	<1
9	0.480 X 0.384H	35	4.555	39.85	3378.08	<1
10	0.471 X 0.385H	38	4.945	46.97	4036.60	<1
	Minimum = 1793.76 psi		Average = 2745 psi		Maximum = 4036.60 psi	
Long-term loading						(minutes)
11	0.483 X 0.383H	18	4.955	22.29	1887.62	1.5
12	0.478 X 0.381H	14	4.955	17.34	1499.41	900
13	0.478 X 0.382H	14	4.555	15.94	1371.14	112 320*
14	0.473 X 0.381H	14	4.946	17.31	1512.64	112 320*
15	0.478 X 0.381H	14	4.675	16.36	1414.67	60
16	0.478 X 0.431H	18	4.955	22.29	1506.18	17
17	0.481 X 0.380H	14	4.675	16.36	1413.26	43 200
18	0.480 X 0.387H	20	4.480	22.40	1869.54	9
19	0.479 X 0.382H	14	4.955	17.34	1488.46	112 320*
20	0.481 X 0.381H	15	4.480	16.80	1443.66	1 200
21	0.480 X 0.382H	18	4.675	21.03	1801.45	0.03

*Test terminated without specimen fracture.

Notes:

1. Specimens were lapped with 12 μm grit and polished with 8 μm slurry.
2. Specimens were beveled with 400 μm mesh and polished with 20 μm compound.
3. Loading was generated by manually applied dead weight at the center of the bar.
4. Tests were conducted in atmospheric environment, 50-100° diurnal variation.
5. All bars were 6.0 inches long.

Table 10. Polished bars of AMTIR-1 under short-term and long-term flexure loading.

LONG-TERM UNIAXIAL FLEXURAL STRENGTH

As in the short-term uniaxial flexural strength tests, audible cracking did not precede specimen failure. The modulus of rupture (table 10) appeared to be a function of time, as was expected. The dispersion between test results was quite large, indicating that there must be many boundary weaknesses or incipient flaws in the material that cause a wide variation of failure stress under sustained loading.

It is obvious from a comparison of the short- and long-term testing that if chalcogenide glass is subjected to less than 50% of its average short-term modulus of rupture (flexural strength), failure due to static fatigue can be forestalled or avoided provided the duration of loading does not exceed 1000 hours. Figure 68 shows a semilog plot of the long-term flexure test data. If the data are plotted on log-log coordinates, those beyond

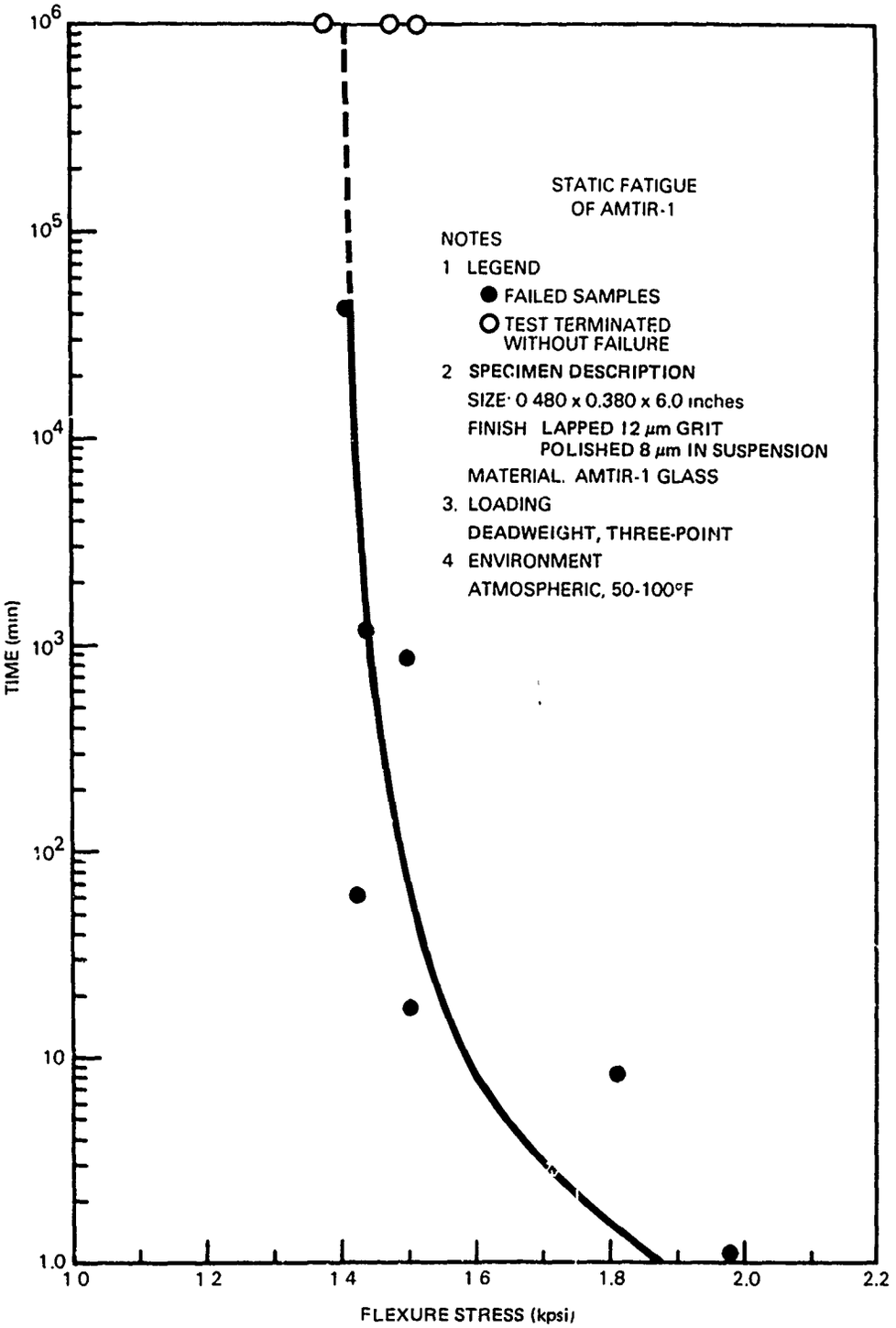

Figure 68. Static fatigue life of AMTIR-1 chalcogenide glass specimens under long-term sustained flexure loading.

about an hour fall on a reasonably straight line. Thus the stress at which failure will occur under long-term loading can be extrapolated far into the future. We can predict with reasonable certainty what the maximum allowable stress level should be in a chalcogenide window or lens under long-term flexure loading even though the test itself extended only for a duration of 1000 hours.

SHORT-TERM BIAXIAL FLEXURAL STRENGTH

There was no audible cracking preceding the catastrophic failure of the test specimens (fig 69). The variation in modulus of rupture between some of the test specimens was quite large (1925 to 2750 psi, table 11). The average modulus of rupture (2255 psi), calculated from the hydrostatic pressure that caused the disks to fail, indicated that the stress level at which fracture occurred was only a little lower than that of specimens under uniaxial flexure loading (2528 psi). The average modulus of rupture of germanium disks of identical dimensions was, as expected, found to be much higher (12 650 psi) than that of chalcogenide glass (2255 psi). However, the range of stresses at which germanium specimens failed (9625 to 16 500 psi) was wider than the range of stresses at which the chalcogenide glass specimens failed (1925 to 2750 psi). Incipient sources of failure seem to be less uniformly distributed in germanium than in chalcogenide glass.

SHORT-TERM BIAXIAL COMPRESSIVE STRENGTH

The spherical sector specimen failed catastrophically, without any previous audible cracking, at 17 000 psi. The force of the implosion fragmented the window into very small pieces (fig 70). The force of impact rounded off the fragment edges,and very little remained of the original planes of fracture. The gasket was totally destroyed (fig 71). Because the original fracture surfaces were flattened and demolished during the failure, the origin of failure was hard to reconstruct. However, it is probable that the origin of rupture was the bearing surface.

CYCLIC BIAXIAL COMPRESSIVE STRENGTH

Failure of the specimens was found to be a function of both the magnitude of loading and the number of cycles. The specimen that was cycled to 9000 psi failed after eight pressure cycles; again the force of implosion was so great that very few of the original surfaces remained for examination of fracture origin (fig 72 and 73). However, sufficient material did remain in place around the seat to indicate that the fracture originated on or near the bearing surface.

The specimen that was pressure cycled to 4500 psi failed noncatastrophically after 215 pressure cycles. The failure would have been catastrophic had the cycling continued somewhat longer; cycling was interrupted because of indications that some fragments had fallen from the internal surface of the window. Subsequent close inspection of the window (fig 74) revealed that there were several large spalls on its concave surface, midway between the apex and the bearing surface. The reason for the appearance of the spalls and their location is unknown, but there is no doubt that catastrophic failure would have resulted had cycling of the window continued. The gasket suffered only minor damage (fig 75).

The window that was pressure cycled to 2250 psi for 500 pressure cycles showed no sign of damage after its removal from the test jig at the conclusion of the test (fig 76). It is not known exactly how many more pressure cycles would have been required to

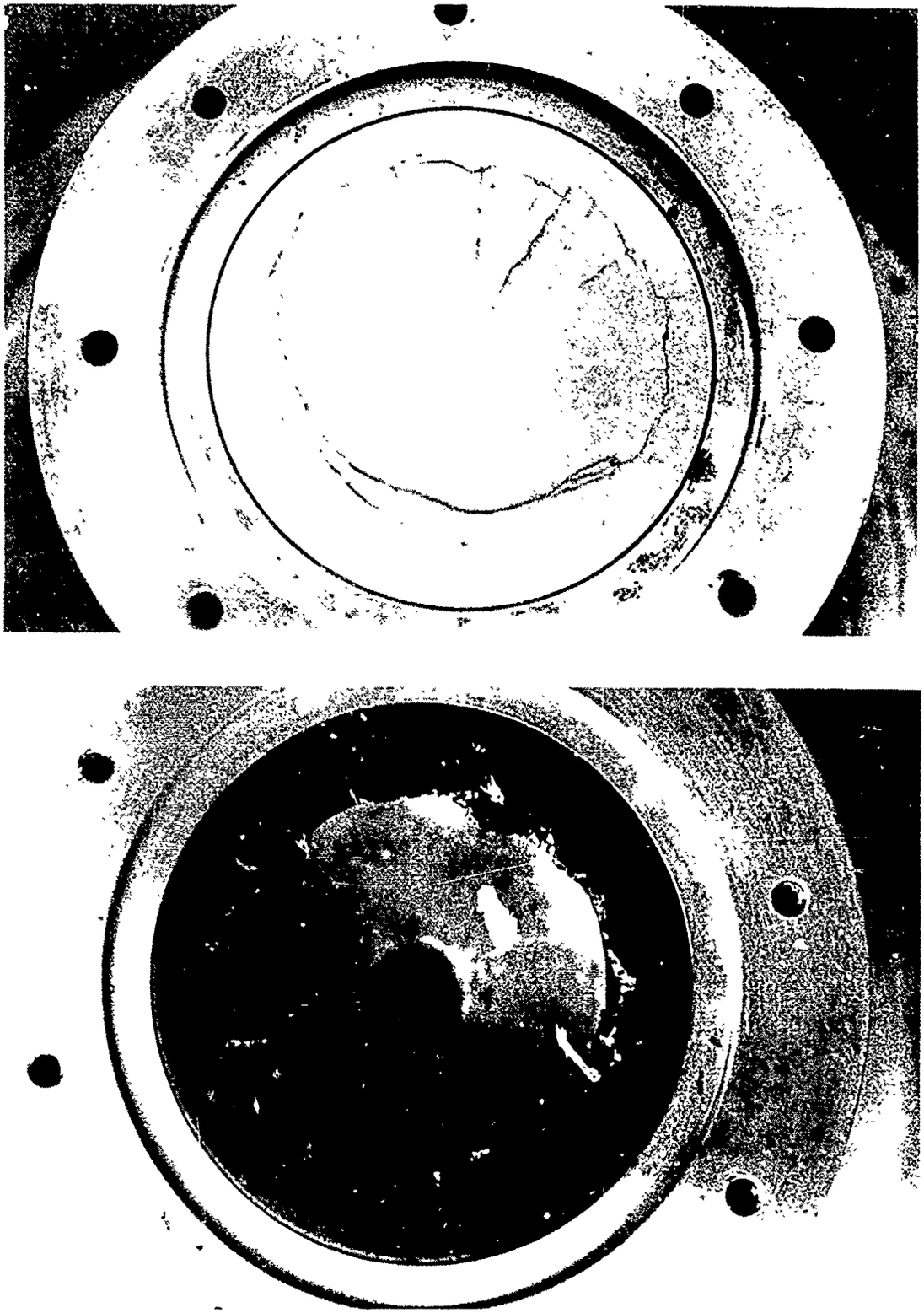

Figure 69. The incipient (top) and catastrophic (bottom) failure of a 3-inch diameter, 0.25-inch thick biaxially flexed AMTIR-1 disk after short-term hydrostatic loading.

Specimen No	Material	Temperature (°F)	Type of Failure	Maximum Stress (psi)
1	Acrylic plastic	76	Catastrophic	18 612
2	Acrylic plastic	77	Catastrophic	20 304
3	Acrylic plastic	77	Catastrophic	17 766
4	Acrylic plastic	77	Catastrophic	16 074
5	Acrylic plastic	77	Catastrophic	15 228
				Minimum = 15 228 Average = 17 596 Maximum = 20 304
6	Germanium	61	Catastrophic	16 500
7	Germanium	69	Catastrophic	11 000
8	Germanium	69	Catastrophic	12 375
9	Germanium	74	Catastrophic	13 750
10	Germanium	70	Partial fracture	9 625
				Minimum = 9 625 Average = 12 650 Maximum = 16 500
11	AMTIR-1	50	Catastrophic	2 476
12	AMTIR-1	50	Catastrophic	1 925
13	AMTIR-1	50	Catastrophic	2 750
14	AMTIR-1	50	Catastrophic	1 925
15	AMTIR-1	50	Catastrophic	2 200
				Minimum = 1 925 Average = 2 255 Maximum = 2 750

Notes:

1. All disks were 3.0 inches OD X 0.25 inch thick, supported in a steel seat with ID = 2.388 covered by a 0.060-inch neoprene gasket.
2. The magnitude of maximum stress in the disks has been calculated.

Table 11. Polished disks under short-term biaxial flexure loading.

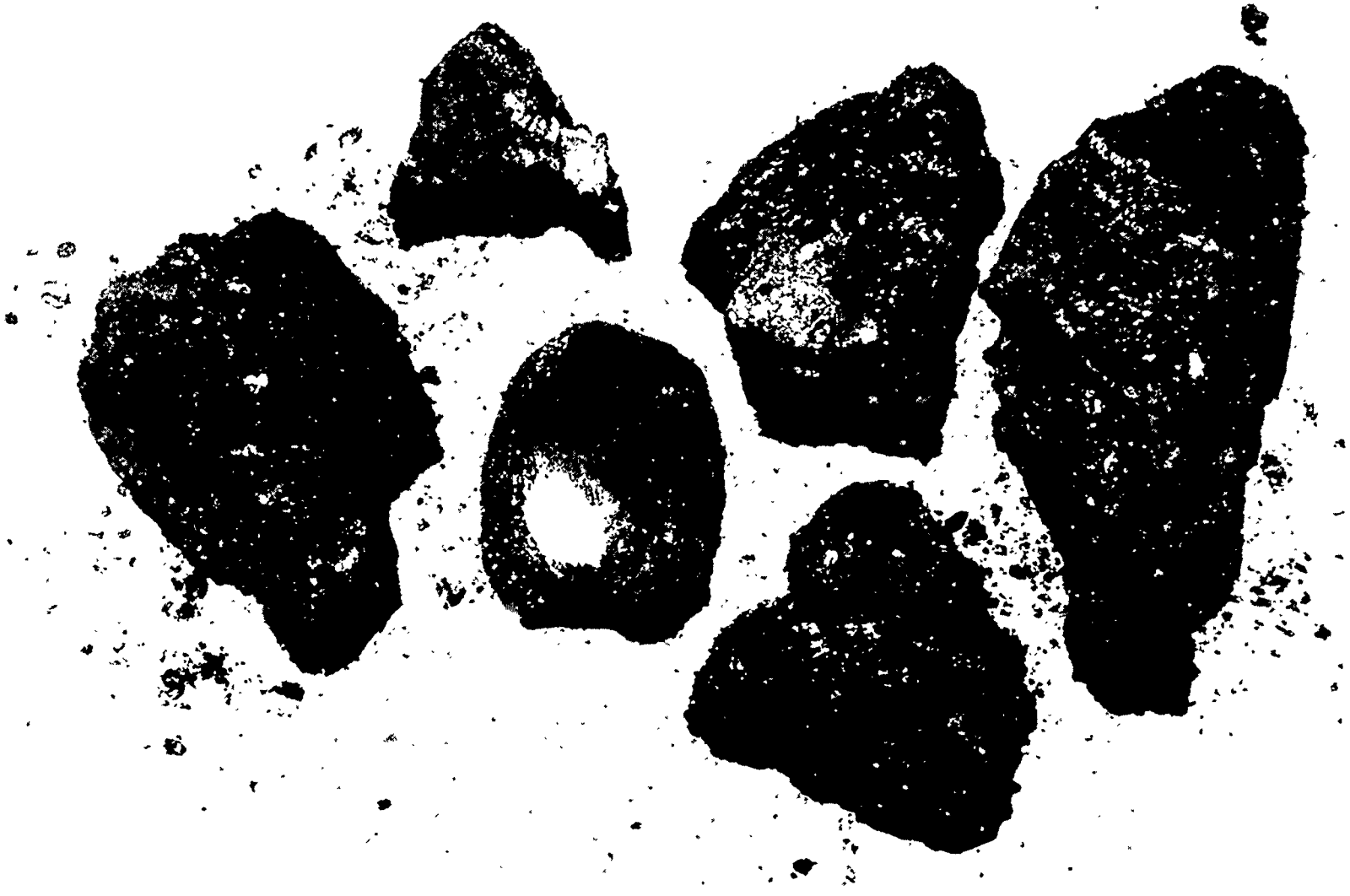

Figure 70. Fragments of AMTIR-1 spherical sector window specimen that failed catastrophically under short-term hydrostatic loading, at 17 000 psi. Note the pulverized edges of fragments subjected to biaxial compressive stresses in excess of 50 000 psi.

Figure 71. The gasket under the spherical sector pressurized to 17 000 psi. The gasket was not the source of failure; identical gaskets were used in prior studies with germanium spherical sector windows pressurized to 20 000 psi.

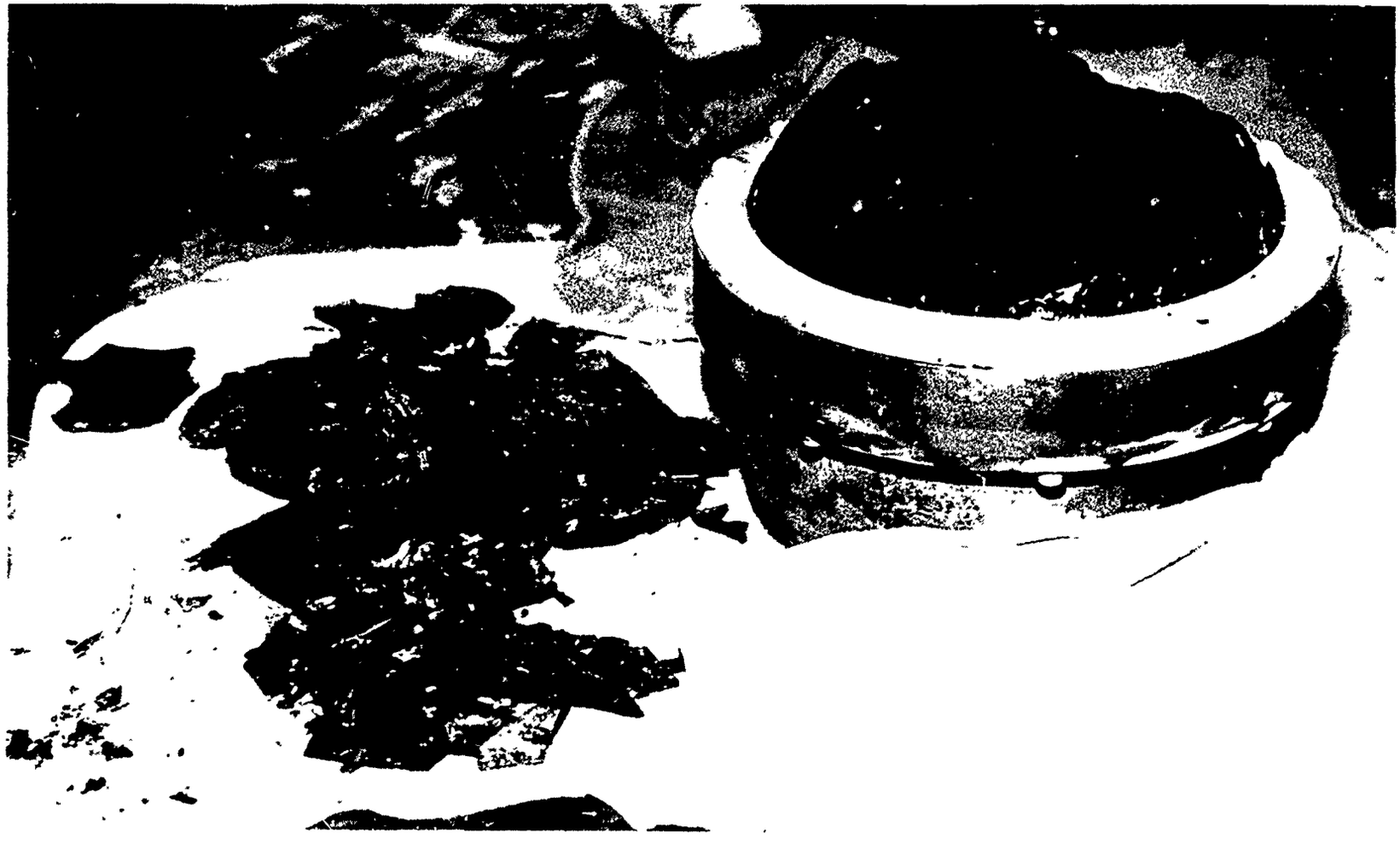

Figure 72. The AMTIR-1 spherical sector window after being pressure-cycled eight times to 9000 psi. Failure occurred on the eighth pressure cycle.

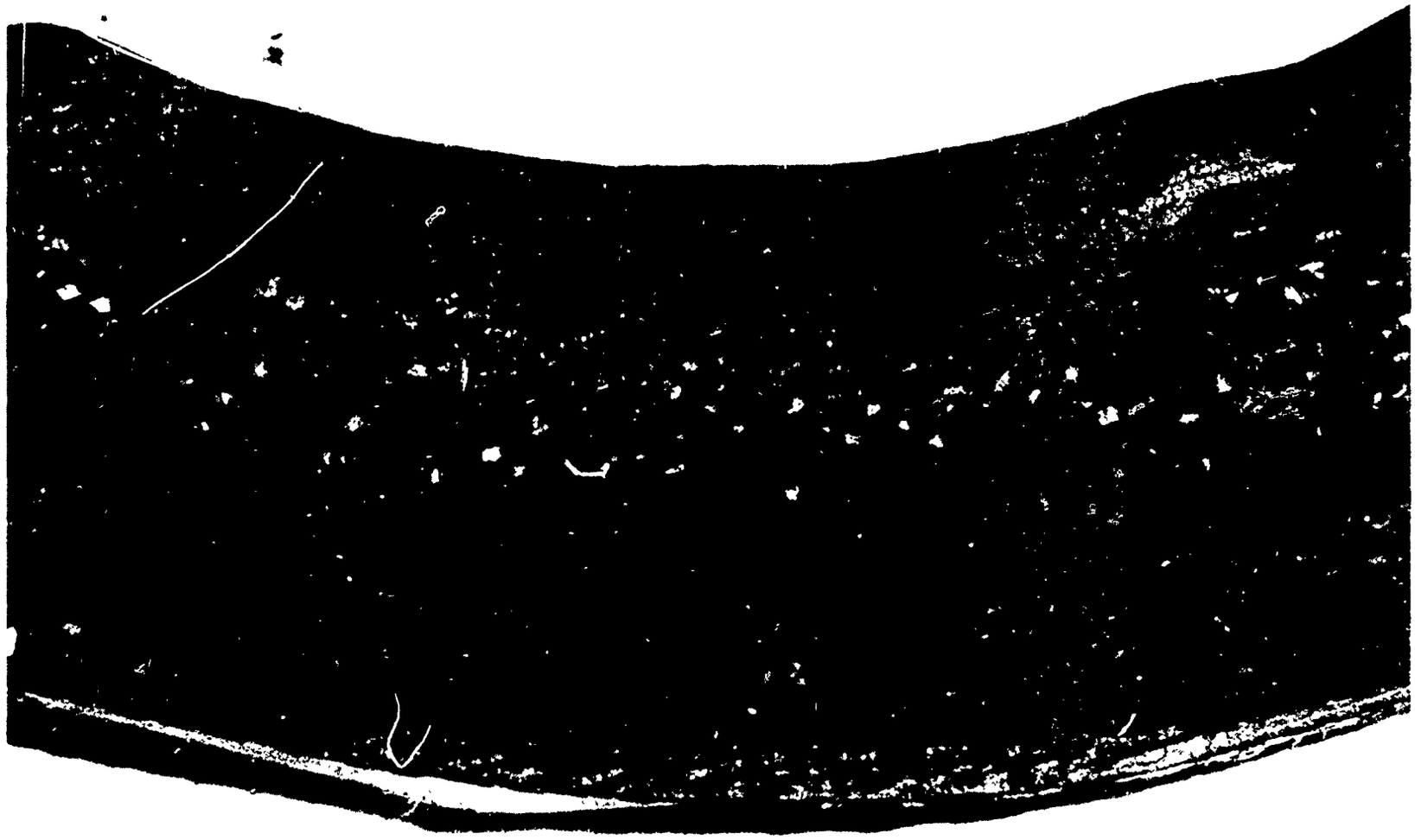

Figure 73. Bearing gasket that was under the spherical sector window specimen cycled eight times to 9000 psi. Note extensive wear of neoprene coating; white threads of nylon cloth have been exposed locally.

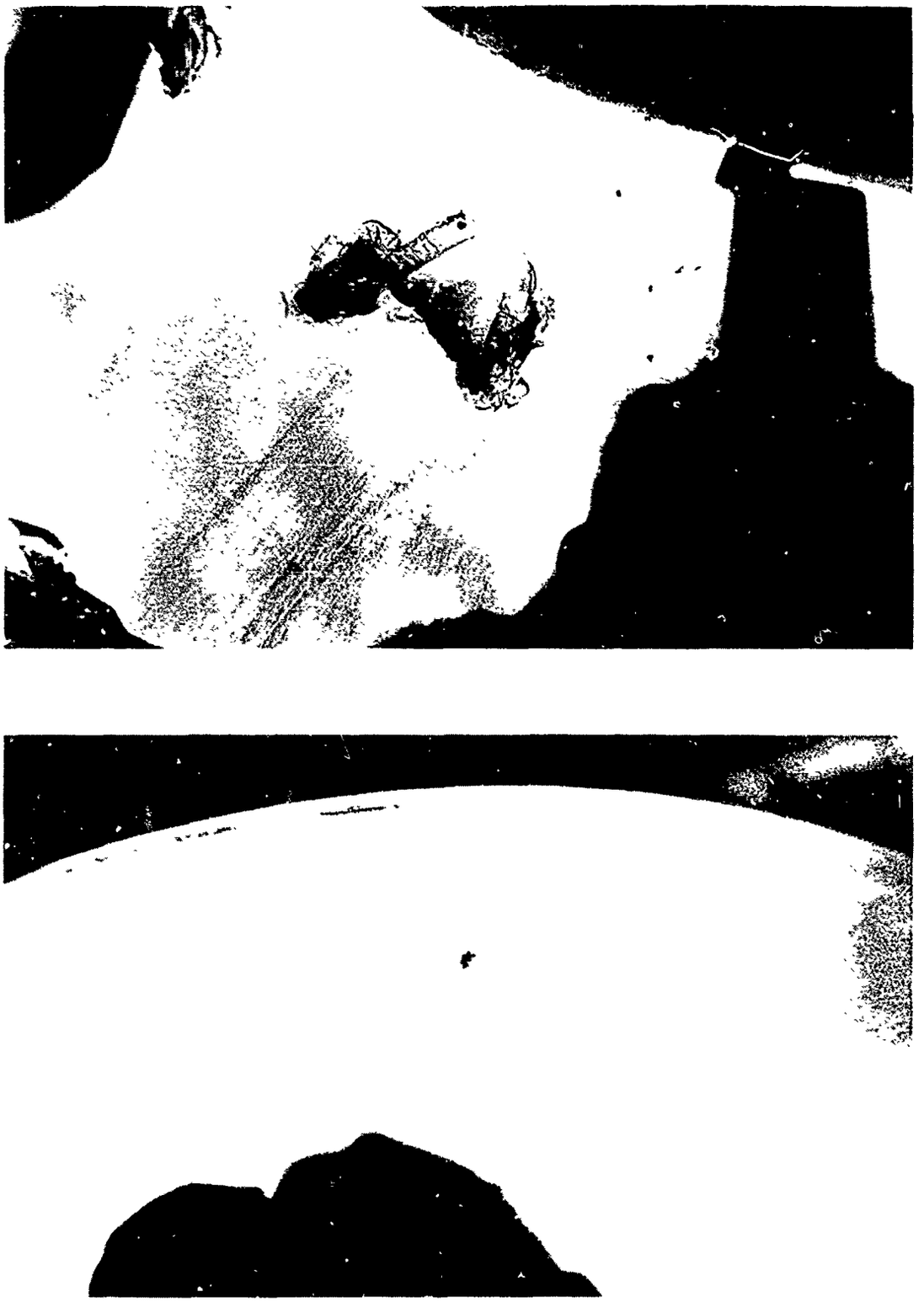

Figure 74. Close-ups of the interior (top) and exterior (bottom) spalls on the AMTIR-1 spherical sector window specimen that was pressure-cycled 215 times to 4500 psi prior to inspection.

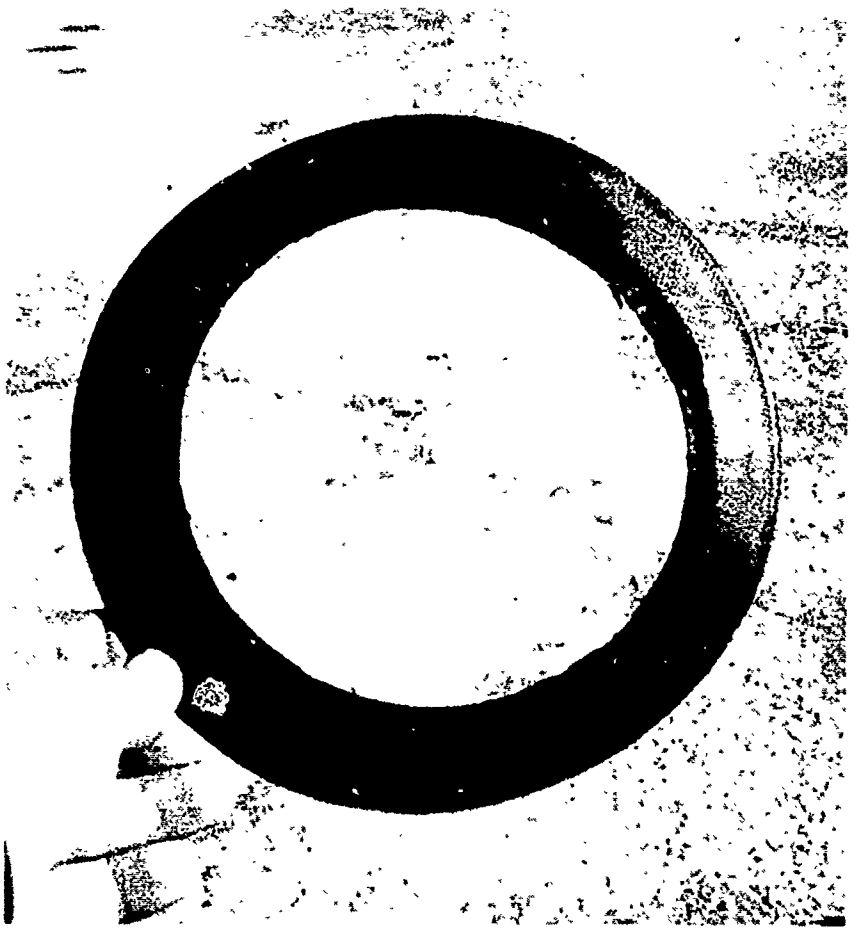

Figure 75. Gasket for the AMTIR-1 spherical sector window specimen cycled 215 times to 4500 psi exhibited only minor wear of the neoprene coating.

Figure 76. The AMTIR-1 spherical sector window specimen cycled 500 times to 2250 psi showed no signs of damage. Similarly, no wear was observed on the bearing gasket.

initiate failure of that window, but it can be safely predicted that a total of at least 1000 cycles would have been required before it would have been damaged sig. ificantly.

On the basis of data generated by this test, a curve was plotted that allows prediction of the fatigue failure of a spherical sector window fabricated from chalcogenide glass and mounted in the NOSC window mounting (fig 77). Because of the linearity of the curve on log-log coordinates, it is possible to extrapolate the known data far into the future with reasonable confidence. There is no doubt that failure of chalcogenide windows can be predicted on the basis of this curve at something above 10 000 pressure cycles if the nominal compressive stress in a sector is held to 2500 psi or less (based on a safety factor of 2).

This cyclic fatigue life applies to spherical sector windows whose dimensional and angular tolerances are comparable to those of the test specimens and which are mounted in window seats whose radial dilation and contraction are identical or very similar to window seats used in this test program.

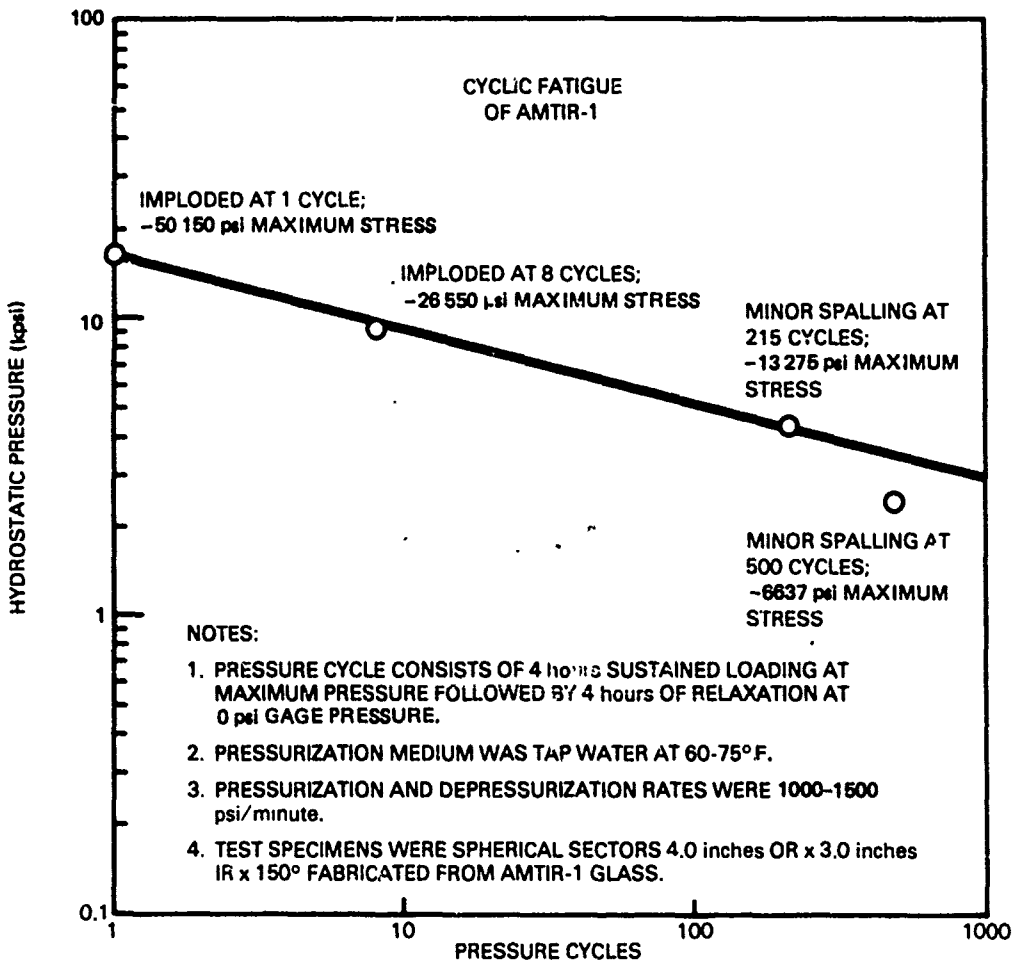

Figure 77. Cyclic fatigue life of AMTIR-1 spherical sector windows on composite gaskets in metallic mounting. Note that the cyclic fatigue life stress at 10 000 cycles is extrapolated to 5000 psi.

DYNAMIC IMPULSE RESISTANCE

The spherical sector specimens failed under a dynamic overpressure loading of only 835 psi (table 12), a significantly lower pressure than the static 17 000 psi required to implode the sector in a prior test. Note that even the appearance of the failed specimen under dynamic pressure (fig 78) was significantly different from that under static pressure (fig 70). Whereas the fragments from the statically imploded spherical segment had smooth edges as the result pulverization of the glass, the edges on the fragments from the dynamically fractured spherical segment were razor sharp. It would seem that failure under static loading is caused by exceeding the material's compressive strength, whereas failure under dynamic loading is caused by exceeding its tensile strength. The tensile stresses in point were generated by the reflection of shock waves inside the spherical segment.

Explosive Charge (g)	Stand-off Distance (feet)	Peak Overpressure (psi)	Test Specimen	Results
9	50	61	005 AMTIR-1	No damage
9	35	83	005 AMTIR-1	No damage
9	25	135	005 AMTIR-1	No damage
9	20	174	005 AMTIR-1	No damage
9	15	225	005 AMTIR-1	No damage
9	10	360	005 AMTIR-1	No damage
9	5	835	005 AMTIR-1	Fractured
9	5	835	006 AMTIR-1	Fractured

Notes:

1. The AMTIR-1 chalcogenide glass spherical sectors had the following dimensions: R_o = 4 in, R_i = 3 in, included angle of sector = 150°
2. The spherical sectors were mounted in window seat 2H654-702100-12 on a fairprene gasket of 0.02-in thickness.
3. The window test assembly was suspended at 50-ft depth in the well, from an overhead crane.
4. All overpressure values have been calculated on the basis of $P_m = k\left(\frac{1/3\ W}{R}\right)^{\alpha}$, where $\alpha = 1.13$, k = 22 500, W = weight in lb, R = standoff in feet, and P = peak pressure in psi.

Table 12. Hydrodynamic impulse testing of AMTIR-1 glass spherical sectors.

CORROSION RESISTANCE

The 3-inch diameter by ¼-inch thick massive chalcogenide glass disks were subjected to preliminary evaluation of corrosion resistance in the marine environment. The transmission through the specimens actually improved after 4 months of continuous immersion in seawater in San Diego Bay (fig 79). The improvement was insignificant (ie less than 5%) but still measurable. It is postulated that the improved transmission of the test specimens was due to minor surface oxidation or the deposition of an oxide layer on the chalcogenide glass. Since chalcogenide glass oxide has a lower index of refraction than the glass itself, the oxide layer acts as a low-grade, inefficient antireflective coating.

Figure 78. Failed AMTIR-1 spherical sector window after a 9-gram pentolite charge was set off 5 feet above it, generating a dynamic overpressure of 835 psi at the window.

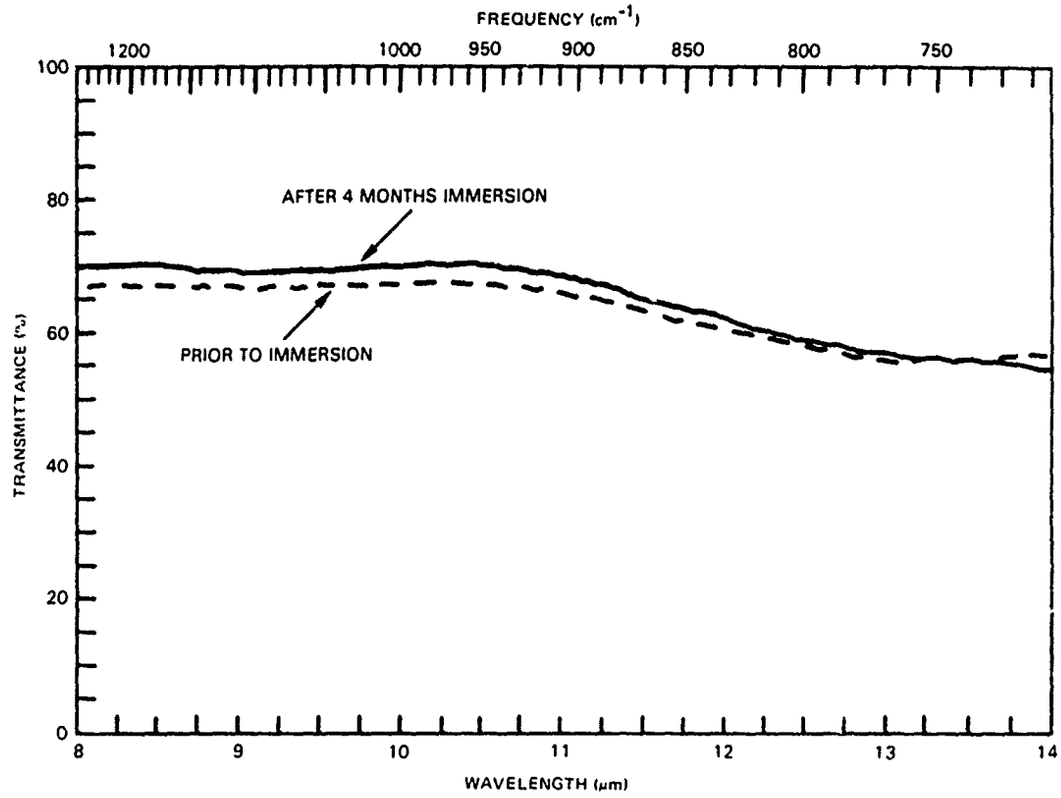

Figure 79. Transmittance versus wavelength for the 3-inch diameter 0.25-inch thick AMTIR-1 glass disks, both prior to and after immersion in seawater for 4 months.

TEST RESULTS – CORROSION RESISTANCE OF CHALCOGENIDE-GLASS-COATED SPECIMENS

3-INCH DIAMETER DISK

The 3-inch diameter by ¼-inch thick germanium disk coated on one side with a 0.001-inch thick chalcogenide glass layer was used as a test specimen for preliminary evaluation of such coating in the marine environment. As with the massive chalcogenide glass specimen, the transmission through the chalcogenide-glass-coated specimen actually increased after 4 months of immersion in seawater in San Diego Bay (fig 80). Again the improvement was insignificant, averaging less than 5%. As with respect to the massive chalcogenide glass, it is postulated that the formation of a thin surface oxide layer caused the improvement in transmission. Detailed observation of the surface detected neither pinholes in the chalcogenide glass layer nor deterioration of the substrate. If pinholes did exist in the coating originally, the seawater did not effect their expansion into craters.

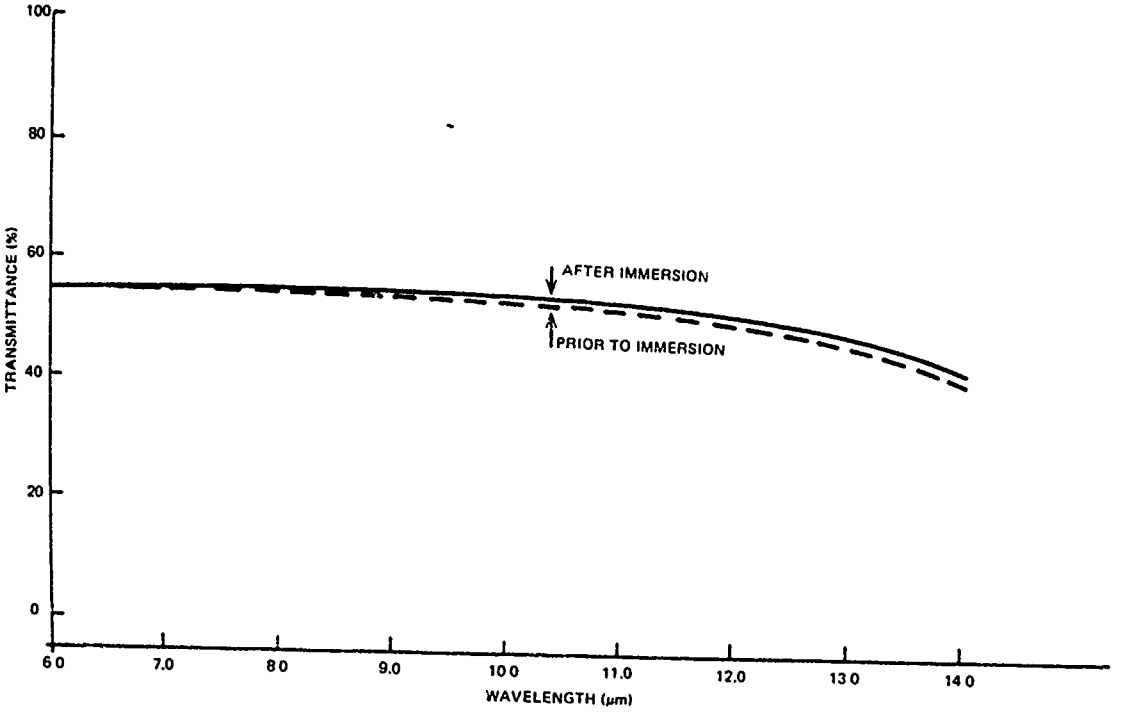

Figure 80. The transmittance of 0.25-inch thick germanium disk, coated on the wetted surface with 0.001-inch thick AMTIR-1 chalcogenide glass, both prior to and after 4-month exposure to seawater.

There are two possible reasons for the total absence of cratering in the substrate: either pinholes are totally absent in the glass coating or, if pinholes are present, the glass coating adhered well to the germanium. Good adherence would impede the process by which corrosion byproducts on germanium lift the edges of the coating around the pinhole and thus facilitate cratering. Which of these postulates is correct remains to be seen. It is very probable that both have some validity; ie, pinholes are very few because of the 1-mil thickness of the coating and, if there are some pinholes, the corrosion tends not to propagate from the pinholes because of the good adhesion of the chalcogenide glass to the germanium substratum.

8-INCH DIAMETER DISK

After 4 months of continuous submersion in seawater in San Diego Bay, there was no decrease in transmission through (1) the specimen coated on the wetted surface with a 0.001-in thick layer of chalcogenide glass and on the dry surface with Optic Electronic XF457 antireflective composition (fig 81 and 82), (2) the specimen coated on the dry surface with Optic Electronic XF457 antireflective composition and on the wetted surface with chalcogenide glass with an Optic Electronic XF508 antireflective composition overlay (fig 83 and 84), or (3) the germanium specimen (serving as a standard of comparison) coated with the multilayer AR coating Exotic Materials 40100 (fig 85 and 86).

Minute observation of the wetted surfaces failed to detect cratering or other indications of corrosion in the two specimens coated with chalogenide glass. The specimen that was coated on the wetted surface with the Exotic Materials 40100 coating had minute pinholes, some of which were already showing enlargement. From a comparison of the three 8-inch specimens, a general conclusion can be made that the least deterioration after 4 months of continuous exposure was shown by the germanium specimen coated with chalcogenide glass with an AR overlay. The most corrosion took place on the specimen coated with Exotic Material's 40100 multilayer antireflective coating, which previous tests at NOSC have shown to be the most durable of all standard AR coatings on the market.

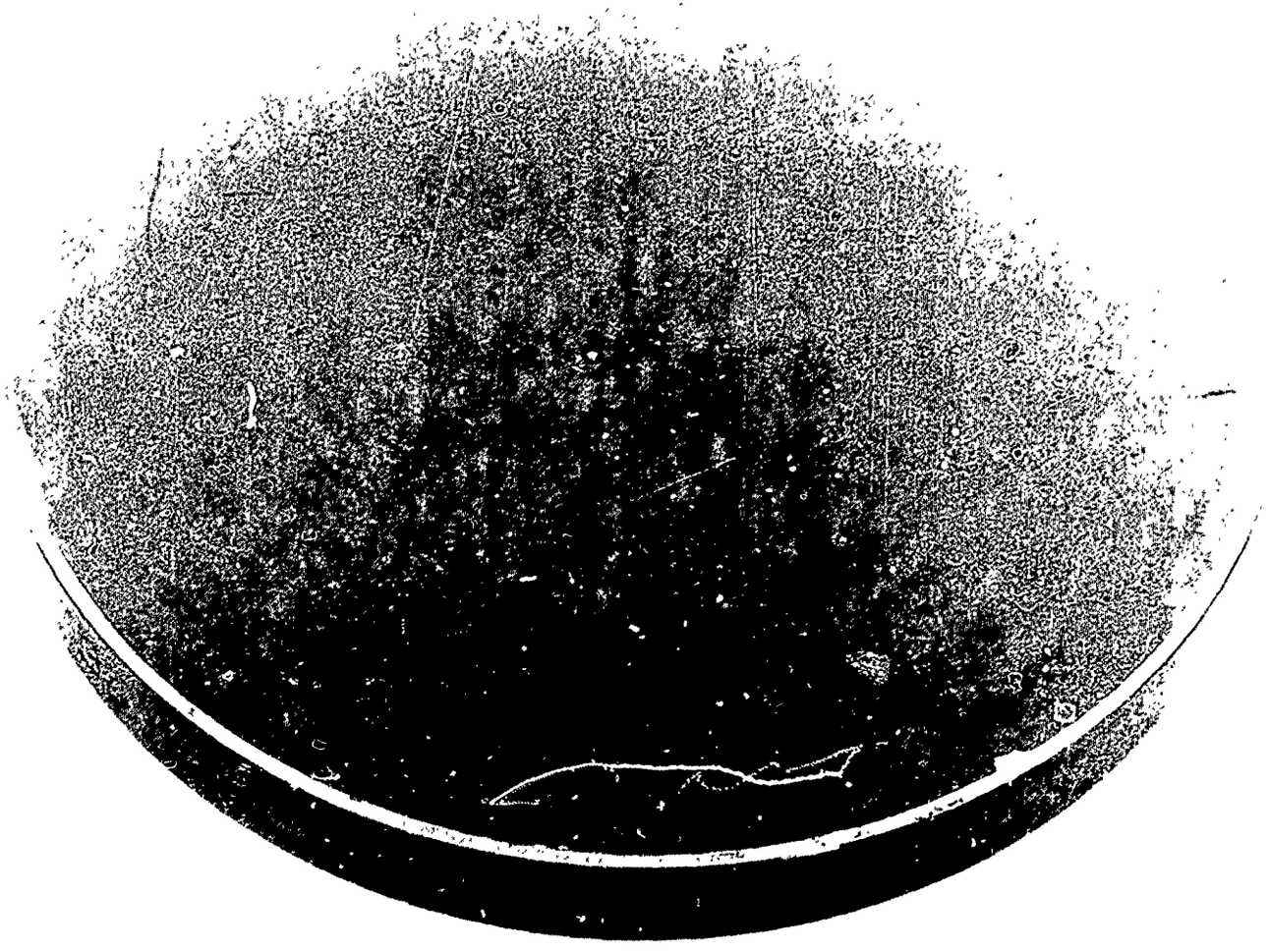

LRO 2697-7-81

Figure 81. The wetted AMTIR-1 glass coated surface of germanium specimen whose transmittance is shown in figure 82, after 4 months of exposure to seawater in San Diego Bay.

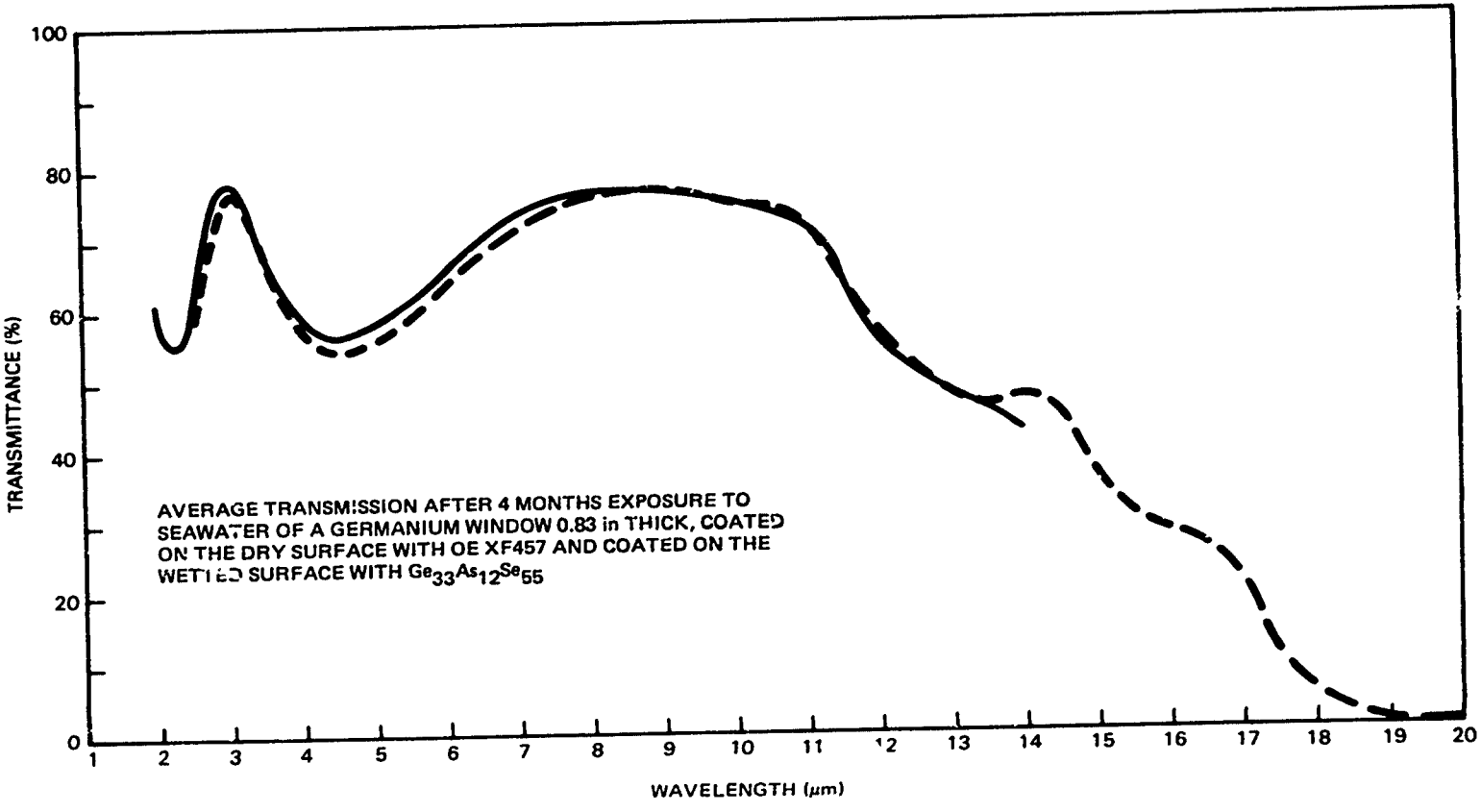

Figure 82. Average transmittance of a germanium window 0.83 inch thick coated on the dry surface with Optic Electronic antireflective composition XF457 and on the wetted surface with AMTIR-1 glass, after 4 months of exposure to seawater. Dashed line shows the transmittance prior to seawater exposure (from fig 37).

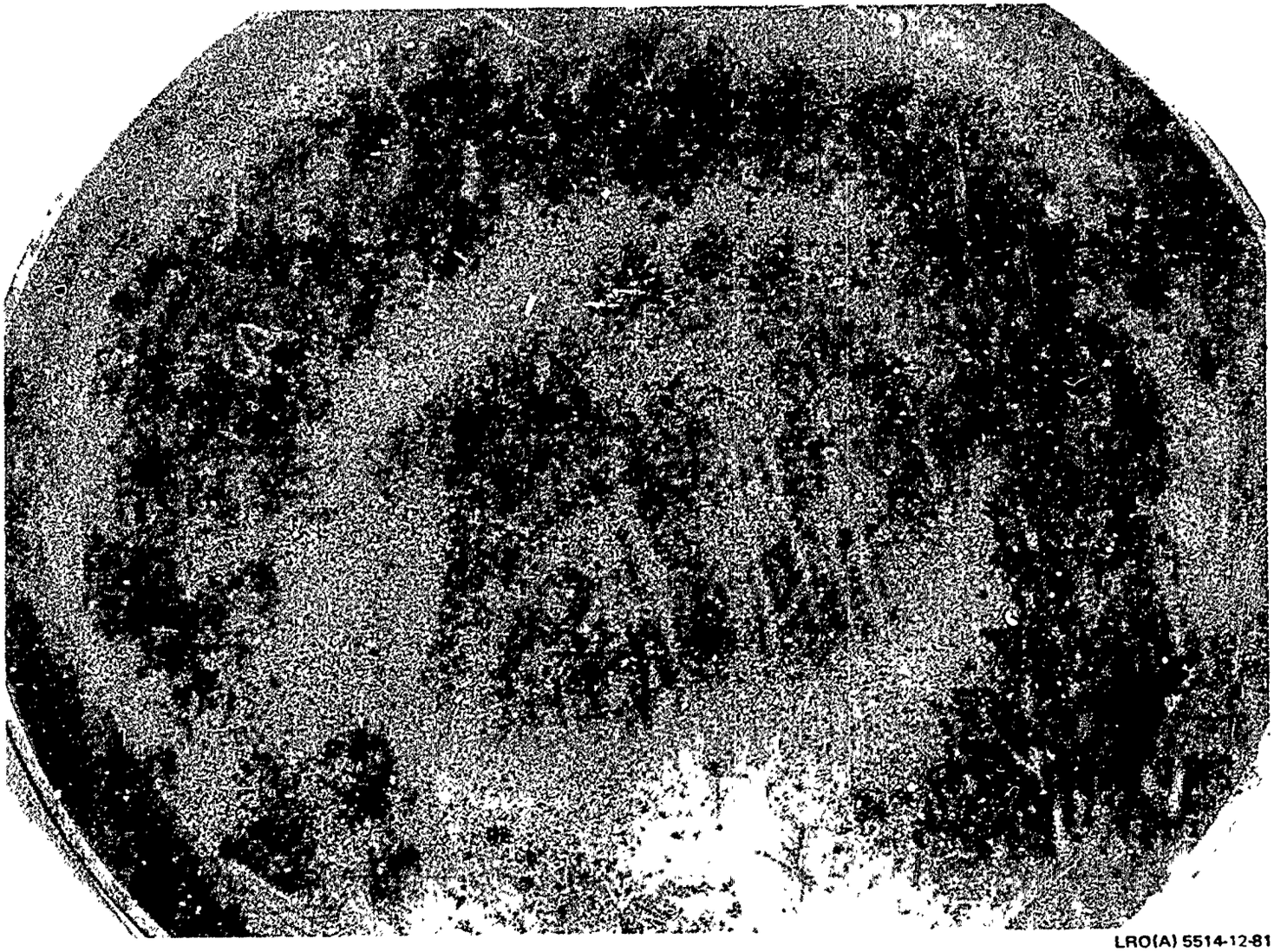

LRO(A) 5514-12-81

Figure 83. The wetted surface of germanium specimen whose transmittance is shown in figure 84, after 4 months of exposure to seawater in San Diego Bay. Note that the multilayer AR coating XF508 on top of the AMTIR-1 layer shows some signs of deterioration even though there is no measurable decrease in transmittance.

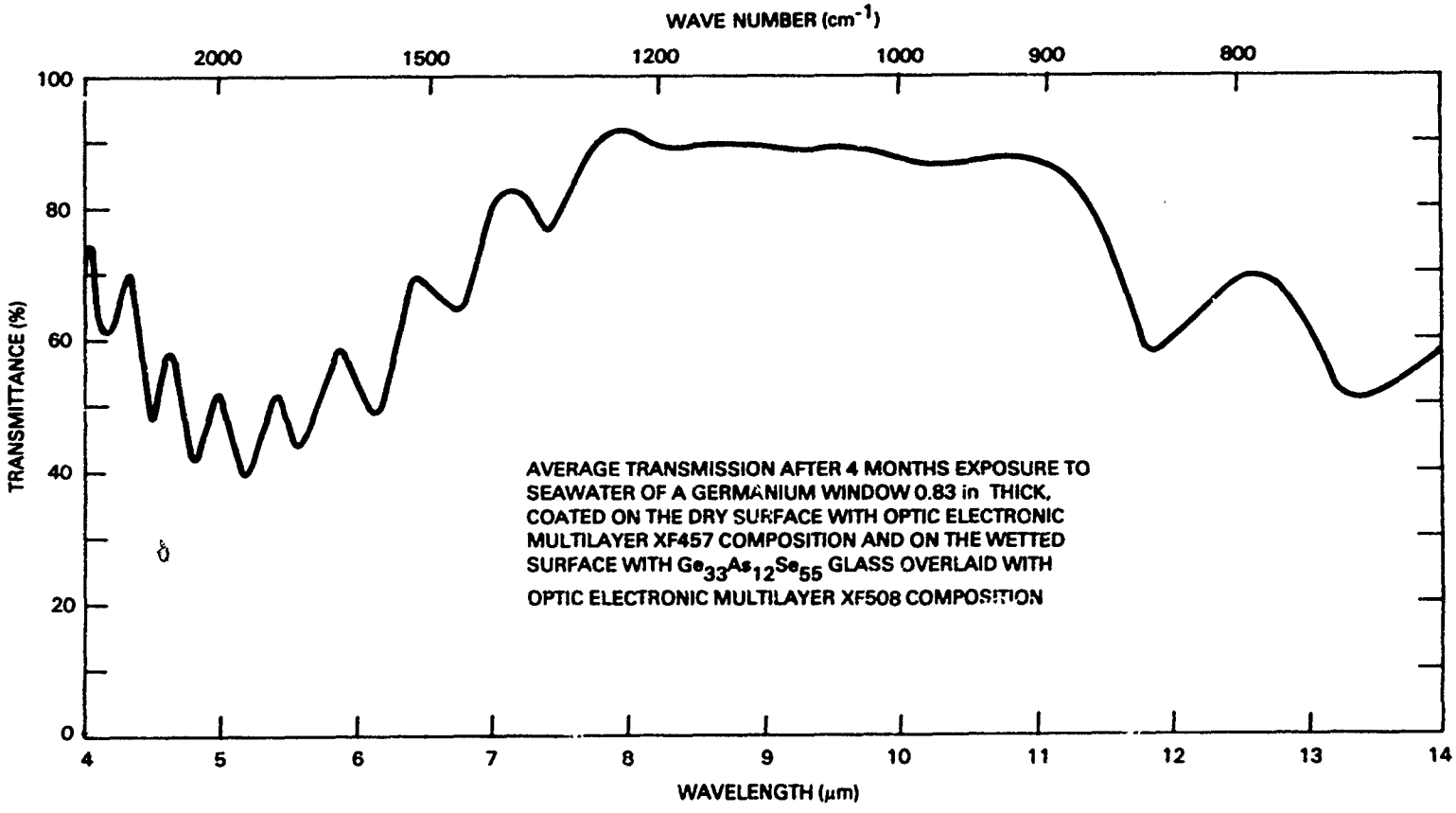

Figure 84. The transmittance of a germanium specimen coated on the dry surface with Optic Electronic antireflective composition XF457 and on the wetted surface with AMTIR-1 glass and Optic Electronic antireflective composition XF508, after 4 months of exposure to seawater. Figure 38 shows the transmittance prior to seawater exposure.

LRO 2690-7-81

Figure 85. The surface of the specimen coated on both sides with Exotic Materials multilayer AR coating composition 40 100, after 4 months of exposure to seawater. There are some minor corrosion craters in the surface even though there is no measurable decrease in transmittance.

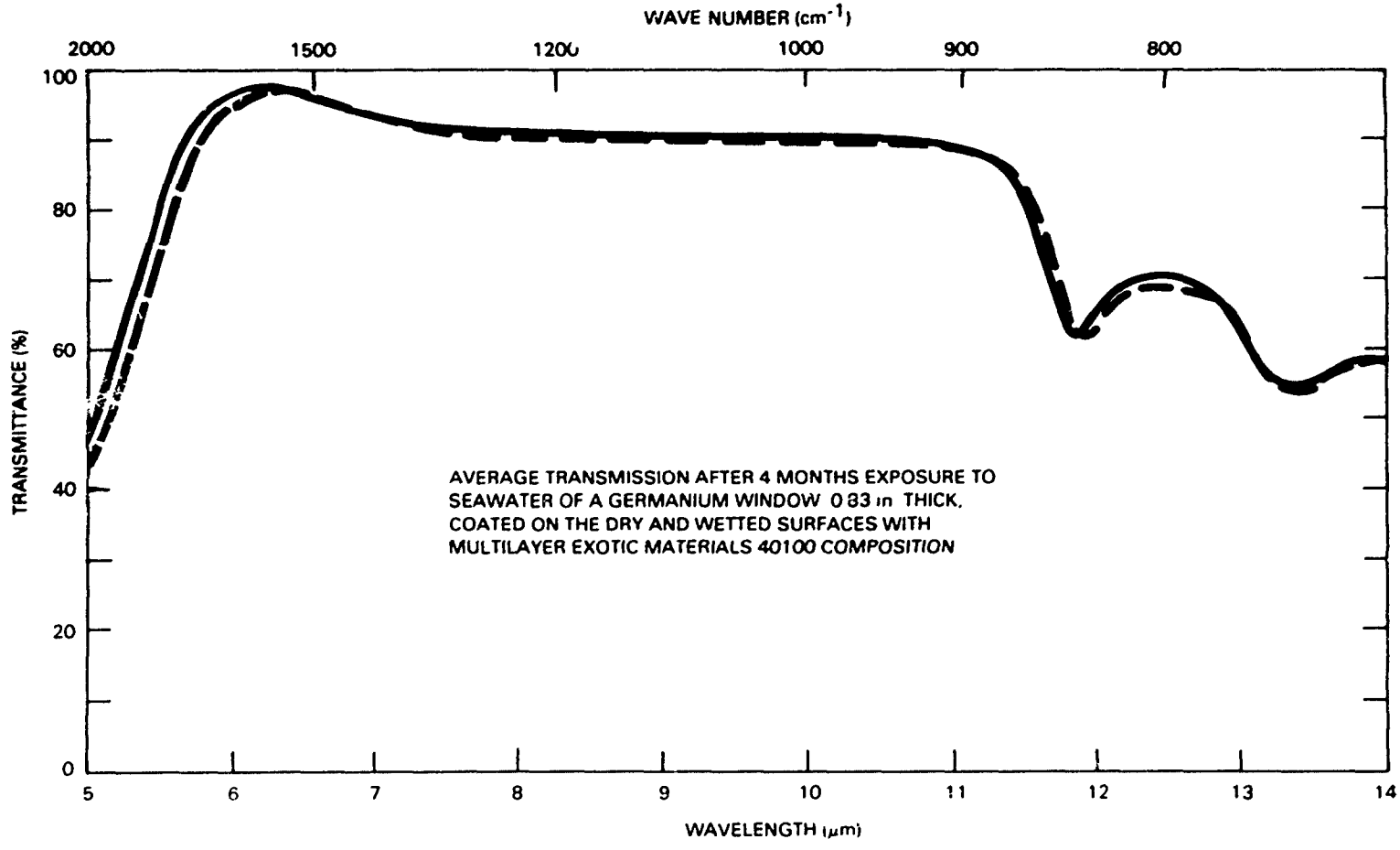

Figure 86. The transmittance of a germanium specimen coated on both surfaces with Exotic Materials multilayer AR coating composition 40100, after 4 months of exposure to seawater. The dashed line shows the transmittance prior to seawater exposure (from fig 39).

10-INCH DIAMETER HYPERHEMISPHERE

Although the hyperhemispherical window did not show any of the typical signs of deterioration during its 4-month submersion in seawater, some deep scratches were seen around the equator of the specimen when it was retrieved from the water. The scratches penetrated the chalcogenide glass layer, and there was some etching of the germanium beneath. Since no natural explanation could be found for the marred surface, the damage was assumed to be due to unauthorized human interference. The performance of the chalcogenide glass layer on the hyperhemispherical specimen that had incurred no scratches was identical to that of the chalcogenide glass layer on the flat disk specimens, indicating that a chalcogenide glass layer can be applied as successfully to complicated shapes as to plane windows.

DISCUSSION OF PHYSICAL PROPERTIES

MASSIVE CHALCOGENIDE GLASS

The average short-term uniaxial compressive strength of chalcogenide glass was found to be on the order of 21 000 psi (table 8). This is considerably lower than the average compressive strength of germanium, which in previous testing was found to be about 64 000 psi. The average short-term uniaxial flexure strength of chalcogenide glass was also found to be significantly lower than that of germanium: 2500 psi vs 11 500 psi for germanium (ref 24).

Similar results were obtained for test specimens under long-term uniaxial flexure loading. Chalcogenide glass exhibited static fatigue just as germanium did in previous testing. For sustained loading (up to 1000-hour duration) the flexural stress on a massive chalcogenide window in an air environment must not exceed 1400 psi to avoid catastrophic failure of the window under load. The corresponding maximum flexural strength applicable to germanium as sustained loading that avoids catastrophic failure for up to 1000 hours is 10 000 psi. The modulus of elasticity of chalcogenide glass is 3.19×10^6 psi, as compared to 1.49×10^7 psi for germanium.

The difference in physical properties between the two materials is an inherent difference of material. It is not due to the test parameters, since in both cases the materials were prepared, finished, and tested identically. It would appear that, in a comparison of both short- and long-term structural properties, chalcogenide glass is significantly weaker than germanium. This should be taken into account when chalcogenide glass is used as the structural material for windows subjected to significant pressure loading. This difference in structural properties, established with test specimens under uniaxial loading, is confirmed by the test results from the disk specimens that were subjected to biaxial loading.

The average short term biaxial flexure strength of chalcogenide glass (2250 psi) is significantly lower than that of germanium (12 650 psi). The difference is not significant between the strength of chalcogenide glass under uniaxial vs biaxial loading or between the strength of germanium under uniaxial vs biaxial loading. But the spread of test values for germanium under short- and long-term loading is significantly higher than for chalcogenide glass, indicating that the distribution of incipient fracture sources in germanium is inherently less uniform than in chalcogenide glass. In any case, a design stress value can be selected which will insure that a chalcogenide glass window will not fail prior to a specified number of hours of sustained or cyclic loading.

The biaxial compression test results show that for chalcogenide glass, the short-term compressive strength (≈50 000 psi) and the cyclic fatigue life (≈2500 psi at 10 000 cycles) are significantly less than the corresponding values for germanium (≥100 000 and ≥25 000 psi). It is also apparent that the cyclic compressive fatigue life of both chalcogenide glass and germanium can be extrapolated into the future. The difference in magnitude of short-term and cyclic biaxial compressive strength of glass versus germanium has been hard to establish. The magnitude of the difference is at minimum a factor of five, judged on the following basis: a germanium spherical sector of identical dimensions as the chalcogenide spherical sector was cycled 300 times to 20000 psi without failure, whereas the chalcogenide glass specimen that was pressure-cycled to 4 500 psi showed signs of failure within 200 cycles.

The factor of five for the difference in cyclic compression fatigue strength between chalcogenide glass and germanium is similar to the factor of about five to six which differentiates the short-term and long-term flexural strength of the two materials. From these data it would appear that as a matter of general comparison chalcogenide glass possesses approximately 1/5 the strength of germanium under short-term and long-term loading applications. This by no means renders the chalcogenide glass undesirable. It simply indicates that the design factors or design stresses applicable to germanium are totally inapplicable to chalcogenide glass. Safe performance of chalcogenide glass can be expected under the various types of loading encountered in service only if design stresses are based on test data for chalcogenide glass.

The dynamic tensile strength (impulse resistance) of chalcogenide glass has been found to be about the same as that of germanium. Tests have shown that chalcogenide glass spherical sector windows fail at about the same dynamic pressure loading as germanium windows of identical dimensions (835 psi vs 1100 psi – ref 24). Test data seem to indicate that germanium windows do not possess an inherent advantage over chalcogenide windows in resisting dynamic pressure impulses generated by above- or below-water explosions. This is surprising since both the tensile and compressive strengths of germanium are known to be higher than those of chalcogenide glass by at least a factor of five.

On the basis of data generated in this study one can establish several stress levels applicable to the design of chalcogenide glass windows and lenses. The magnitude of stress level used in the design to a large degree depends on what kind of a loading the window will be subjected to in service. If a window is to be subjected only to a few pressure cycles, the stress level used in design can be much higher than that for a window which is routinely pressurized and depressurized, such as one intended for an IR system on a submarine. On the basis of these considerations two design stress levels can be postulated. One applies to windows and lenses that are to be subjected to a design stress loading only in an emergency, such as an underwater explosion. The other is used for applications in which the design stress level is reached periodically or many times during the life of the window, such as for equipment mounted on a submarine and periodically subjected to dives to operational depths.

For applications where the design stress level is reached only several times during the life of the chalcogenide glass window, a nominal compressive stress level of 9000 psi and a nominal flexural stress level of 900 psi are recommended. For applications where the window is periodically subjected to the design stress level, the recommended compressive design stress level is 4500 psi and the flexural stress level is 450 psi. These recommended stress levels are based on test data from this study and on the experience accumulated by the authors during the testing of glass, germanium, and other brittle materials.

For a new-design system that is to use chalcogenide glass windows, a prototype window should without question be designed and subjected to the operational scenario that is envisioned for the system. By this means the designer may if desired select somewhat higher stress levels. If the operational scenario to which the specimen is subjected supports the chosen design stress level, it should be employed instead of the one recommended in this report.

Note that surface scratches and roughness affect the flexural strength of chalcogenide glass much less than that of other stronger materials, such as germanium. For chalcogenide glass the comparison of the modulus of rupture for specimens which were only ground but not polished with those that were both ground and polished shows that there is no significant difference. In contrast, the short-term modulus of rupture (strength) differs significantly for polished and unpolished germanium specimens. Why the modulus of rupture (flexural strength) of chalcogenide glass is not affected by lack of polishing is not known. It is postulated that it is because in chalcogenide glass the bond between individual molecules is much weaker than it is in crystalline materials such as germanium. The practical result of this observation is that chalcogenide glass windows probably can tolerate a larger number of scratches in service prior to losing their structural strength than can other materials like germanium. This feature is useful because chalcogenide glass in service will see significantly more scratches than germanium; it is much softer and much more susceptible to scratching during cleaning than germanium and other harder materials.

CHALCOGENIDE GLASS COATINGS

This study indicates that it is feasible to sputter a thick layer of chalcogenide glass on a germanium substratum and that the coating layer later exhibits good attachment to the substratum even during stressing with large temperature fluctuations. When tested with the Sebastian I test arrangement, the tensile strength between the coating and the germanium substratum was on the order of 4 to 6 kpsi (ref 22). An additional advantage of placing a thick layer of chalcogenide glass on germanium is that transmission through the germanium substratum is enhanced – not as much as it would be with a high-performance AR coating, but nevertheless by a significant percentage. Finally, the use of a chalcogenide glass layer appears to provide the germanium substratum with unexcelled protection against seawater corrosion; and transmission through this surface layer does not appear to deterioriate with time, in contrast to typical AR coatings, including the new carbon-based AR coatings. The lack of deterioration is probably due to the fact that chalcogenide glass does not absorb water. Any products of corrosion that might form on the surface of the glass act like AR coatings, further enhancing transmission through the glass. Chalcogenide glass coatings adhere quite well and can be applied by a standard coating technique to large and complex shapes. There appear to be no size or configuration limitations for application of this type of coating to germanium substrata.

Because chalcogenide glass coatings can be applied in any thickness, a layer can be used for repair or resurfacing of a germanium window whose surface has been ground down to such an extent that it has lost its original figure, or radius. By applying a thick layer of chalcogenide glass and subsequently grinding or polishing the lens or window down to the appropriate conformation, a very complex and expensive lens shape that otherwise might be lost because of corrosion or external figure destruction during repolishing operations could be reclaimed.

It is not presently known whether chalcogenide glass coatings would perform as well on other IR transparent substrata that are attacked by seawater, such as zinc selenide, sodium chloride, or potassium chloride. It is highly probable that the coating affords as good protection for these substrata as it does for germanium, provided it can be made to adhere without the presence of pinholes. The experimental data generated in this study, however, do not extend beyond germanium substrata. To determine how well the coating would perform with other substrata would require further studies.

CONCLUSIONS

Chalcogenide glass is extremely well suited for construction of windows and IR systems that are exposed to a marine environment. Totally uncoated chalcogenide glass windows on IR systems have an average transmission of about 65–69%. When coated on the dry surface only with the standard AR zinc sulfide/thorium fluoride coating, they have an average transmission of about 80–82%. And when coated with a high-grade multilayer AR coating on both the wetted and the dry surface, they have an average transmission of 95–97% in the 8–11 μm range. The projected life of a chalcogenide glass window uncoated on the external surface is at least 1 year. Standard grinding and polishing techniques can be used to fabricate windows of any size and any shape from chalcogenide glass, provided the designer takes into consideration the low tensile, compressive, and thermal shock resistance properties of the material.

Thick chalcogenide glass coatings on germanium substrata provide the same corrosion resistance as massive chalcogenide glass. Germanium coated on the dry side with an AR coating and on the wetted side with a chalcogenide glass layer has an average transmission of 75% in the 8–11 μm range. A further AR overlay on the chalcogenide glass raises the transmission through the germanium window to about 87% over the same range.

RECOMMENDATIONS

It is recommended that on IR systems exposed to a marine environment chalcogenide glass be considered both as a prime construction material and as a coating for windows of other materials. Whether chalcogenide glass is used as the primary material for windows or as a coating on germanium windows, it will extend the life of such windows in the marine environment to at least 1 year. In contrast, the life of current standard AR-coated germanium windows is less than 6 months. Because chalcogenide glass provides such a tremendous potential reduction in expenditures as window or window-coating material, its use where feasible is encouraged.

REFERENCES

1. Naval Air Development Center Report of Action Group JAG-1, State of the Art of Airborne Forward Looking Infrared (FLIR) Technology, vol 1, edited by PM Moser, August 1976.
2. Lloyd, JM, Thermal Imaging System, Plenum Press, New York, London, 1975.
3. The Infrared Handbook, edited by WL Wolfe and GJ Zissis, Infrared Information and Analysis Center, Environmental Research Institute of Michigan, Ann Arbor MI, 1979.
4. Levitt, RS, and T Conklin, Infrared Imaging, Heating Up, Industrial Research, July 1977.
5. Hilton, A, Infrared Transmitting Glasses as Optical Materials in Passive Systems, Society of Photo-Optical Instrumentation Engineers, Proceedings, vol 131, 1978.
6. NOSC TR 633, Resistance of Coated and Uncoated IR Windows to Seawater Corrosion, Phase V – Summary, by JD Stachiw and SL Bertic, 1 February 1981.
7. Frerichs, R, paper on the new As_2S_3 glasses, Physical Review, vol 78, p 643, 1950.
8. Frerichs, R, New Optical Glasses with Good Transparency in the Infrared, Journal of the Optical Society of America, vol 43, p 1153, December 1953.
9. Fraser, WA, and J Jerger Jr, paper 57, Arsenic Trisulfide: A New Infrared Transmitting Glass, reported in Journal of the Optical Society of America, vol 43, p 332, April 1953.
10. Billian, CJ, and J Jerger, Servo Corp of America Contract NONR 3647 (00), 1943, Contract NONR 4212 (00), 1964.
11. Hilton, AR, and M Brau, New High Temperature Infrared Transmitting Glasses, Infrared Physics, vol 3, p 69, July 1963.
12. Hilton, AR, CE Jones, and M Brau, New High Temperature Infrared Transmitting Glasses – II, Infrared Physics, vol 4, p 213, December 1964.
13. Hilton, AR, CE Jones, and M Brau, New High Temperature Infrared Transmitting Glasses – III, Infrared Physics, vol 6, p 183, 1966.
14. Patterson, RJ, and M Brau, 129th Meeting of the Electrochemical Society, May 1966.
15. Jones, C, and H Hafner, Contract AF33 (615) 3963, October 1963.
16. Savage, JA, and S Nielsen, Preparation of Glasses Transmitting in the Infra-red Between 8 and 15 Microns, Physical Chemistry of Glasses, vol 5, no 3, p 82, June 1964.
17. Myuller, RL, LA Bardokow, and ZV Borisova, Journal of the University of Leningrad, vol 10, p 94, 1962.
18. Hilton, AR, JJ Hayes, and MD Rechtin, Chalcogenide Glasses for High Energy Applications, Texas Instruments Inc Contract N00014-73-C-0367, Technical Report 1, January 1974.
19. NOSC TR 421, Resistance of Coated and Uncoated IR Windows to Seawater Corrosion, JD Stachiw and SL Bertic, 1979.
20. Technical Report AFAL-FR-73-340, Development of Deicing Methods of Chalcogenide Glass Windows for Reconnaissance and Weapon Delivery, SN Rea and RS Wriston, Texas Instruments Inc, 1973.

21. Maissel, LI, and R Glang, Handbook of Thin Film Technology, McGraw-Hill, New York, 1970.

22. Herrmann, WC Jr, and JR McNeil, Ion Beam Deposited Ge-As-Se Glass for Applications in the 1 μ to 16 μ Wavelength Region, 12th Annual Symposium on Optical Materials for High Powered Lasers, Boulder Colorado, 30 September 1980.

23. Stachiw, JD, Transparent Structural Materials for Underwater Research and Exploration, Industries Atomique et Spatiales, vol 18, no 3, p 71-94, 1974.

24. NOSC TR 565, High Pressure Viewports for Infrared Systems, Phase I – Germanium, JD Stachiw, September 1980.

25. NOSC Technical Report NUC TP-393, Glass or Ceramic Spherical Shell Window Assembly for 20,000 psi Operational Pressure, JD Stachiw, May 1974.

26. Stachiw, JD, Hyperhemispherical Viewports for Undersea Applications, Journal of Engineering for Industry/ASME Transactions, vol 101, no 3, 1979.

27. Stachiw, JD, and WL Loucks, Design Parameters for Germanium Windows Under Uniform Pressure Loading, Society of Photo-Optical Instrumentation Engineers, Proceedings, vol 131, 1978.

APPENDIX A

DESIGN CONSIDERATIONS

DESIGN STRESSES

Although the measured short-term flexure strength for AMTIR-1 is in the 1600 to 4000 psi range, the effects of surface scratches, chips, pits, and static or cyclic fatigue can lower it to the 1000 psi level. For this reason, it is considered prudent to restrict the magnitude of maximum tensile design stress in an AMTIR-1 window to 450 psi. The value of maximum tensile stress may be increased to 900 psi if the window is subjected neither to constant loading of long duration nor to a high number of load cycles and if the surface in tension is protected from scratches or abrasions by appropriate hard coatings. In applications where the window has to survive only a single loading of short duration (in a missile, for example) the maximum tensile stress may be increased to 1000 psi.

The maximum design stress in compression can be significantly higher than in flexure, since the measured short-term compressive strength of AMTIR-1 is in the 18000 to 25000 psi range and since static and cyclic fatigue as well as surface scratches affect compressive strength far less than flexural strength. For windows which will see extended sustained loading and/or a large number of loading cycles (up to 10000) at maximum design stress, the value of that stress should not exceed 2250 psi. For applications where the windows will not see extended sustained loadings and/or a large number of cyclic loadings ($\leqslant$1000) at maximum design stress, the value of maximum design stress can be safely increased to 4500 psi. In applications where the window has to survive only a single loading of short duration (for example, in a missile), the maximum compressive design stress may be increased to 9000 psi.

That such high design stress values are feasible was shown by the testing of spherical sectors in this study: no failure took place even though the peak compressive stress was approximately 6500 psi and the 500 cyclic load applications were each of 4-hour duration. However, these values were achieved only by meticulous attention to bearing surface finish, dimensional and angular tolerances, and seat design.

WINDOW DESIGN

Unless operational requirements absolutely forbid it, windows for high-pressure service should always assume the shape of a spherical sector with the included spherical angle in the 60–330° range (fig 7). Where the thickness of the window is to be optimized, the spherical included angle must be limited to the 140–160° range; experiments with glass and plastic spherical sectors have shown that sectors with included angles in that range can withstand higher bearing stresses without cracking than sectors with any other angle. If the design pressure is no greater than 1000 psi, windows with plane surfaces also may be used.

The bearing surfaces on spherical sectors must be normal to the spherical surfaces. The edges of the bearing surface shall terminate in large, smooth chamfers (0.020–0.040 inch), since it is known that the inner edge of a sector is never under high compressive stress and is sometimes even under low tensile stress. If chipped and nicked sharp corners on brittle glass are not eliminated by chamfering prior to assembly, they will act during loading as stress risers that may, even at a very low tensile stress level at a particular point, initiate fracture of the bearing surface.

The dimensional, angular, and surface-finish tolerances imposed on the bearing surface of the window all must of necessity be tight to preclude the presence of stress risers in the form of point or line contacts between the mating bearing surfaces of the window and the seat. Special attention must be paid to the finish on the bearing surface, because the radial component of stress on that surface is generally tensile. After the surface is ground with progressively finer compounds, the final operation should be lapping with 8 μm compound.

MOUNTINGS

Mountings for IR windows under external pressure must meet the same design criteria as mountings developed successfully in the past for glass or ceramic structural components under external pressure loading (ref 26). These criteria are rather straightforward, but failure to heed them invariably leads to premature fracture of any brittle window. The criteria can be summarized in two statements:

1. The radial dilation or contraction of the seat on the mounting under the combined actions of the pressurized window, the hydrostatic pressure, and the pressurized housing should be uniform around its circumference.

2. The radial dilation or contraction of the window circumference and the rotation of the window's bearing surface should be matched by the corresponding radial dilation or contraction and rotation of the seat on the mounting.

In practice, it is impossible to meet both criteria completely. Thus every mounting design is an imperfect attempt to meet these ideal criteria. If compromises have to be made, they are best made in the realm of matching the radial contraction or dilation of the window to that of the mounting rather than in the realm of assuring uniform radial displacement or minimal angular rotation of the mounting. Unless the design stresses are set excessively high, the compliant elastomeric gasket between the mating surfaces will take care of minor angular or diametrical displacements of the seat relative to the window's bearing surface, under hydrostatic loading.

Additional requirements are placed on mountings subject to hydrodynamic forces and shock forces such as drag, lift, or wave slap. The mountings must be rigid enough to prevent the window from shifting or being detached by these nonuniform forces, yet must not generate significant tensile stresses in the windows under these conditions or under hydrostatic loads.

There are two practical mounting techniques currently in use to satisfy these requirements: semirigid mounting and compliant mounting. In the first, the window is mechanically affixed (rigidly connected) to the sensor housing, commonly by placing it in a prepared oversized recess in the housing and filling the space between the window and the mounting with casting epoxy or silicone rubber. This method is acceptable for simple shapes such as flat or cylindrical windows exposed to low hydrostatic pressure. A major shortcoming is the difficulty of removing the window for refurbishment or replacement.

The technique based on a compliant mounting is more satisfactory for higher pressures, more complex window shapes (eg, hyperhemispheres), and window refurbishment. A compliant mounting allows the window and housing to deform independently while a watertight seal and minimized tensile stresses are maintained. The mating bearing surfaces of the window and mounting are allowed to slide with respect to one another, with a compliant gasket distributing the bearing loads. Figure A1 illustrates a method for achieving the

desired compliance for a hyperhemispherical window (ref 26). The mounting employs a conical seat and elastomeric O-rings to both seal the window and hold it in place. Because highly compressed elastomeric O-rings exert considerable, but uniform, bearing pressure against its exterior and interior surfaces, the window is held securely against the seat of the mounting without the generation of local stress concentrations in the window. In addition, the compliance of the O-rings and bearing gasket allows for differential expansion or contraction between the window and the mounting as the result of static pressure, hydrodynamic drag, wave slap, or temperature variations, without generation of stresses in the window. The presence of compliant barriers in the form of O-rings and bearing gaskets between the window and the mounting also serves as a shock absorber against high-frequency vibration of the housing generated by vortex shedding, wave slap, or ship's engines. It should be noted that even in a compliant mounting with a conical seat, the magnitude of compressive stresses across the bearing surface of the window varies significantly. In the absence of the conical seat and compliant mounting, however, the peak stress would be significantly higher and probably would cause the window to fail at a much lower hydrostatic loading. Figure 27 illustrates a compliant mounting for a spherical sector window. The basic difference between this mounting and the one for hyperhemispheres is that the retaining ring is located on the exterior rather than the interior of the window. Where the retaining ring is on the outside, it generates only compressive stresses in the window and thus can be clamped down tighter than allowed for the interior retaining ring in hyperhemispheres, where tensile stresses are generated in the window during tightening of the retaining ring. The compliant mountings shown in figures 27 and A1 have been used successfully with plastic, glass, and germanium windows.

SEALING

The marine environment imposes one condition more extreme than that experienced by IR sensors in aerospace applications – exposure to moisture. It is well known that optical systems are very intolerant of even minor amounts of moisture. Moisture can fog lenses, corrode precision parts, and eventually make a sensor inoperable. IR systems are equally vulnerable; the window and housing must be completely sealed from external seawater. All sealing configurations for marine applications must be compliant in order for the seal to be maintained during differential expansions and contractions resulting from pressure, temperature changes, or external forces. The three major categories of seals are cast-in-place types, compressed gaskets, and O-rings.

The cast-in-place seal can be an epoxy or a silicone rubber compound that is poured into the bearing interface area and allowed to cure. It depends primarily on adhesion to the window and housing surfaces and therefore is useful only for relatively low external pressure.

Compressed gaskets are fabricated from cured elastomeric materials, usually synthetic rubber. A gasket is cut so as to conform to two mating surfaces and is then clamped in place mechanically. Compressed gaskets have several advantages over cast-in-place seals: they resist higher pressures, they make it possible to remove and refurbish the window, and, since they are identical in design and form, performance is relatively easy to duplicate. The primary drawback of a gasket seal is that for it to function properly, the retaining ring must be clamped very tightly. Otherwise, the gasket will not be sufficiently precompressed.

The O-ring seal is widely recognized as a modern, cost-effective, and reliable sealing technique for a wide range of pressures. A large variety of O-ring thicknesses and materials is commercially available. For proper functioning of the O-ring seal, the IR system designer must match the size of the O-rings to the grooves in the mounting and must use an appropriate clamping arrangement for holding the window in the housing. As can be seen in the mounting for hyperhemispherical windows (fig A1), this may involve the sandwiching of O-rings between the clamp and the window as well as between the window and the housing. Such a seal design eliminates high-point loading and resultant tensile stresses that might fracture the window during tightening of the retaining ring. In the design of the grooves for O-rings, care must be taken to provide adequate restraint for the window without generating unacceptable tensile stresses in it. The peak stresses generated on the interior surface in the meridional direction by tightening the split retaining ring against the internal O-ring seal should be kept below 500 psi so that no opportunity is presented for microcracks to grow larger. The advantages of O-ring seals include improved repeatability of performance, tolerance to higher pressure, and commercial availability of replacement seals.

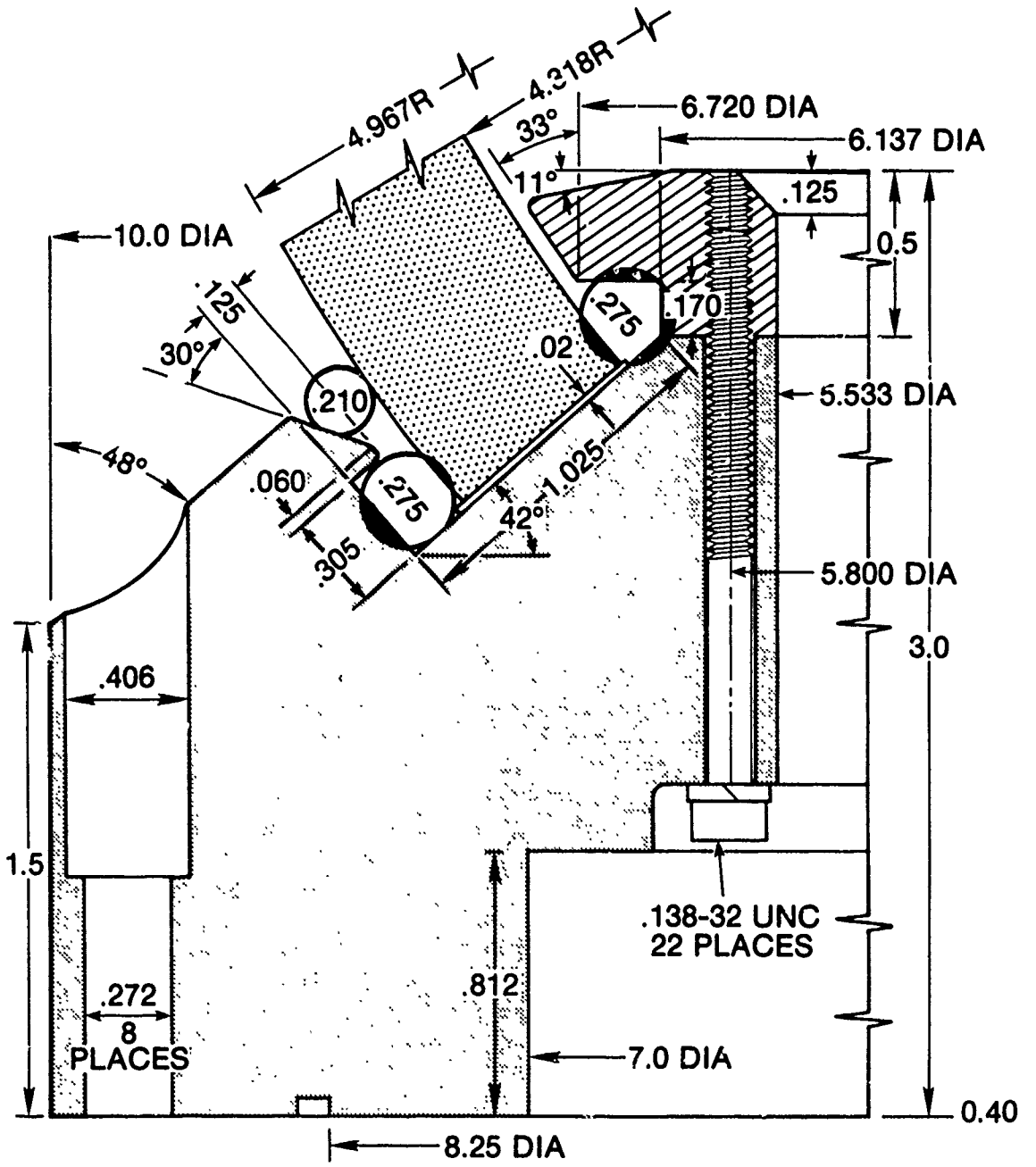

Figure A1. Compliant mounting design for brittle windows of hyperhemispherical shape subjected to static and dynamic pressure loading, vertical and transverse vibration, and lateral impact. Rated for 10000 psi service when fabricated from Ti-6Al-4V alloy.

APPENDIX B

FUTURE DEVELOPMENTS *

After many years of relative stability, the cost of germanium took a dramatic turn upwards during 1981. The weight percentage of germanium in AMTIR-1 is 31.37. The cost of germanium is the largest single item of cost in the production of AMTIR-1 and thus controls the cost of the elements used in making windows (table B1). With both the impendent and the longer range anticipated cost increases of germanium, the situation will worsen, leading to increased cost of AMTIR-1 glass. A possible alternative glass similar in properties but less expensive from a materials cost viewpoint should be sought.

	Cost ($/kg)	
Date	Germanium	AMTIR-1 Elements
1977	250.00	108.96
1978	250.00	108.90
May 1979	275.00	116.80
November 1979	325.00	132.64
January 1980	448.50	171.22
July 1980	705.50	250.55
December 1980	800.00	280.20
1981	960.00	321.12

Table B1. Germanium cost.

As-Se GLASSES

Fortunately, the germanium-arsenic-selenium glass system was identified some years ago as the best source of infrared glass for FLIR applications. Many glass compositions have been studied in detail in this country and abroad. Table B2 is a summary of the results of one such study carried out by Savage et al at the Royal Radar Institute (England). Examination of the table reveals that there are numerous glasses with the transparency and the desired infrared dispersion for 8–12 μm applications. The last glass in the table corresponds to the composition of AMTIR-1. Several of the glasses have dispersions that may be better suited to color-correct germanium systems. Three are very low in germanium content (10%) and thus support our purpose of reduced cost. Arsenic selenide glass ($As_{40}Se_{60}$), the first one in the table, contains no germanium at all. The cost for the elements required to compound a kilogram of the glass is shown in table B3. A comparison shows that the cost of germanium is the dominant factor (greater than 50%) for all glass compositions containing that element. Only arsenic selenide glass avoids the problem of the escalating cost of germanium.

*Appendix B was contributed by AR Hilton of Amorphous Materials Inc, Garland, Texas.

	T_g (°C)	T_x (°C)	30-180°C Thermal Expansion Coefficient	Density (g/cm^3)	Refractive Index (n)			8-12 μm Dispersion
					At 8 μm	At 10 μm	At 12 μm	
$As_{40}Se_{60}$	178	286	21.0×10^{-6}/°C	4.62	2.7840	2.7789	2.7728	159
$Ge_{20}Se_{80}$	154	–	24.8×10^{-6}/°C	4.37	2.4071	2.4027	2.3973	143
$Ge_{10}As_{20}Se_{70}$	159	–	24.8×10^{-6}/°C	4.47	2.4649	2.4594	2.4526	119
$Ge_{10}As_{30}Se_{60}$	210	–	19.0×10^{-6}/°C	4.51	2.6254	2.6201	2.6135	135
$Ge_{10}As_{40}Se_{50}$	222	–	20.9×10^{-6}/°C	4.49	2.6108	2.6067	2.6016	176
$Ge_{20}As_{10}Se_{70}$	209	–	20.5×10^{-6}/°C	4.41	2.5628	2.5583	2.5528	156
$Ge_{30}As_{10}Se_{60}$	345	519	13.7×10^{-6}/°C	4.36	2.4408	2.4347	2.4271	104
$Ge_{30}As_{15}Se_{55}$	351	528	12.8×10^{-6}/°C	4.42	2.4972	2.4914	2.4840	113
$Ge_{30}As_{20}Se_{50}$	361	469	11.7×10^{-6}/°C	4.47	2.5690	2.5633	2.5560	120
$Ge_{33}As_{12}Se_{55}$	368	539	12.0×10^{-6}/°C	4.41	2.5002	2.4942	2.4867	111

Table B2. Physical and optical properties of GeAsSe glasses.

Composition	Cost ($/kg)*	Percentage of Cost due to Germanium
$As_{40}Se_{60}$	$ 54.70	0
$Ge_{20}Se_{80}$	167.40	84
$Ge_{10}As_{20}Se_{70}$	111.40	63
$Ge_{10}As_{30}Se_{60}$	117.10	60
$Ge_{10}As_{40}Se_{50}$	122.60	57
$Ge_{20}As_{10}Se_{70}$	173.00	81
$Ge_{30}As_{10}Se_{60}$	240.20	88
$Ge_{30}As_{15}Se_{55}$	243.00	87
$Ge_{30}As_{20}Se_{50}$	245.80	86
$Ge_{33}As_{12}Se_{55}$ (AMTIR-1)	250.41	88

*1980 price levels ($/kg):

Ge – 750
As – 89
Se – 33

Table B3. Cost of elements used to compound infrared glasses, based on 1980 price levels.

Fortunately, arsenic selenide glasses have been made and sold commercially for years. Eastman Kodak once marketed a glass containing 8% arsenic. Servo Corporation prepared large amounts of arsenic selenide $As_{38.7}Se_{61.3}$ for use in heat detectors for railroad systems. Numerous papers are found in the literature describing its properties. Texas Instruments at one time made arsenic selenide $As_{40}Se_{60}$ in large pieces and characterized it during a US Air Force funded program. The pertinent physical and optical properties of arsenic selenide glass (AMTIR-2) along with those of AMTIR-1, TI 1173, zinc sulfide, Raytheon zinc selenide, and germanium are given in table B4.

Table B4 shows that the refractive index, transmission range, and dispersion of As-Se would be as good or better than the other glasses. Its hardness is less than that of AMTIR-1 and TI 1173 but greater than that of zinc selenide. Its high thermal expansion coupled with relatively low thermal conductivity make it susceptible to heat shock. The rupture modulus of all three glasses is significantly less than that of germanium, ZnS, and ZnSe. The upper use temperature is only about 150°C, much below that of the other glasses. Since its reflection losses are greater than 20%, a reflection coating is necessary. Absorption in the 8–12 μm region is slightly less than that of either TI 1173 or AMTIR-1.

FABRICATION PROCESS

The process used at Amorphous Materials to compound and cast glass plates is carried out in one sealed high-purity quartz system. Vacuum distillation – one of the main purification steps for the glass – can be used to process all the glasses in table B4. The process parameters that must be determined by trial and error are distillation temperature and casting temperature. Correct selection of these parameters is arrived at iteratively by measuring the optical properties of various experimental castings produced under trial sets of process parameters and, on the basis of such evaluations, adjusting the parameters toward improving the quality of each next batch.

APPENDIX B RECOMMENDATIONS

Since the primary source of germanium, a strategically important material, is abroad, and since its cost is progressively increasing, it is recommended that an extensive research program be initiated involving the entire family of chalcogenide glasses, with the objective of defining their optical and structural properties.

Property	AMTIR-1	AMTIR-2	TI 1173	ZnS	ZnSe	Germanium
Composition	$Ge_{33}As_{12}Se_{55}$	As-Se	$Ge_{28}Sb_{12}Se_{60}$	ZnS	ZnSe	Ge
Transmission range	0.9-16 μm	0.9-16 μm	1.0-16 μm	0.5-22 μm	0.5-16 μm	2-18 μm
Refractive index (n) at 10 μm	2.4975	2.7710	2.6036	2.19	2.403	4.0025
Thermal change in n	72×10^{-6}/°C	–	91×10^{-6}/°C	43×10^{-6}/°C	52×10^{-6}/°C	400×10^{-6}/°C
Hardness (Knoop)	170	110	150	215	100	850
Thermal expansion coefficient	12×10^{-6}/°C	20×10^{-6}/°C	14×10^{-6}/°C	7.85×10^{-6}/°C	8.5×10^{-6}/°C	6×10^{-6}/°C
Thermal conductivity (cal/cm·s·°C)	6.0×10^{-4}	5.5×10^{-4}	5.0×10^{-4}	4.0×10^{-2}	4.3×10^{-2}	1.4×10^{-2}
Specific heat (cal/g·°C)	7.2×10^{-2}	–	6.6×10^{-2}	11.2×10^{-2}	8.5×10^{-2}	7.4×10^{-2}
Density (g/cm^3)	4.40	4.66	4.67	4.08	5.27	5.33
Modulus of rupture, annealed (psi)	2700	2500	2500	15000	7500	10500
Young's modulus (psi)	3.2×10^6	2.65×10^6	3.1×10^6	10.8×10^6	9.75×10^6	1.49×10^7
Shear modulus (psi)	1.3×10^6	1.03×10^6	1.2×10^6		3.8×10^6	5.96×10^6
Poisson's ratio	0.26	0.29	0.26	0.27	0.28	0.25
Glass trans temp, T_g (°C)	405	163	295		–	937 (MP)
Upper use temp (°C)	310	150	200	200	>300	200
Dispersion						
3-5 μm	194	182	174		177	102
8-12 μm	115	170	110		57	970
Reflectivity (%)	18.3	22.2	19.8	17	17	36
Trans max (uncoated) (%)	69	64	67	69	69	53
Absorption at 10.6 μm, per cm	0.01	<0.01	0.01	2×10^{-1}	$1\text{-}5 \times 10^{-3}$	0.02

Table B4. A comparison of AMTIR-1, AMTIR-2, TI 1173, zinc sulfide, zinc selenide, and germanium.